GEOTECHNICAL EXTREME EVENTS RECONNAISSANCE (GEER) ASSOCIATION

Turning Disaster into Knowledge

Geotechnical Reconnaissance of the 2016 M_w6.3 Meinong Earthquake, Taiwan

Lead Authors:
Joseph Sun (PG&E), Tara Hutchinson (UCSD), Kevin Clahan (LCI), Farnyuh Menq (UT), Eric Lo (UCSD), Wen-Jong Chang (NCKU), Chi-Chin Tsai (NCHU), Kuo-Fong Ma (NCU)

Contributing Authors[1]:
Michael Hess, Falko Kuester, Dominique Meyer, Vid Petrovic, Sabrina Trinh (UCSD)

GEER Association Report No. GEER-046

[1] The following authors from UC San Diego contributed to data processing and model generation in the present Appendices to the main report.

Version 2: July 14, 2016

FUNDING SOURCES

Funding for the reconnaissance from February 14 - 19, 2016 was provided by the U.S. National Science Foundation (NSF). Participation of the GEER Steering Committee personnel in coordinating and reviewing the report was also made possible by the NSF. The work of the GEER Association, in general, is based upon work supported in part by the NSF through the Geotechnical Engineering Program under Grant No. CMMI-1266418. The GEER Association is made possible by the vision and support of the NSF Geotechnical Engineering Program Directors: Dr. Richard Fragaszy and the late Dr. Cliff Astill. GEER members also donate their time, talent, and resources to collect time-sensitive field observations of the effects of extreme events. Any opinions, findings, and conclusions or recommendations expressed in this material are those of the authors and do not necessarily reflect the views of the NSF.

In support of GEER's vision, in-kind support from U.C. San Diego (UCSD), Univ. of Texas at Austin (UT), Lettis Consultants International (LCI), and Pacific Gas & Electric Company (PG&E) was provided for this reconnaissance effort. Additional local support in Taiwan was provided by National Cheng Kung University (NCKU), National Central University (NCU), National Chung Hsing University (NCHU), Taiwan Water Resources Agency (TWRA), and Sinotech Engineering Consultants Inc. (Sinotech). Several local practitioners also volunteered their time and provided technical and logistical assistance.

CONTENTS

List of Figures

List of Tables

1. INTRODUCTION

In response to the heavy damage reported for the Mw 6.3 (ML 6.4) Meinong Earthquake that hit southern Taiwan at 3:37 am local time, February 6, 2016 (11:57 am February 5, 2016, Pacific Standard Time), the GEER Steering Committee dispatched a reconnaissance team to Taiwan. The reconnaissance team was selected and formed on Monday (February 8, 2016), departed for Taiwan on Friday (February 13, 2016), and arrived and started their reconnaissance effort on Sunday (February 14, 2016) after the conclusion of rescue and recovery effort. The reconnaissance effort continued for about a week and the team returned on February 20, 2016.

1.1 Activities

The main activities for each day are summarized below. Specific sites visited by the GEER team are shown on Figures 1-1 and 1-2 and summarized in Table 1. Where possible, remote sensing equipment (unmanned aerial vehicle; UAV and light-detection and ranging; LiDAR) were deployed at specific sites. Three-dimensional models developed using these data are available in the part 2 report series.

Day 1 (Sunday 2/14): The GEER team met with Prof. Kuo-Fong Ma (馬國鳳) of the National Central University 國立中央大學 (NCU) and was debriefed on the seismicity and ground motion characteristics that had accumulated to that point.

Day 2 (Monday 2/15): The team then met with Prof. C.T. Lee (李錫堤) of NCU and several students to receive a geological summary and presentation with supporting documents. The GEER team leader received the first Meinong earthquake debriefing from the National Center for Earthquake Engineering Research 國家地震中心 (NCREE) in the afternoon, while part of the Team traveled to Tainan and began field reconnaissance by documenting levee failures on the Tsengwen River (曾文溪) and exploring sites along the Ho Jah Lei fault (後甲理斷層).

Day 3 (Tuesday 2/16): Additional team members arrived, and a kick-off meeting including GEER, Prof. Wen-Jong Chang (張文忠) of the National Cheng-Kung University (國立成功大學), Prof. Chi-Chin Tsai (蔡祁欽) of the National Chung Hsing University (國立中興大學), and faculty members and students from NCKU participating in the GEER program, and another U.S. based reconnaissance team from Degenkolb Engineers. In the afternoon, GEER Team 1 visited 3 levee failure/distress sites along the Tsengwen River and performed UAV and LiDAR surveys at all three locations. GEER Geology Team investigated several damaged and collapsed buildings along Hwy 182 east of Tainan and in the city of Xinghua (新化) along Hwy 20; liquefaction features and associated damage in the historic district in Guanmiao (關廟); and a well expressed N-S trending lineament along the west side of the Guanmiao Valley.

Day 4 (Wednesday 2/17): GEER Team 1 visited 3 liquefaction sites and observed building performance in those areas including: the Annan District 安南區, the North District南區, and the West Central District中西區. GEER Geology Team observed slope failure of the channel

embankment and damage to the Da Chueng bridge; mapped the western Guanmiao hills fold structure, had two drone teams fly UAV surveys along the geomorphic Guanmiao lineament; examined the Longtsuan fault (龍船斷層) and boundaries of the mainshock uplift area; and visited liquefaction features in the Xinshi (新市) neighborhood. GEER Team 2 split at the end of the day and a portion of the team visited two collapsed building sites and performed ground vibration monitoring (King's Town Bank 京城銀行and Guiren area歸仁區).

Day 5 (Thursday 2/18): GEER Team 1 visited 3 liquefaction sites: (1) Xinshi (新市) where residential buildings were constructed over liquefied soils, (2) Xinhua area (新化) where repeated liquefaction occurred during this earthquake and in the 2010 Jiasian earthquake (甲仙地震), and (3) Guanmiao area (關廟) closer to the epicenter where a village of older adobe-type residential buildings were constructed over liquefied soil and non-liquefied soils. UAV and LiDAR surveys were performed at each of the sites. GEER Geology Team travelled to Taipei for a meeting with Prof. Kuo-Fong Ma (馬國鳳) of National Central University 國立中央大學 (NCU) and was interviewed for a Taiwan News special on the Meinong earthquake. GEER Geology Team left Taiwan that evening. GEER Team 2 split at the end of the day and visited collapsed building sites (Weiguan Building (維冠大樓) and King's Town Bank (京城銀行) and performed ground vibration monitoring at the two sites.

Day 6 (Friday 2/18): GEER Team 1 visited Wenhe Street 文和街 (West Central District中西區), where a mixture of old and newer residential buildings that experienced ground liquefaction where different performances were observed. GEER Team 1 also walked a western-most region of the Yanshuei river bank (鹽水溪高灘地) on banks to the North near Annan and South of Annan, to determine if liquefaction occurred along the river bank where extensive liquefaction was observed in the nearby Annan District less than 100 m away. Team 2 revisited Guanmiao area (關廟) to perform a UAV survey, visited a collapsed abandoned building (Wanglin Hotel – Guiren旺林飯店歸仁館) and performed ground vibration monitoring. GEER Team 1 also split and visited the Beian Bridge (北安橋). The GEER team held a closing meeting at NCKU in the evening.

Day 7 (Saturday 2/19): GEER team departs Taiwan.

Day 8 (Tuesday 2/23): One GEER Team member visited Haidian Junior High School (海佃國中) in Annan District.

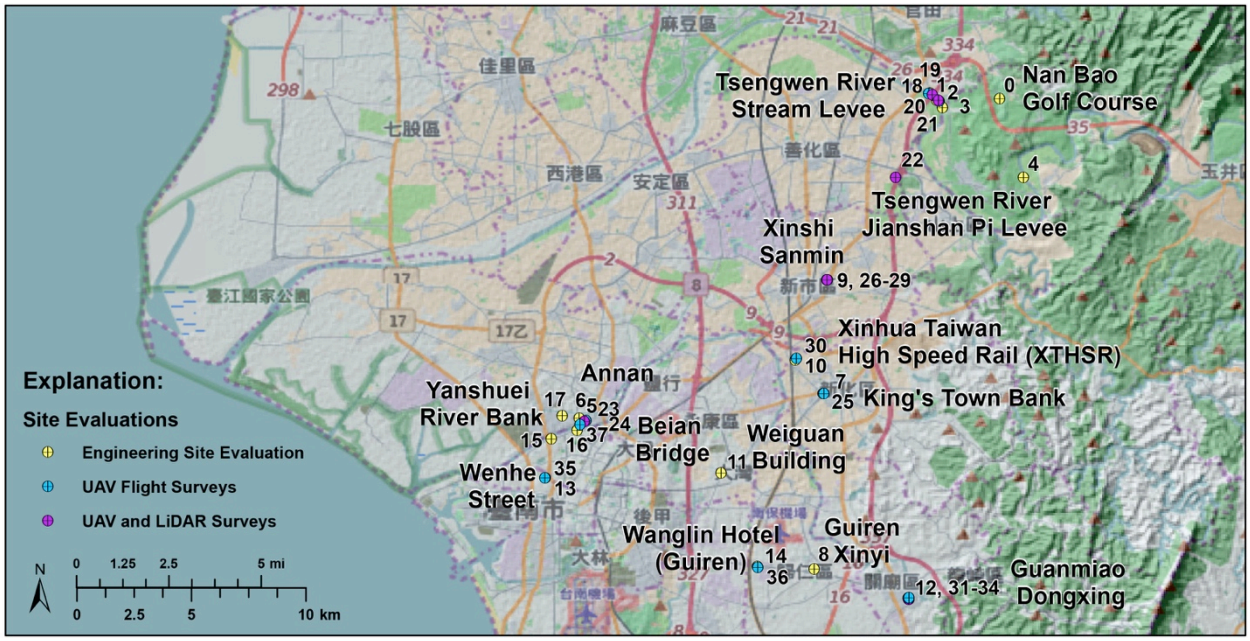

Figure 1-1: GEER Team site evaluation locations, including locations of unmanned aerial vehicle (UAV) and LiDAR surveys.

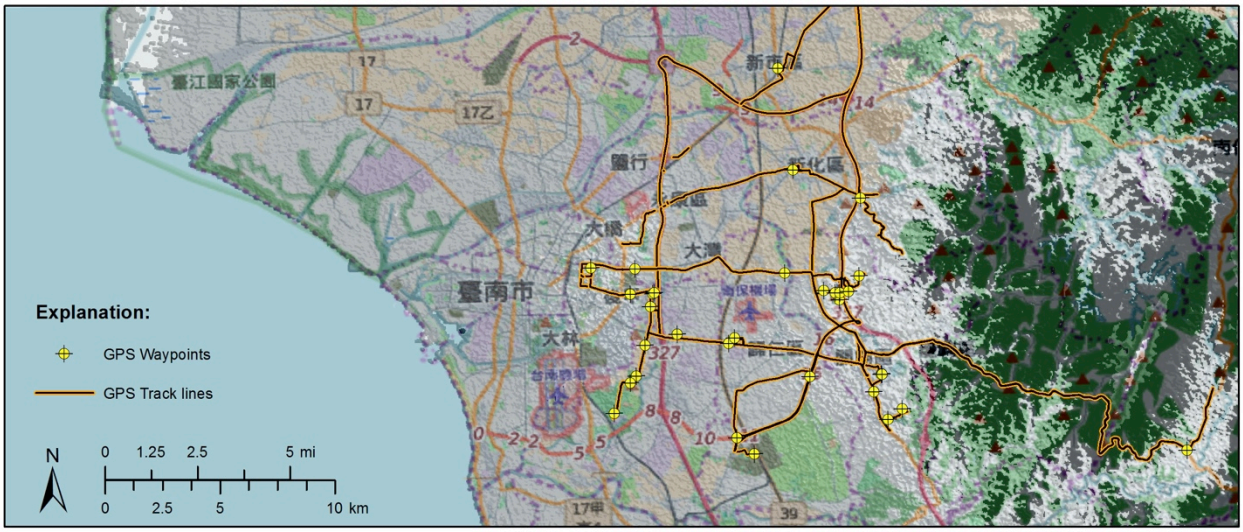

Figure 1-2: GEER Geology Team track log and waypoint location map.

Site Name	*Name In Report*	*Site #*	*District*	*Chinese Name*	*Date*	*Coordinates*	*Comments*
Nan Bao Golf Course	Nan Bao Golf Course	1	Danei	南寶高爾夫球場	2/13/2016	23.151930, 120.370192	Failure of fill slope (rigid block movement)
Tsengwen River Rixin Down Stream Levee	Rixin Failure No. 1	1	Danei	曾文溪日新護岸下游	2/16/2016	23.154097°,120.342908°	Failed levee, under repair at time of visit
Tsengwen River Rixin Mid Stream Levee	Rixin Failure No. 2	2	Danei	曾文溪日新護岸中游		23.151331°, 120.345572°	Failed levee, under repair at time of visit
Tsengwen River Rixin Up Stream Levee	Rixin Failure No. 3	3	Danei	曾文溪日新護岸上游		23.148416, 120.347761	Failed levee, unrepaired at time of visit
Tsengwen River Jianshan Pi Levee	ErXi Bridge Levee	3	Danei	曾文溪尖山埤堤防		23.121176°,120.379569°	Distressed concreted slab slope protection due to slope movement, evidence of landside liquefaction
Annan	Annan	4	Annan	安南液化區	2/17/2016	23.025585°,120.207441°	Liquefaction-induced damage to residential structures (2-4 stories; backfilled old pond)
Kuo clinic building	Kuo Clinic	5	Annan	郭婦產專科		23.026813°,120.205381°	Liquefaction-induced damage to residential structures (adjacent to hospital on basement)
King's Town Bank	King's Town Bank	6	Sinhua	京城銀行		23.036360°, 120.301000°	Collapsed 11-story commercial building
Guiren Xinyi	Guiren	7	Guiren	歸仁區信義路		-22.967643°,120.297568°	Collapsed 6-story residential building
Xinshi Sanmin	Xinshi	8	Xinshi	新市區三民路	2/18/2016	23.080978°, 120.302724°	Liquefaction-induced damage to residential structures (2-4.5 stories; backfilled old pond)
Xinhua Taiwan High Speed Rail (XTHSR)	HSR	9	Xinhua	新化高鐵		23.049466°, 120.290060°	Repeated freefield liquefaction (1946, 2010, 2016). Satisfactory performance of nearby Taiwan High Speed Rail viaduct structure
Weiguan Building	Weiguan Building	10	Yongkang	維冠大樓		23.005233°, 120.261053°	Collapsed 16-story building (debris has been removed)
Guanmiao Dongxing	Guanmiao	11	Guanmiao	關廟區東興路		-22.955921°,120.334688°	Historical single story adobe and brick homes; combined structural & liquefaction-induced collapse
Wenhe Street	Wenhe	12	North	北區文和路	2/19/2016	-23.003406°,120.192122°	Liquefaction-induced damage to residential structures (2-4.5 stories)
Wanglin Hotel - Guiren	Wanglin	13	Guiren	旺林飯店歸仁館		-22.968561°,120.275314°	Collapsed 10-story building (pancaked-type failure)
Yanshuei River Bank	Yanshuei river bank	14	North	鹽水溪岸		23.018717°, 120.194495°	No visible liquefaction features
Beian Bridge	Beian bridge	15	North	北安橋		23.021954°,120.204664°	Southwest approach shows possible abutment movement
Haidian Junior High School	Haidian	16	Annan	海佃國中	2/23/2016	23.02771°, 120.19879°	Satisfactory foundation performance

Table 1-1: GEER Meinong earthquake team site reconnaissance summary table.

1.2 Team Members

The GEER effort was supported by various agencies and organizations and their support is acknowledged below.

Figure 1-3: Vice Chancellor of National Cheng Kung University (NCKU) addressing the GEER Kickoff Meeting.

Figure 1-4: GEER Kick off Meeting held at National Cheng Kung University (NCKU) attended by GEER Team, NCKU faculty and students, and Degenkolb Reconnaissance Team.

Figure 1-5: GEER Engineering Team, left to right: Wen-Jong Chang, Farnyuh Menq, Chi-Chin Tsai, Eric Lo, Tara Hutchinson, Joseph Sun, and Tong-Ho Tsai.

Figure 1-6: GEER Geology Team, left to right: Wei-Kai Huang, Lun-Wei Wei, Siang-Fu Chuang, Jia-Jyun Dong, Typhoon Huang, and Kevin Clahan.

Figure 1-7: Dinner hosted by the Vice Chancellor of NCKU for the Internal Reconnaissance Effort and NCKU Faculty

GEER Steering Committee members and Staff
Jonathan Bray (Univ. CA Berkeley) – GEER Lead
Rob Kayen (U.S. Geological Survey; Univ. CA Los Angeles) – GEER Coordinator
Fernando "Estéfan" Garcia – GEER Recorder

GEER Reconnaissance Team
Joseph Sun (Pacific Gas &Electric Co.) – Geotechnical Engineer
Tara Hutchinson (Univ. CA San Diego) – Structural Engineer
Kevin Clahan (Lettis Consultants International) – Engineering Geologist
Farnyuh Menq (Univ. Texas) – Geotechnical Engineer
Eric Lo (UCSD) – Development Engineer

GEER Taiwan Team
Wen-Jong Chang (NCKU) – Geotechnical Engineer
Chi-Chin Tsai (NCHU) – Geotechnical Engineer
Kuo-Fog Ma (NCU) – Seismologist
Kuo-Liang Wen (NCU) – Seismologist
Chyi-Tyi Lee (NCU) - Geologist
Jyun-Yan Huang (NCREE) – Seismologist
Tong-Ho Tsai – Structural Engineer
Typhoon Huang – Geologist
Pin-Kun Lu (TWRA) – Civil Engineer
Tian-Yu Wang (Sinotech) – Geotechnical Engineer

GEER Contributing Members
J.J. Dong (NCU) – Geotechnical Engineer
Che-Min Lin (NCREE) – Seismologist
Chun-Shiang Kuo (NCREE) – Seismologist
Chun-Te Chen (NCREE) – Seismologist
Auga Tsai (Sinotech) – Geotechnical Engineer
Lun-wei Wei (Sinotech) – Geotechnical Engineer
Wei-kai Huang (Sinotech) – Geotechnical Engineer
Shih-Hsun Chou (NCKU)
Chen-Han Lin (NCKU)
Ting-Han Hsiao (NCKU)
Han Hsiao (NCKU)
Wei-Chun Lin (NCHU)
Hsing-Wen Lui (NCHU)
Siang-Fu Jhuang (NCU)
Shun-Qiang Zhang (NCU)
Qi-Xuan Zhong (NCU)
Meng Xuan Shi (NCU)

1.3 Focus and Theme

There were some unexpected structural performances, geographical damage patterns, and liquefaction manifestation from the Meinong earthquake compared with prior earthquakes of similar magnitude. As such, this reconnaissance placed emphasis on the following:

- Seismic source characterization
- Influence of geology, structure, and local soil conditions on ground motions
- Liquefaction of fine-grained sands and silty sands
- Performance of buildings and foundations in liquefied soils
- Performance of non-symmetrical and soft story buildings

1.4 Report Organization

Reconnaissance findings are presented in a two-part series. With the first part organized as a conventional report, summarizing the event, geologic setting, seismology, ground response, including the specific detailing of liquefaction-induced damage and a summary of the performance of buildings, slopes, and dams. The second part, provided herein offers a unique "virtual" perspective of the sites visited by the team whereby remote sensing equipment was deployed. This Part 2 report includes compressed 3D-models of key sites that are either interactive or representative of fly-throughs of full-resolution models.

2. GEOLOGIC SETTING

This section presents the regional geologic setting of Taiwan with emphasis on southwest Taiwan and the Chianan Plain which contains the three large cities of Chiayi, Tainan, and Kaohsiung which sustained significant damage from the February 6, 2016, Mw 6.3 Mienong earthquake.

2.1 Regional Geologic and Tectonic Setting

The island of Taiwan is a product of both subduction and collision of the Philippine Sea and Eurasian tectonic plates (Figures 2-1 and 2-2). The active arc-continent (Philippine Sea Plate vs. Eurasian Plate) collisional nature of the plate boundary results in the relatively young and on-going Taiwan orogeny. Using 1990–1995 global positioning system (GPS) data from the Taiwan GPS network, Yu et al. (1997) show the Philippine Sea plate converging at a rate of ~82 mm/yr while longer-term data indicate convergence could be as high as 90 mm/yr (Chen, 2006) with respect to the stable Eurasian Plate (Figure 2-1). Geodetic shortening rates lessen progressively to the west and north (Yu et al., 1997) as Philippine Sea plate motion is transferred to north-south-striking thrust faults beneath Taiwan's Central Range and Western Foothills, and the oblique-reverse Longitudinal Valley fault bounding the western margin of Taiwan's Coastal Range (Figure 2-1).

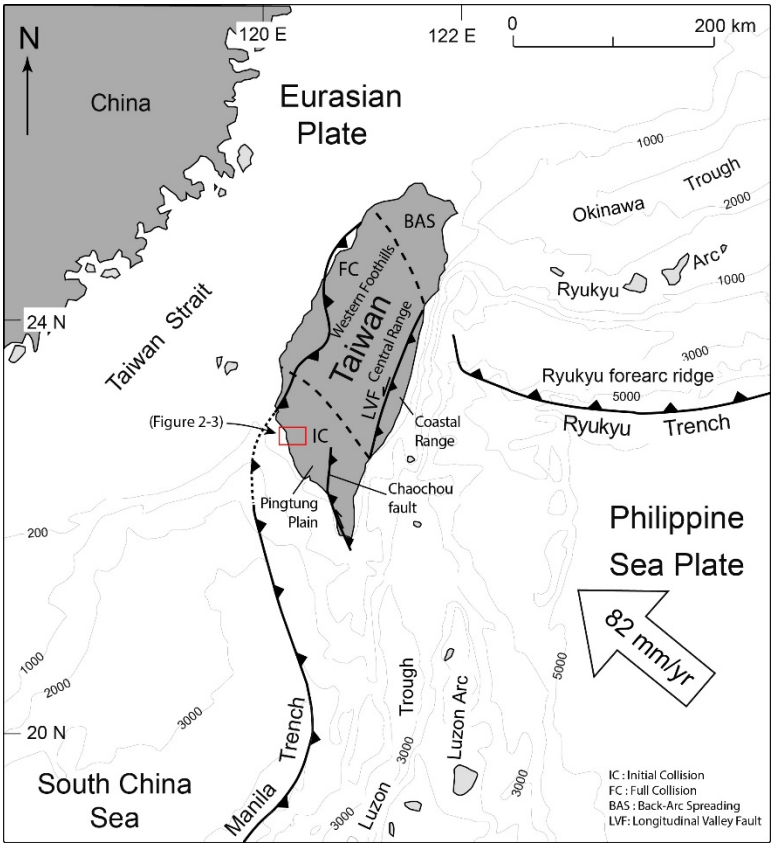

Figure 2-1: Regional Tectonic Map: IC = Initial Collision; FC = Full Collision; BAS = Back-Arc Spreading; LVF = Longitudinal Valley Fault (Modified from Shyu et al. 2005).

Figure 2-2: Geologic Map of Taiwan (CGS, 2000).

Oblique convergence of the Philippine Sea Plate and Eurasian Plate in the Taiwan region results in an 84 mm/yr north–to-south migration of the suture zone (Suppe, 1984), which in turn results in mature structures at the northern end of the island and nascent structures at the very southern end of the island and further south offshore. South of Taiwan, oceanic lithosphere of the Eurasian Plate subducts beneath the Philippine Sea Plate along the Manila Trench, resulting in the Luzon Trough, Luzon Arc, and an accretionary prism (Kaoping Slope [Huang et al., 2006]) that becomes progressively wider and more deformed to the north of this collision, eventually emerging as southwest Taiwan. The central part of Taiwan is characterized by an arc-continent collision (Figure 2-1) where the Luzon arc collides with the last vestige of Eurasian oceanic lithosphere and the margin of the Eurasian continental lithosphere. This collision results in: (a) docking of the Luzon arc on the eastern side of Taiwan, and (b) uplift and exhumation of the Eurasian continental basement (Huang et al., 2006). Docking and northward translation of the

Luzon Arc and associated basin strata, which make up Taiwan's coast range, is largely accommodated by the oblique reverse Longitudinal Valley fault (Figures 2-1, 2-2, and 2-3). This structure alone accommodates up to 40% of the total shortening between the Philippine Sea and Eurasia plates. Wu et al. (1997) indicate that mountain building in Taiwan's central range is accommodated through both low-angle thrust (detachment) faults and extrusion of higher velocity mid-to-lower crustal materials. At the very northern end of the island, collision gives way to extension and orogenic collapse, the Philippine Sea Plate reverses subduction polarity, and the Ryukyu arc and Okinawa trough impinge on the foundering Central Range (Figure 2-1). Shyu et al. (2005) subdivide Taiwan into several distinct structural domains which are discussed in more detail below (Figure 2-3).

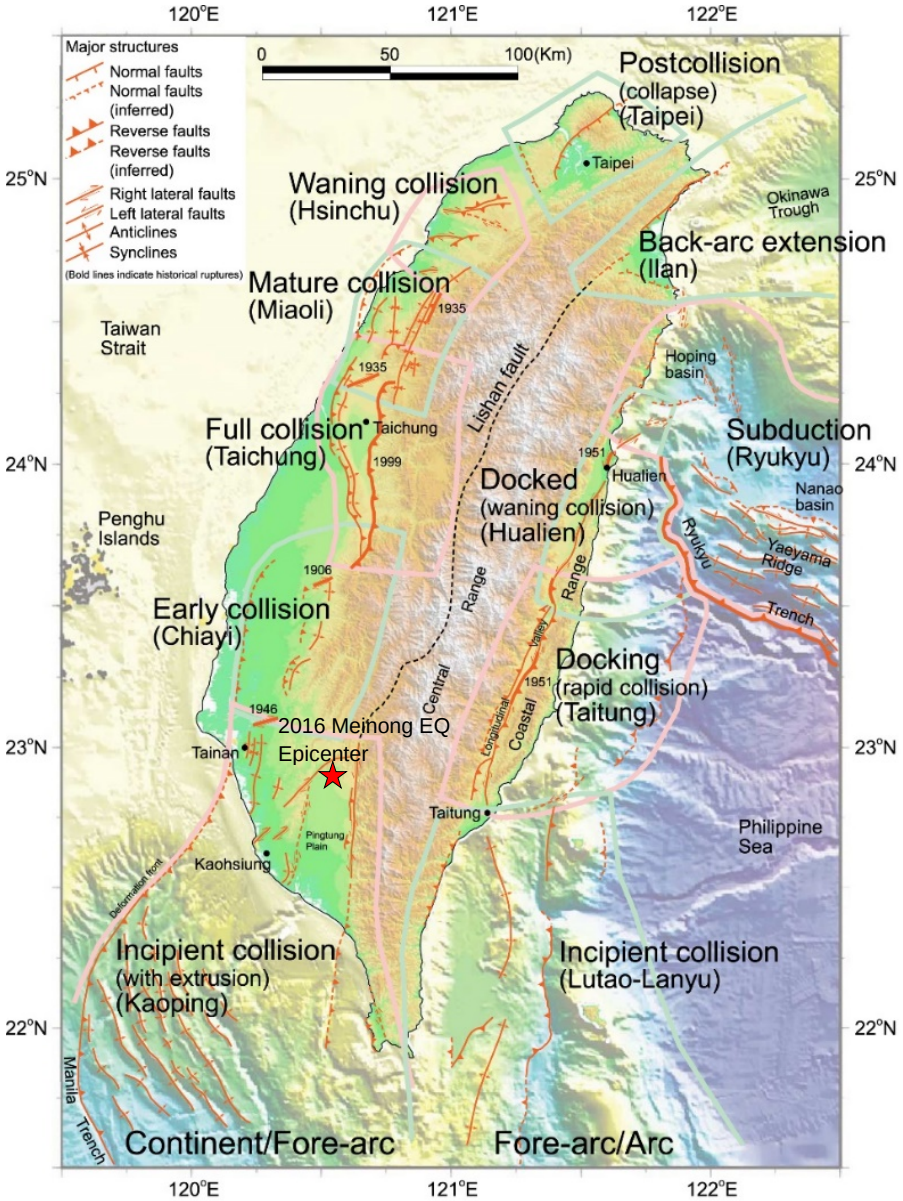

Figure 2-3: Geologic structure map of Taiwan showing separate neotectonic or structural domains as proposed by Shyu et al. (2005).

Orogenic collision in Taiwan began about 5 million years ago in the north (Suppe, 1987; Teng, 1990) and progressed southward during continued collision where it reached the middle of the island about 3 million years ago (Teng, 1990). Presently, collision in southern Taiwan has just begun (Huang et al., 2000; Kao et al., 2000). Thus, given the general southward migration of younger tectonic structures and associated stratigraphy, southern and southwest Taiwan represents the youngest sub-aerial reach of Taiwan's active collisional orogeny (Figures 2-2 and 2-3).

The February 6, 2016, Meinong earthquake occurred in an area with a relatively high rate of W-SW geodetic motion and seismicity (Figures 2-4, 2-5, and 2-6). Approximately 90 M 6.4+ events having occurred within 250 km of the February 5, 2016 Meinong earthquake over the preceding century (USGS, 2016). Several of these earthquakes have been destructive with numerous human fatalities including: a M 7.3 in December 1941 between cities of Tainan and Chiayi which claimed several hundred lives; the 1946 M 6.1 Hsinhua earthquake which caused 74 fatalities; a M 5.7 earthquake 70 km to the north of the February 2016 event in July 1998 caused 5 fatalities; a M 7.0 event in December 2006, 120 km to the south, caused 2 fatalities; the March 4, 2010, M 6.4 Jiashan earthquake located several kilometers east of the Meinong earthquake epicenter; and the Chi-Chi earthquake, a M 7.6 event in September 1999 located just over 100 km north-northeast of the February 2016 event, which caused widespread destruction and almost 2,500 fatalities.

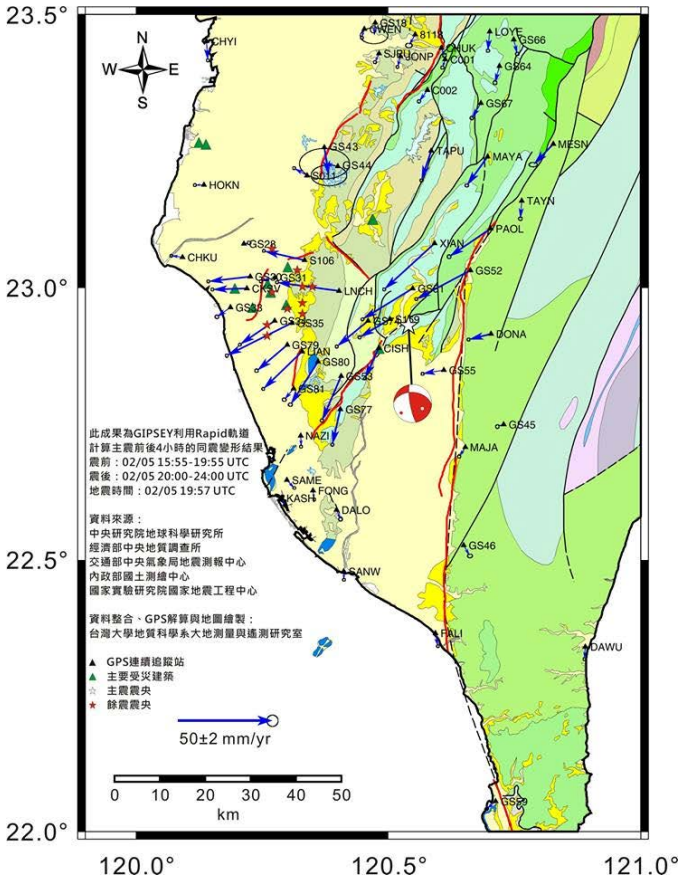

Figure 2-4: Geologic and Geodetic Map of Southwest Taiwan showing relative crustal motions.

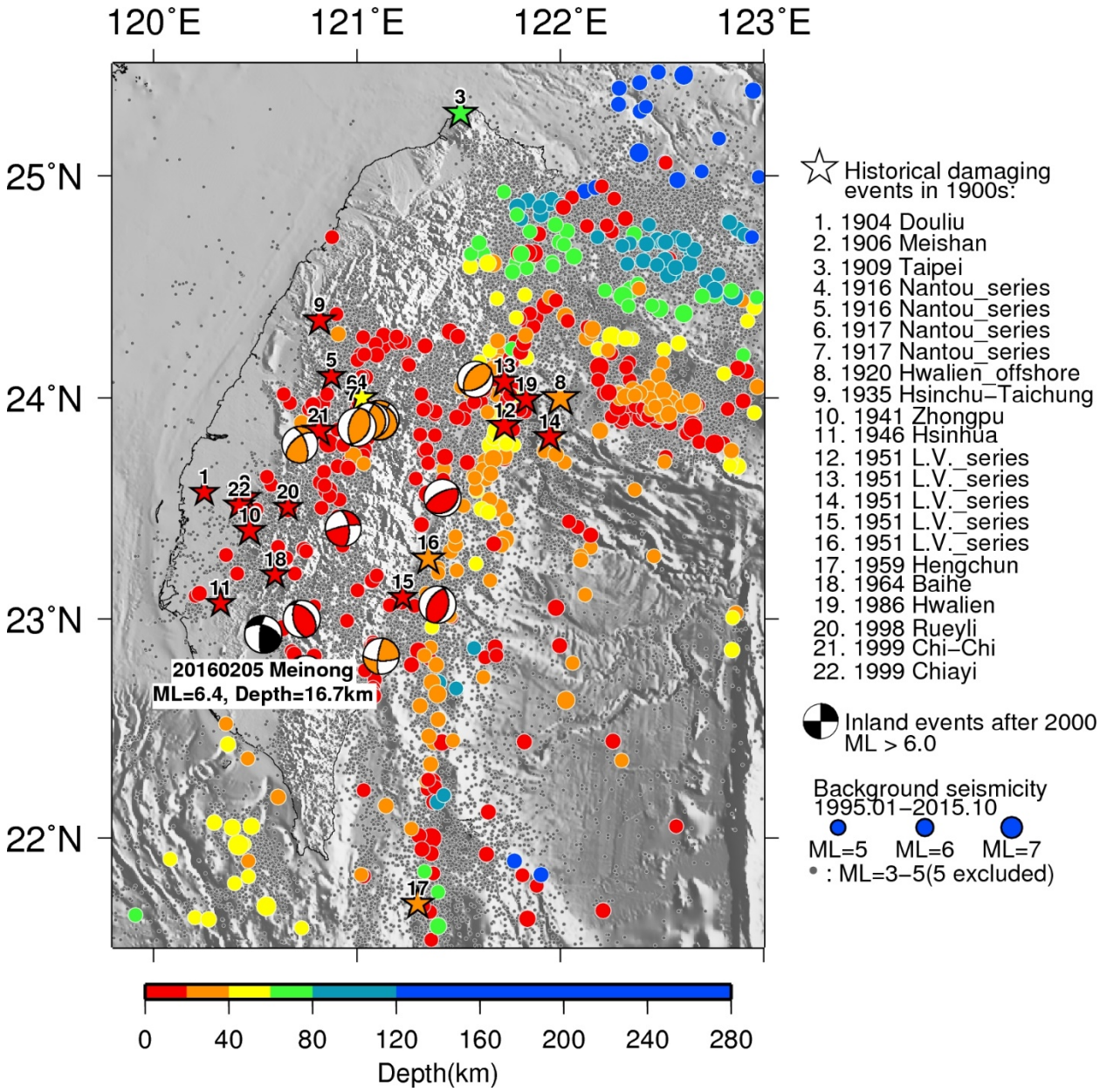

Figure 2-5: Historically damaging earthquakes and selected seismicity of Taiwan (courtesy of Kuo-Fong Ma, 2016).

2.2 Geologic and Tectonic Setting of Southwest Taiwan

The geology of southwest Taiwan, and the Tainan area in particular, is described here in more detail as most of the earthquake related damage from the 2016 Meinong earthquake is concentrated in this area. Southwest Taiwan, which includes the 2016 Meinong epicenter as well as the cities of Tainan and Kaoshiung, consists of shallow marine bedrock from the continental shelf that is being uplifted and deformed as part of crustal shortening during orogenic collision.

According to Shyu et al. (2005), southwest Taiwan and the area of the 2016 Meinong earthquake are located in the Kaoping structural domain which is underlain by the last remnant of the South

China Sea oceanic lithosphere subducting beneath the Philippine Plate to the east (Figure 2-6). The onshore Kaoping structural domain is dominated by the western fold and thrust belt which is rapidly deforming late-Tertiary bedrock and Holocene alluvium of the Chainan Plain by prominent N-S trending folds, as well as, emergent and "blind" reverse thrust faults between the city of Tainan and the Western Foothills (Figures 2-3 and 2-7). The Kaoping domain also includes the Pingtung plain between the Central Range and the Western Foothills, where Holocene subsidence is occurring at rates up to 13 mm/yr (Shyu et al., 2005). The Pingtung Plain is bounded by NE-SW trending left lateral oblique strike-slip faults (Figure 2-3).

Several additional active faults in the southwest region of Taiwan are well expressed geomorphically including (from west to east; Figure 2-7): the Frontal Thrust which comes onshore to the north of Tainan; the Ho Jah Lei fault on the eastern margin of the Tainan Tablelands; the Longtsuen fault within the Western Foothills; the Chishan fault along the western border of the Pingtung Plain, and the Chaochou fault along the eastern margin of the Pingtung Plain and the western margin of the Central Range (Figure 2-7).

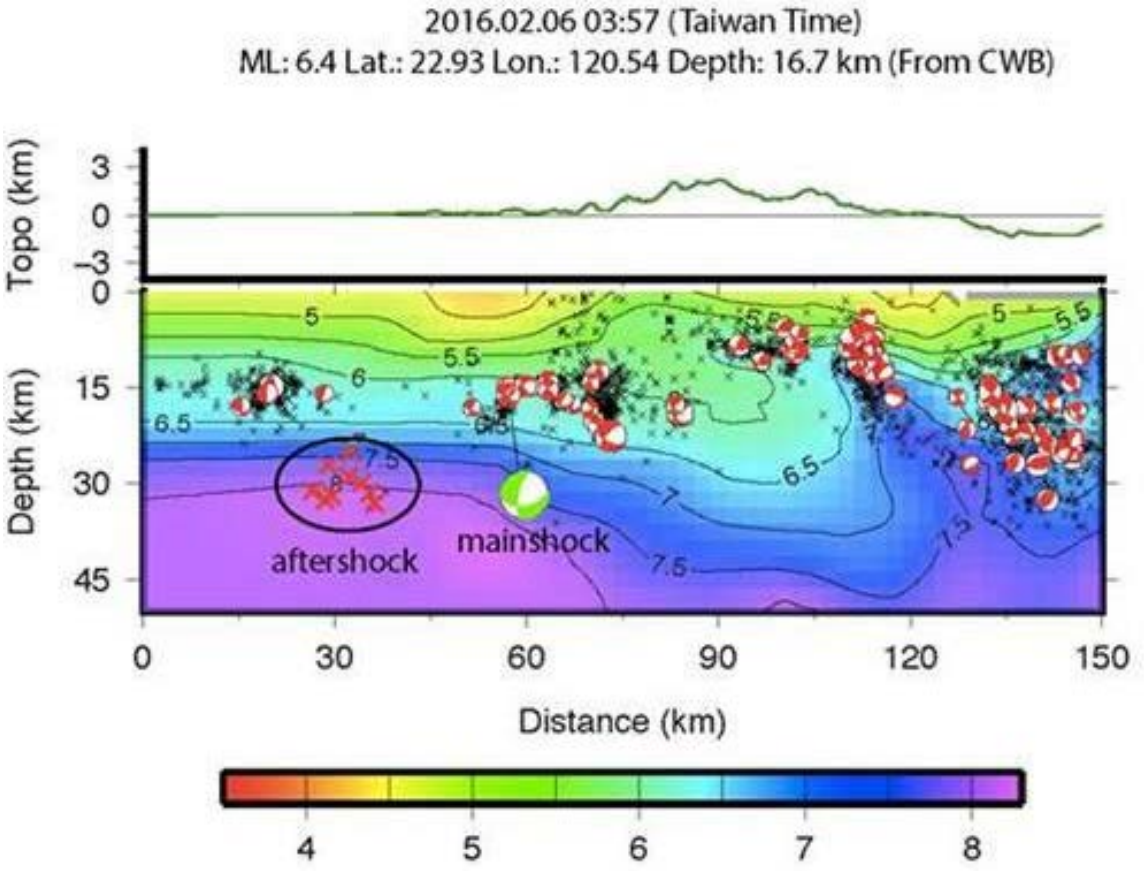

Figure 2-6: Seismic profile of Southern Taiwan showing the location of the February 6, 2016, Meinong earthquake (mainshock) as well as associated aftershocks (circled).

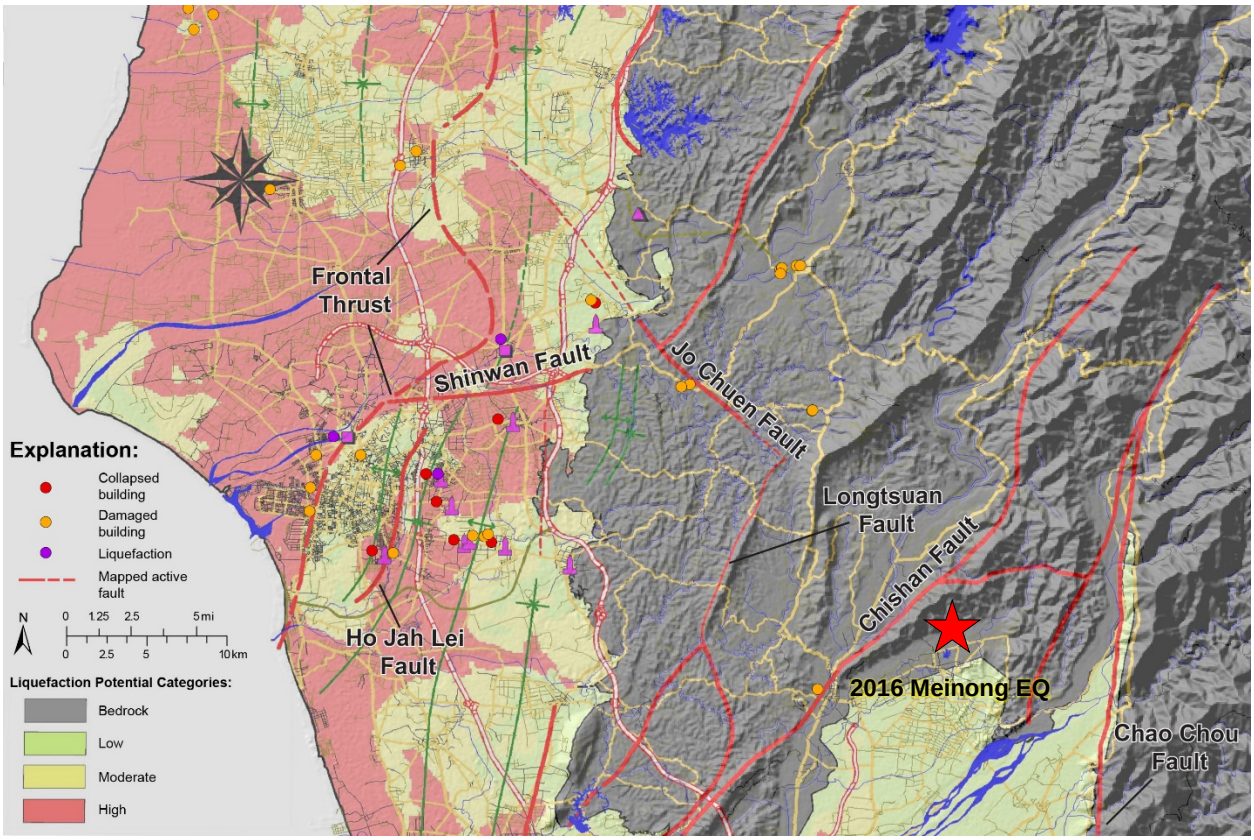

Figure 2-7: Liquefaction Potential and Fault Location Map of Southwest Taiwan (courtesy of Prof. C.T. Lee).

The Quaternary geomorphology of the Tainan area reflects the cyclic behavior and subsequent uplift of the nearshore marine environment (Figures 2-8 and 2-9). The history of accretion and uplift as recorded in the stratigraphy of the Tainan area can be divided into four stages: (1) deposition of Miocene to Pleistocene continental slope fine to coarser grained marine deposits which consist of intercalated sandstones and shales and is located within the western portion of the Western Foothills (Figures 2-8 and 2-9); (2) deposition of the Holocene, shallow marine Tainan Fm sandstone which is reportedly on the order of up to 200 m thick; (3) deposition of Holocene marine terrace deposits along the margin of the Western Foothills; and (4) deposition of the shallow Dawan marine estuarine deposits consisting of fine sand and silts which are reportedly between 2750 and 300 years old and on the order of 20 to 40 m thick in places (Figure 2-9).

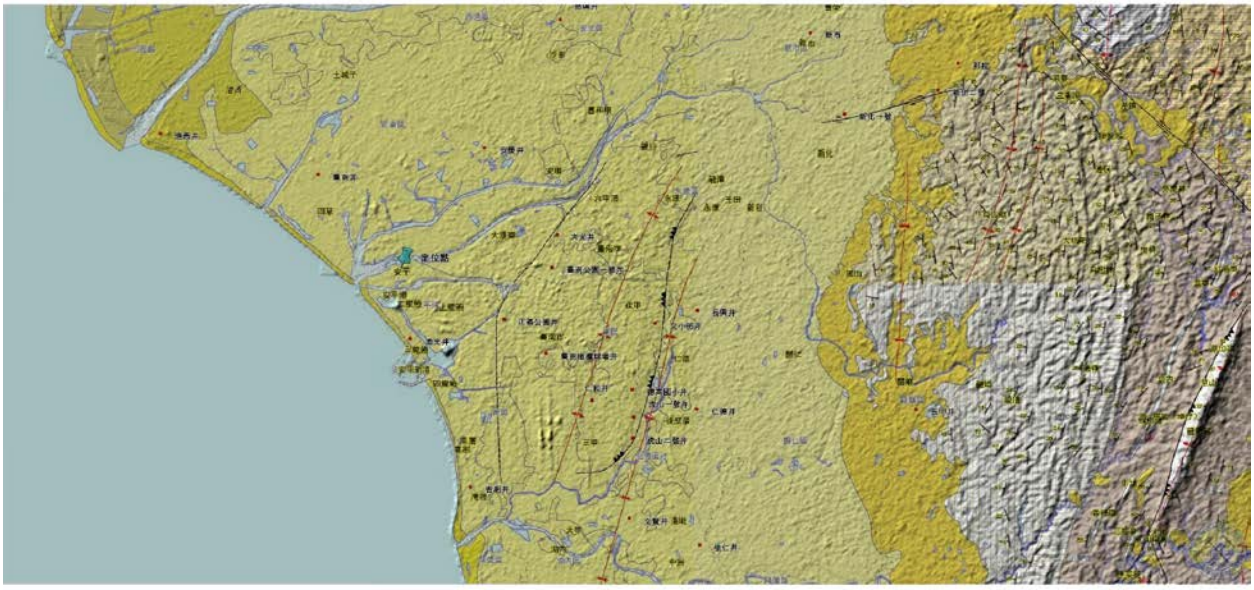

Figure 2-8: Geologic Map of the Tainan Area (CGS, 2005).

The ongoing shortening and associated folding and faulting in the region has produced topographic highs consisting of the more cemented Tainan Fm, as well as topographic lows that have been filled by the Dawan estuarine deposits (Figure 2-9). These topographic features are referred to as the Tainan Tablelands and the Dawan Lowlands, respectively, and are the result of ongoing N-S trending faulting and folding within the Tainan area (Figure 2-9). The Holocene Tainan and Dawan Fms underlie areas of moderate and high liquefaction potential in the Tainan area, respectively (Figure 2-7). Evidence for the poor performance of these young deposits during the Meinong earthquake can be seen on Figures 2-7 and 2-9 where collapsed buildings, damaged buildings, and buildings effected by liquefaction are primarily located within the loose fine sand and silt deposits of the Dawan lowlands.

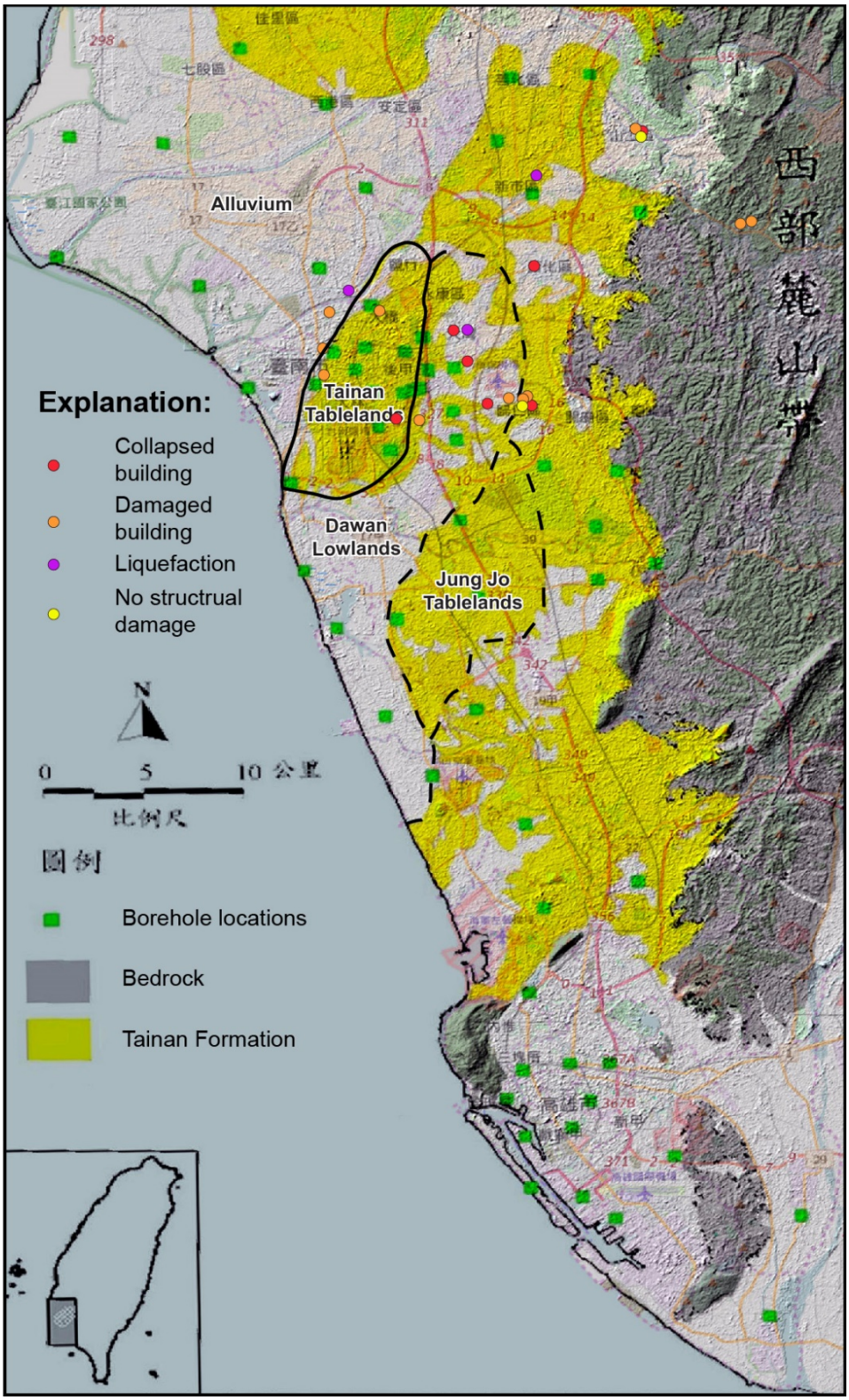

Figure 2-9: Quaternary geologic map of the Tainan area (Courtesy of Prof. C.T. Lee). Includes locations of building damage reports from the February 6, 2016, Meinong earthquake (courtesy of Prof. Chi-Chin Tsai).

2.3 Geologic Reconnaissance of the Proposed Guanmiao Fault

As part of the GEER field investigations during the week of February 14, 2016, several days were spent reviewing known geologic structures including the Ho Jah Lei fault, Longtsuan fault, and the fold and thrust belt of the Western Foothills including the hills west of the Guanmiao Valley (Figure 2-10). Interferometric Synthetic Aperture Radar (InSAR) data supplied by the JPL-Caltech Advanced Rapid Imaging and Analysis (ARIA) project, provided important evidence for vertical ground displacement associated with the Meinong earthquake (Figures 2-11 and 2-12). The InSAR data show vertical displacement and uplift of over 12 cm across the Western Foothills as well as distinct uplift of over 10 cm within the Guanmiao Hills west of the Guanmiao Valley. The Western Foothills highly deformed and are bounded to the east by the Longtsuan fault as shown on Figure 2-12. A schematic cross section across southwestern Taiwan is shown on Figure 2-13.

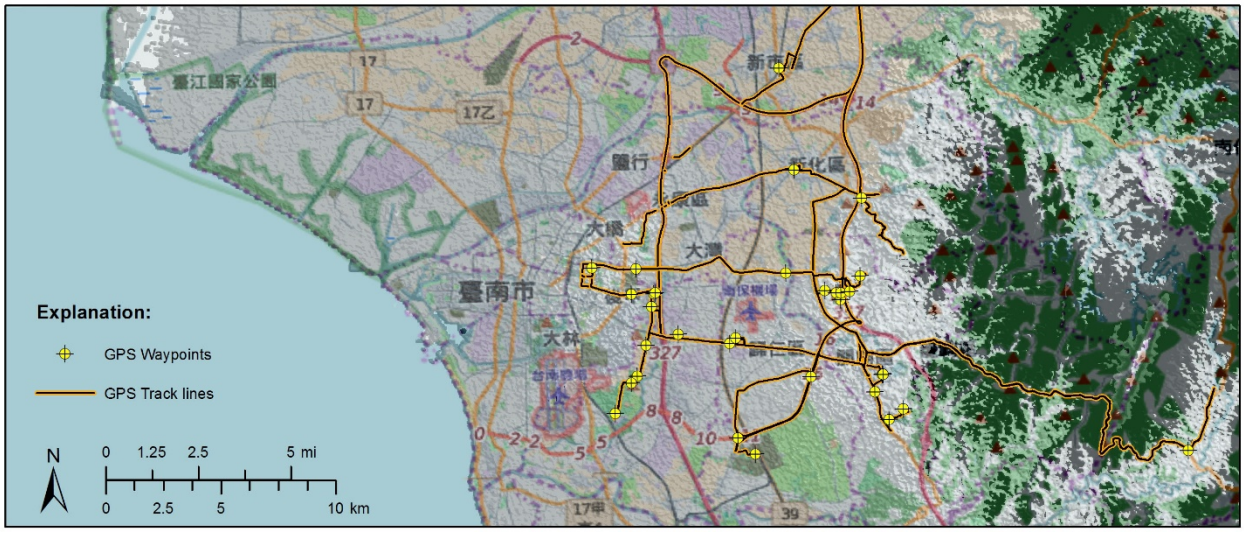

Figure 2-10: GEER Geology Team Track Log and Waypoint Location Map.

A sharp N-S trending displacement lineament separating the area of uplift (Guanmiao Hills) and the down-dropped Guanmiao Valley shows up very clearly on the InSAR imagery. This sharp displacement lineament appears to delineate a west-dipping, N-S trending fault along the western margin of the Guanmiao Valley, now referred to as the Guanmiao Fault. Existing geologic maps indicate synclinal folding is present in the Guanmiao Valley (CGS, 2005) and Prof. C.T. Lee of National Central University, has discussed a possible fault in this location but no published evidence of faulting has been previously mapped along this sharp displacement lineament that moved during the 2016 Meinong earthquake.

Several days were spent inspecting this lineament and mapping the structure of the hills to the west that are shown to have uplifted during the recent Meinong EQ. As part of our field reconnaissance we collected aerial imagery from two unmanned aerial vehicles (U.A.V. or drones) along approximately 4-5 km of this lineament north of Hwy 3 between Guanmiao and Xinhua. This imagery allowed us to create a 3-D digital elevation model (DEM) to more accurately examine the geomorphic characteristics along this sharp lineament.

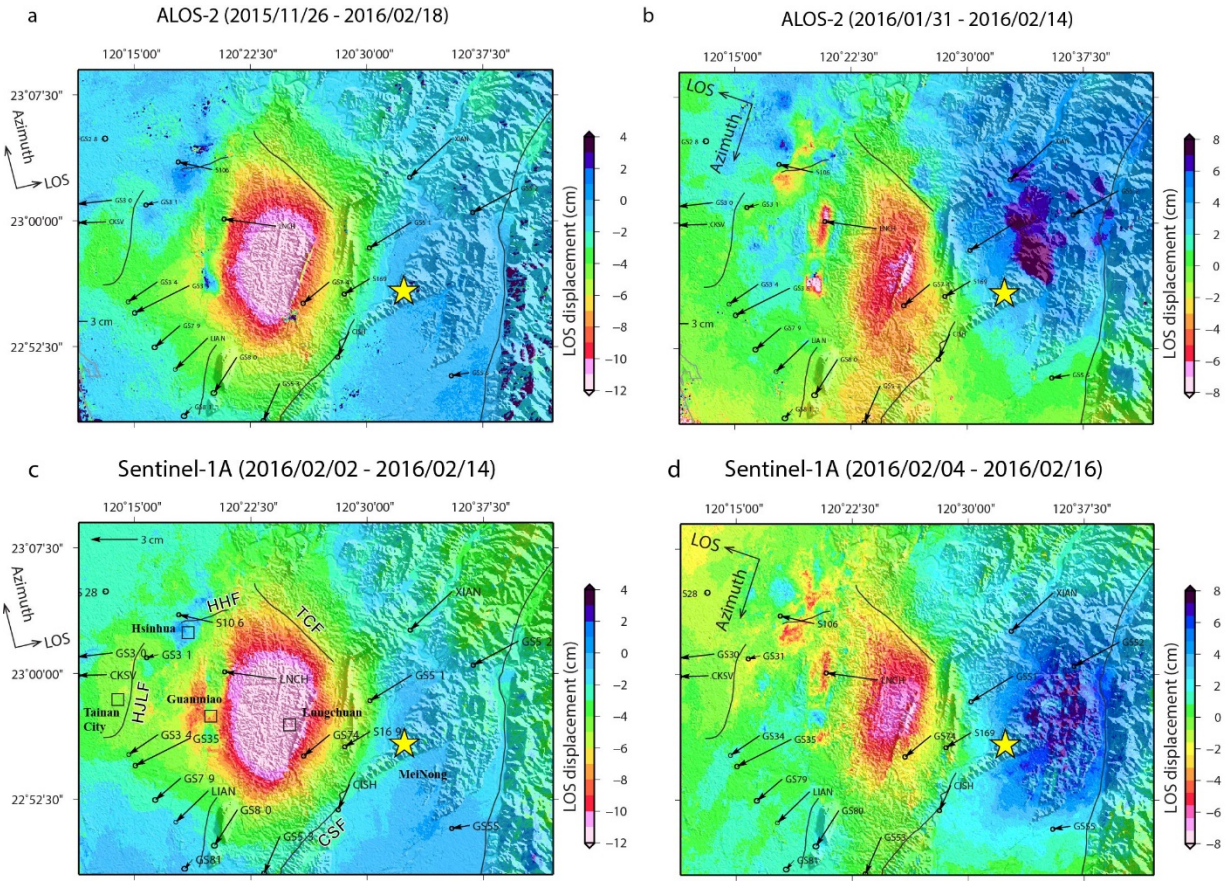

Figure 2-11: InSAR data of the 2016 Meinong earthquake region showing regions of vertical uplift (red/white) and settlement (blue) and lateral displacement vectors (courtesy of C. Liang and M. H. Huang and JPL-Caltech Advanced Rapid Imaging and Analysis [ARIA] project); Original ALOS-2 data are copyright by Japanese Aerospace Exploration Agency (JAXA); the Sentinel-1 images contain Copernicus data.

A transect of the Guanmiao Hills indicate that the bedrock structure of the hills to the immediate west of the lineament are comprised of several parallel N-S trending ridges and valleys that are controlled by folding. This relatively tight fold structure appears to terminate along a N-S trending linear geomorphic escarpment on the eastern side of these hills at the proposed Guanmiao fault and the Guanmiao Valley (Figures 2-14 and 2-15). This strong geomorphic lineament (scarp) is aligned with the InSAR displacement lineament and supports the interpretation that the sharp displacement lineament observed on the InSAR data is fault rather than fold related (Figure 2-12 and 2-15). Our field reconnaissance also located two fresh line cracks that cross the width of a roadway along and parallel to the Guanmiao fault scarp near Xinhua (Figure 2-16). However, these fault coincident cracks could be related to shaking and are not definitive evidence of fault displacement. No conclusive evidence of surface rupture from the Meinong earthquake was evident nor was any reported along any geologic structures in southwest Taiwan.

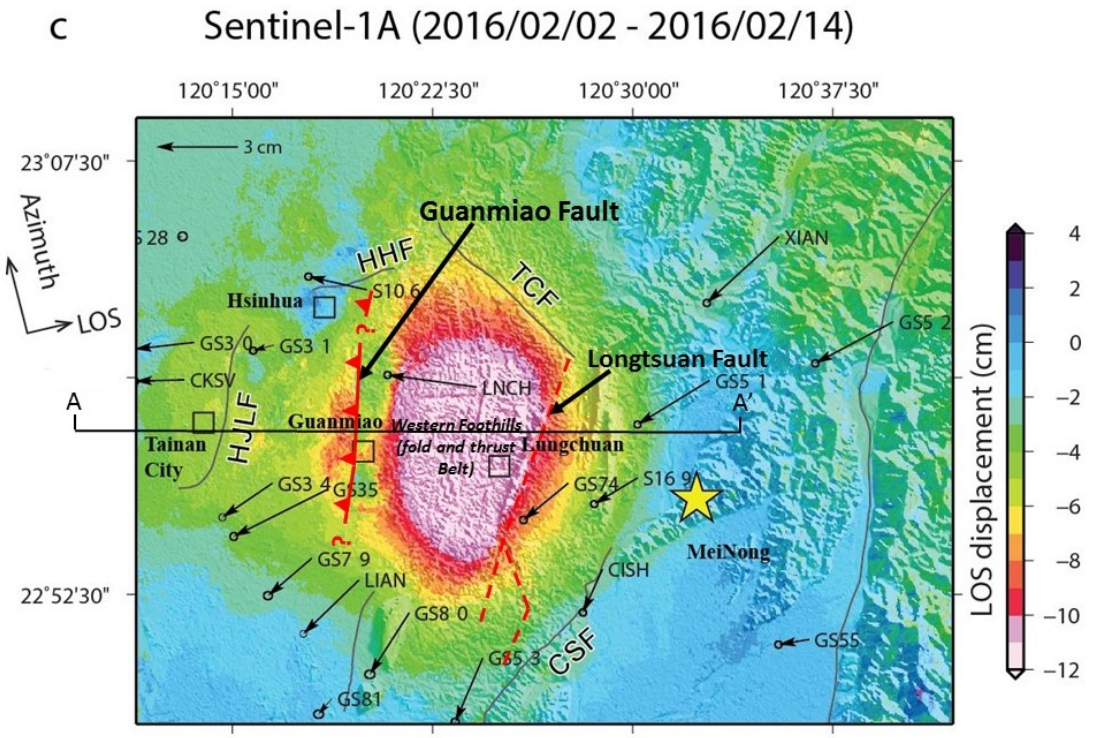

Figure 2-12: Interpreted InSAR image showing the Guanmiao fault and uplift of the Western Foothills Fold and Thrust Belt; See Figure 2-13 for cross section (courtesy of M. H. Huang and JPL-Caltech Advanced Rapid Imaging and Analysis [ARIA] project); the Sentinel-1 image contain Copernicus data.

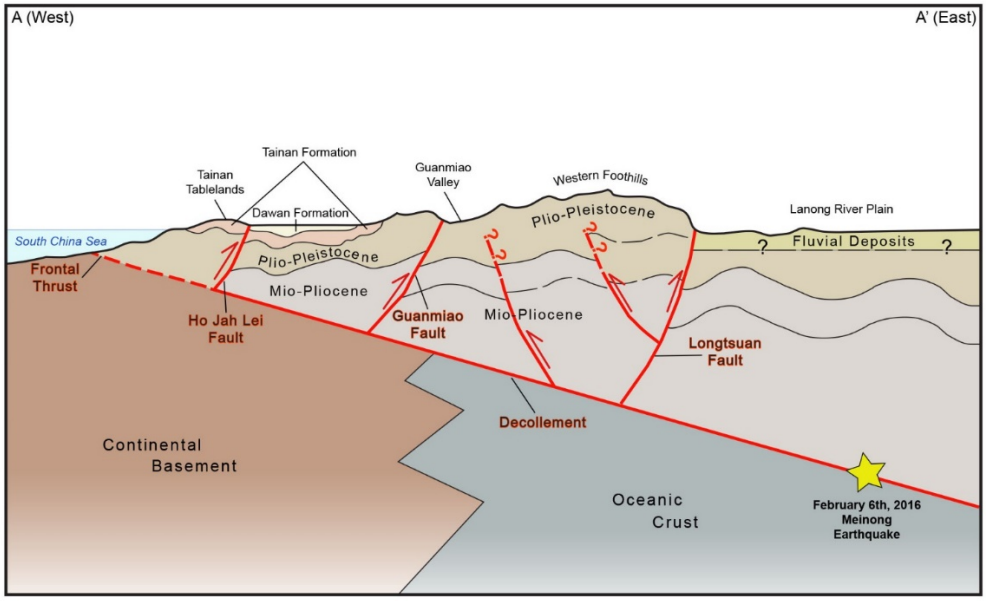

Figure 2-13: Schematic cross section, E-W across southern Taiwan (See Figure 2-12 for cross section location).

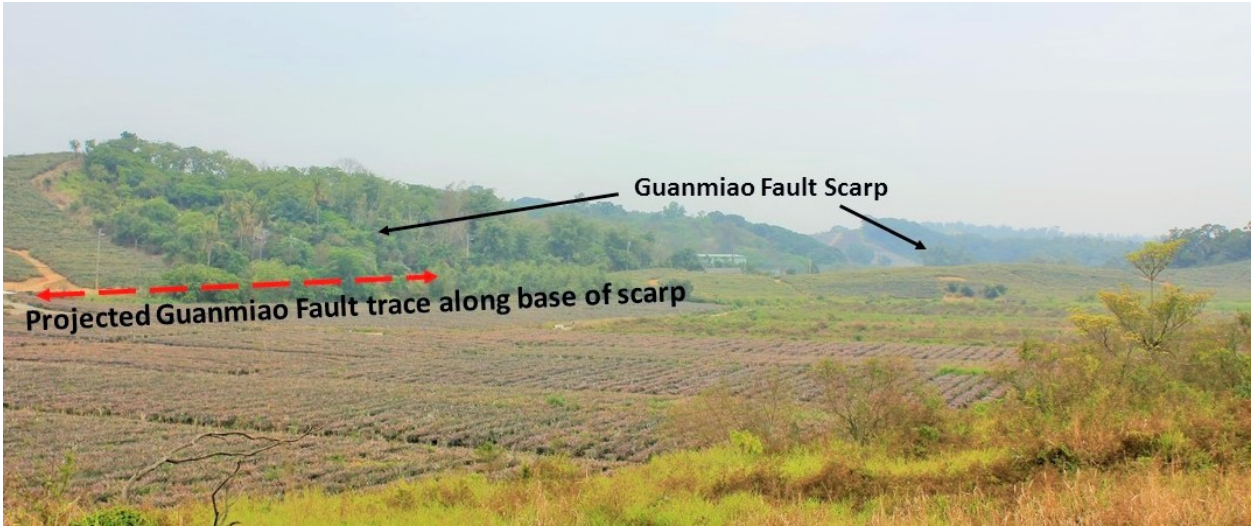

Figure 2-14: View to the northwest of the N-S trending linear Guanmiao Fault scarp (Lat. 22° 59' 41.69" N; Long. 120° 19' 40.98" E).

In Chapter 3 we discuss the complex nature of the seismology of the Meinong earthquake. More work is still required but potentially there may be supporting evidence that uplift along the Guanmiao fault may have occurred as part of a triggered slip event from either the mainshock of the 2016 Meinong earthquake or a possible second event that occurred seconds later and appears to be more closely located near the Guanmiao fault at depth. Movement along the west dipping Guanmiao fault would place part of Tainan (the eastern area comprised of the Dawan lowlands) on the hanging wall (Figure 2-13). In theory, this potential second event and movement along the Guanmiao fault may help to also explain the increased levels of earthquake effects and damage in Tainan City.

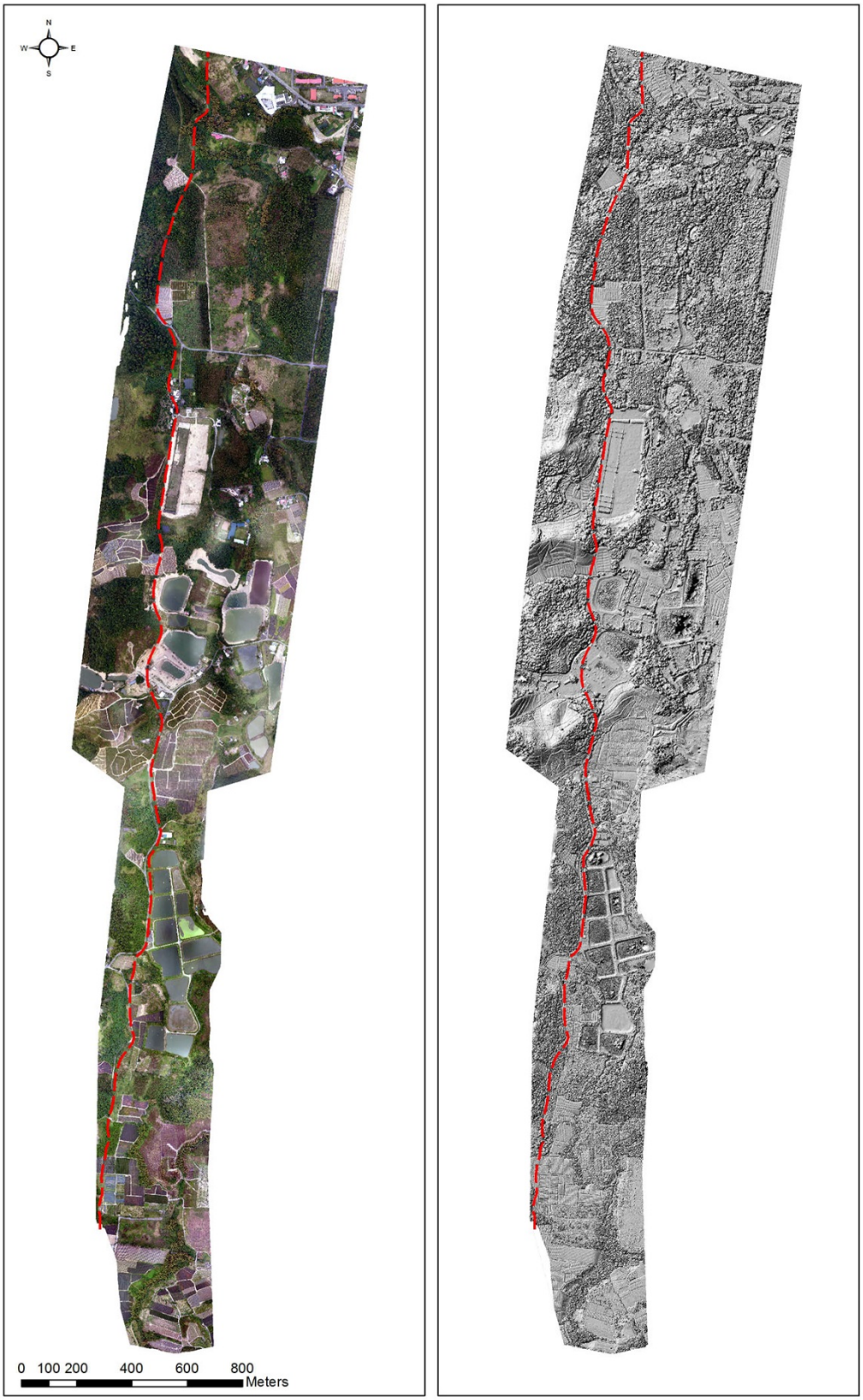

Figure 2-15: Orthophoto mosaic (left) and DEM imagery collected from UAV photographs along the Guanmiao Fault (shown in red) between Guanmiao and Xinhua, Taiwan.

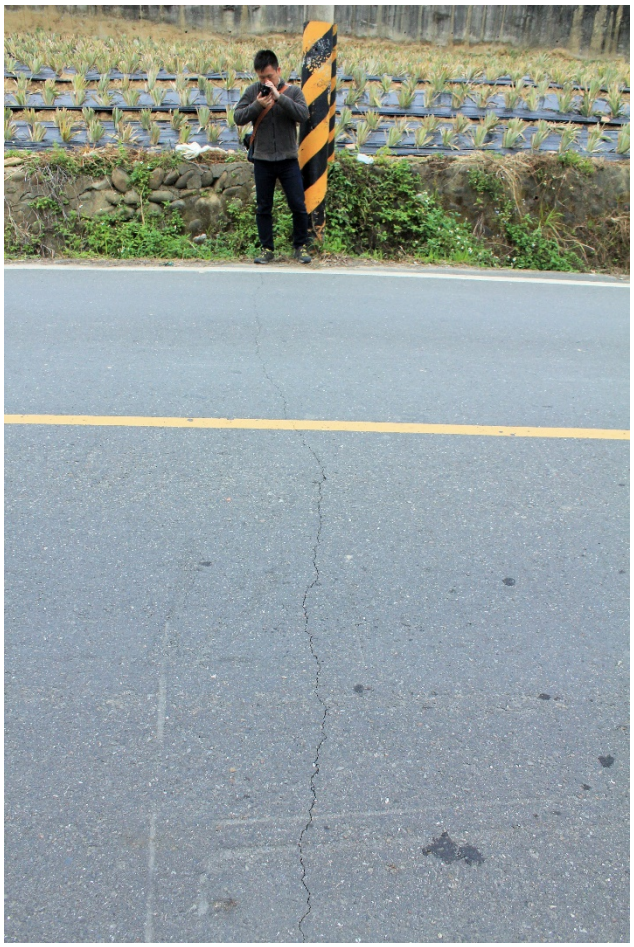

Figure 2-16: View to the north along one of two fresh line cracks within a roadway near Xinhua. The crack is parallel to and aligned with the mapped projection of the Guanmiao Fault but is not conclusive evidence for surface rupture (Lat. 23° 01' 28.30''N; Long. 120° 19' 40.87" E).

3. SEISMOLOGICAL INFORMATION AND RECORDED GROUND MOTIONS

3.1 Historical and Recent Earthquakes

Since 2000, 12 $M_L \geq 6.0$ earthquakes have occurred beneath the island of Taiwan, including this recent 6 February 2016 M_L=6.4 Meinong earthquake (Figure 3-1 and Table 3-1). The recent Meinong earthquake produced significant damage to nearby cities, especially when compared to other $M_L \geq 6.0$ inland earthquakes, which typically produced only minor damage. Table 3-1 lists the properties of the 12 $M_L \geq 6.0$ earthquakes which vary from M_L6.2 to M_L6.7. Most of these earthquakes occurred at moderate depths ranging between 12 and 27 km and all of these earthquakes were not associated with any previously known active faults and ruptured along 'blind' faults that did not reach the ground surface. The 4 March 2010 M_L=6.4 Jiashan earthquake was very similar in location, size, and focal mechanism to the Meinong earthquake. The Jiashan earthquake ruptured from the southeast to northwest along a northeastern dipping blind fault plane (Lee et al., 2013, and Hsieh et al., 2014). In addition to the 2010 Jiashan earthquake, two other distinct earthquakes are the Nantou earthquakes in 2013 with M_L=6.2 and M_L=6.5, respectively, in Central Taiwan.

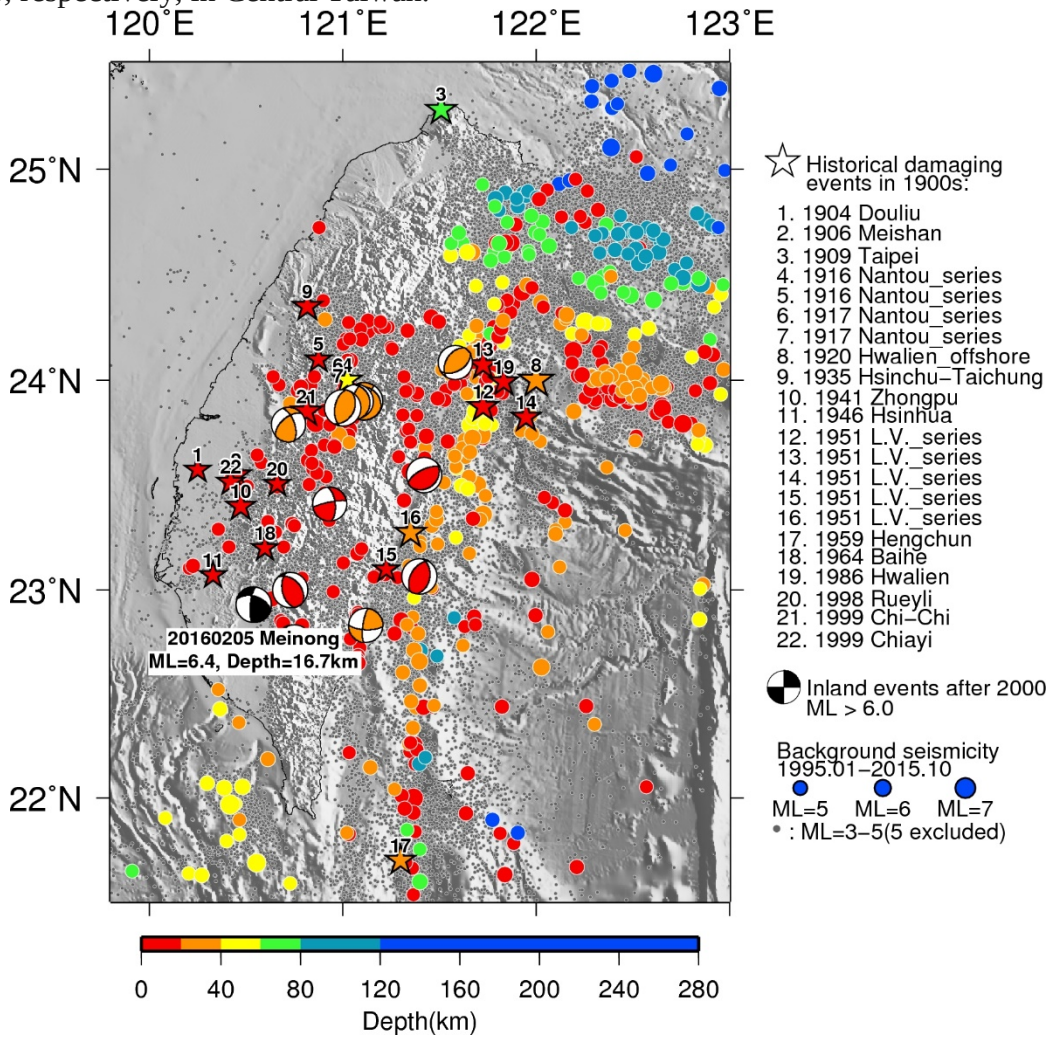

Figure 3-1: Historically damaging earthquakes and selected seismicity of Taiwan.

Table 3.1 M_L>=6.0 inland events after year 2000 (CWB location, and BATS depth and focal mechanism)										
Event date	Time (UTC+8)	Lon.	Lat.	Dep. (km)	M_L (CWB)	M_W (BATS) (*gCMT)	Strke	Dip	Rake	Note
2000/06/11	02:23:29	23.901	121.109	27	6.7	6.07	296.4	24.33	-7.8	
2000/07/29	04:28:08	23.411	120.933	12	6.1	5.65	354	62.89	10.9	
2000/09/10	16:54:46	24.0853	121.584	26	6.2	5.7	213.3	44.67	70.6	
2003/12/10	12:38:14	23.0667	121.398	18	6.4	6.58	8.82	42.16	72.8	Chengkong earthquake
2006/04/01	18:02:19	22.830	121.120	22	6.2	6.05	92.4	70.18	165	
2009/11/05	17:32:53	23.79	120.72	22	6.2	5.6*	229.51	56.74	144.6	
2010/03/04	08:18:53	23.000	120.730	18	6.4	6.3*	318.1	41.39	67.6	Jianshan earthquake
2012/02/26	10:35:00	22.75	120.75	15	6.4	5.9*	161.12	36.65	114.1	Wutai earthquake
2013/03/27	10:03:20	23.900	121.070	20	6.2	5.54	344.4	22.51	61.8	Nantou earthquake
2013/06/02	13:43:04	23.870	121.000	23	6.5	5.73	29.75	36.86	106	Nantou earthquake
2013/10/31	20:02:09	23.550	121.420	17	6.4	5.81	49.25	25.7	77.3	Ruisui earthquake
2016/02/06	03:57:27	22.930	120.540	16	6.4	6.3	288.4	51.02	19.8	Meinong earthquake

*BATS Mw systematic bias by about 0.4 from 2009-2012 (Wen-Tzong Liang, personal communication)

Table 3-1: $M \geq 6.0$ earthquakes (inland) post-2000 C.E.

Historically, there have been 22 damaging earthquakes in Taiwan during the last century as shown in Figure 3-1. These damaging earthquakes brought some unfortunate casualties to human lives. The most destructive have been the 21 April 1935 M=7.1 Hsinchu-Taichung earthquake and the 21 September 1999 M=7.3 Chi-Chi earthquake, which resulted in more than 3200 and 2400 deaths, respectively (Table 3-2). These historically damaging earthquakes occurred primarily at relatively shallow depths, and were mostly associated with active faults that ruptured the ground surface. The frequency of historically deadly and damaging earthquakes is nearly 2 per decade with most of these damaging earthquakes located in central western and eastern Taiwan.

The majority of the historical earthquakes since 1900, that have caused significant damage and casualties, are mostly located across central Taiwan where the Philippine and Eurasian plates are actively colliding and the geologic structures that nucleate these earthquakes are more mature and typically are expressed at the ground surface. As described in Chapter 2 (and shown in Figure 2-3), active collision of the Philippine and Eurasian plates has migrated from the north, approximately 5 mya, to the south of Taiwan where collision is incipient and relatively young. The $M_L \geq 6.0$ earthquakes (Fig. 3-1) that are occurring in southwest Taiwan are typically located on developing faults that may not reach the ground surface but are often manifested as folds that uplift of the ground surface as part of the western fold and thrust belt.

Table 3.2 Historical damaging earthquakes in 1900s											
No.	Evt. Name	Year	Month	Day	Time(UTC+8)	Lat.	Lon.	Dep.	Mag.	Death	Injury
1	Douliu	1904	11	6	04:25	23.575	120.25	7	6.1	145	157
2	Meishan	1906	3	17	06:43	23.55	120.45	6	7.1	1258	2385
3	Taipei	1909	4	14	03:53	25.28	121.51	75	7.3	9	51
4	Nantou_series	1916	8	28	15:27	24	121.025	45	6.8	16	159
5	Nantou_series	1916	11	15	06:31	24.1	120.875	3	6.2	1	20
6	Nantou_series	1917	1	5	00:55	24	120.975	Very shallow	6.2	53	106
7	Nantou_series	1917	1	7	02:08	23.95	120.975	Very shallow	5.5	0	21
8	Hwalien_offshore	1920	6	5	12:21	24	122	20	8.3	5	20
9	Hsinchu-Taichung	1935	4	21	06:02	24.35	120.817	5	7.1	3279	12119
10	Zhongpu	1941	12	17	03:19	23.4	120.475	12	7.1	360	729
11	Hsinhua	1946	12	5	06:47	23.07	120.33	5	6.1	74	474
12	L.V._series	1951	10	22	05:34	23.875	121.725	4	7.3	68	856
13	L.V._series	1951	10	22	11:29	24.075	121.725	1	7.1		
14	L.V._series	1951	10	22	13:43	23.825	121.95	18	7.1		
15	L.V._series	1951	11	25	02:47	23.1	121.225	16	6.1	17	326
16	L.V._series	1951	11	25	02:50	23.275	121.35	36	7.3		
17	Hengchun	1959	8	15	16:57	21.7	121.3	20	7.1	17	68
18	Baihe	1964	1	18	20:04	23.2	120.6	18	6.3	106	650
19	Hwalien	1986	11	15	05:20	23.992	121.833	15	6.8	15	62
20	Rueyli	1998	7	17	12:51	23.508	120.661	6	6.2	5	28
21	Chi-Chi	1999	9	21	01:47	23.852	120.816	8	7.3	2444	10002
22	Chiayi	1999	10	22	10:19	23.517	120.423	16.6	6.4	0	254
Report from Central Weather Bureau:											
Report 1:	http://scman.cwb.gov.tw/eqv5/research/21vol/MOTC-CWB-87-E-11.pdf										
Report 2:	http://scman.cwb.gov.tw/eqv5/research/39vol/MOTC-CWB-93-E-15.pdf										

Table 3-2: Historically damaging earthquakes in the 1900's.

3.2 Regional seismicity and recorded earthquakes

Statistically, Taiwan experiences about 600 M>3.0 earthquakes every year, among that, about 20 earthquakes with M>5.0. Most of the earthquakes that occur in the east and northeast of Taiwan are associated with the collision of the Philippine Sea plate and Eurasian plate and the Ryukyu subduction system. Figure 3-1 also shows the distribution of the M_L >5.0 earthquake since 1995 with the background seismicity of M_L >3.0. Since the deployment of the Central Weather Bureau Taiwan Seismic Network (CWBSN), and Broadband Array in Taiwan for Seismology (BATS) by the Institute of Earth Sciences, Academia Sinica since 1993, the earthquake catalog has a complete magnitude of Mc=2, and automatic determination of earthquake focal mechanism from centroid moment tensor (CMT) by BATS. In addition to the seismic network, a Taiwan Strong Motion Implementation Program (TSMIP) was also established in year 1993 to provide near real-time strong motion shaking and intensity map of a felt quake. Fig. 3-2 shows the distribution of the seismic network in Taiwan along with GPS and strainmeter stations.

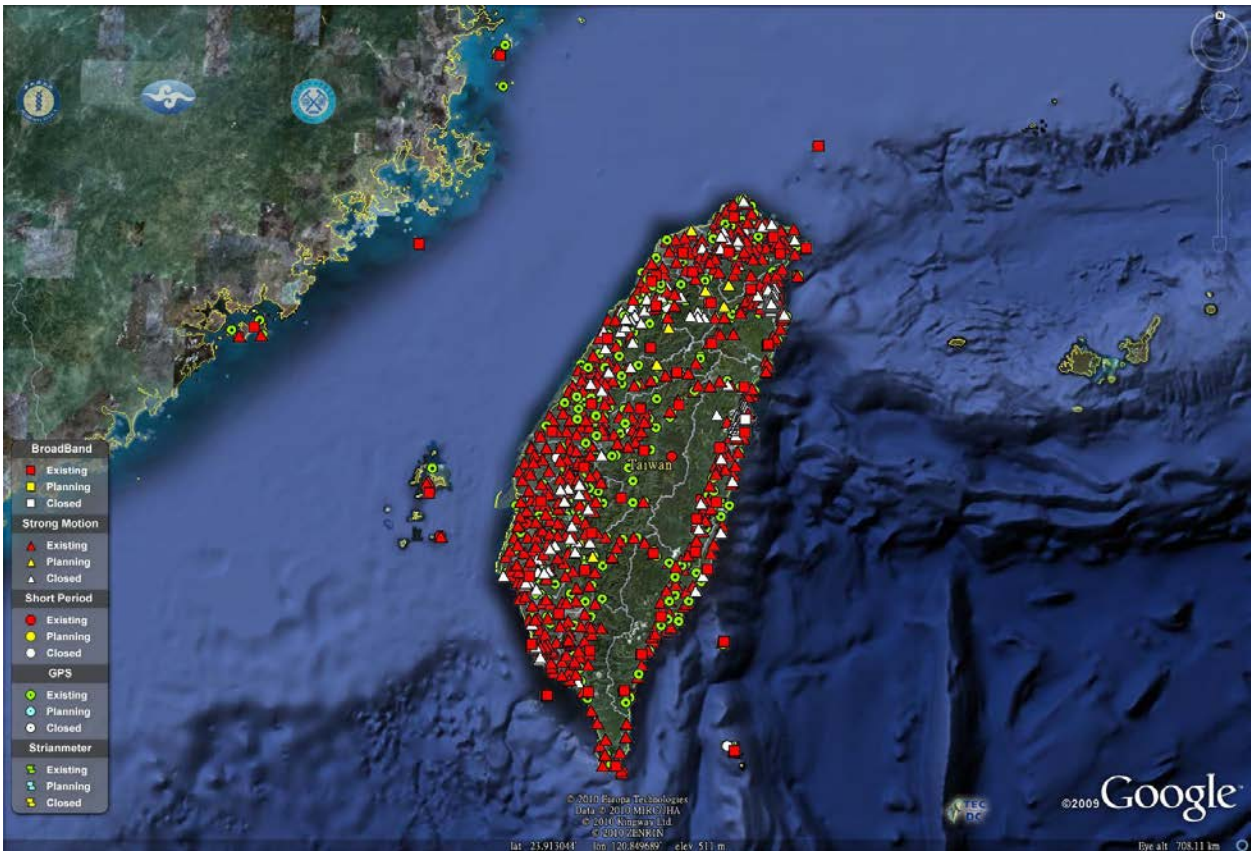

Figure 3-2: Taiwan strong motion, broadband, GPS, and strainmeter station locations

3.3 Recorded Ground Motions (PGA contour or Intensity)

Figure 3-3 shows the Intensity map from Central Weather Bureau and PGA distribution of the Meinong earthquake from the real-time strong motion network. About 1/3 of Taiwan experienced an intensity V shaking, which was scaled with a PGA of 80 to 250 gal. A noted feature for this earthquake is a long period velocity pulse that was observed in many stations near Tainan. Figure 3-4 shows the velocity waveforms of station W21B of P alert station. The long period velocity pulse is distinct with a large PGV of about 1 m/sec. P alert is the instrument implemented for earthquake early warning (EEW). The instrument is not on a free-field, but, mainly installed on the 1st or 2nd floor of elementary schools (Wu et al., 2013). These stations performed very well during the earthquake to provide an instant temporal shaking map[2]. Despite the non-free field and low cost of P alert stations, the stations provide instant real-time records to give the first glimpse of the waveforms as the observation of the 1-sec velocity pulse, which might be the main cause of the damage in Tainan.

[2] See: http://palert.earth.sinica.edu.tw/palert_media/gif/2016/20160205195727_1.gif

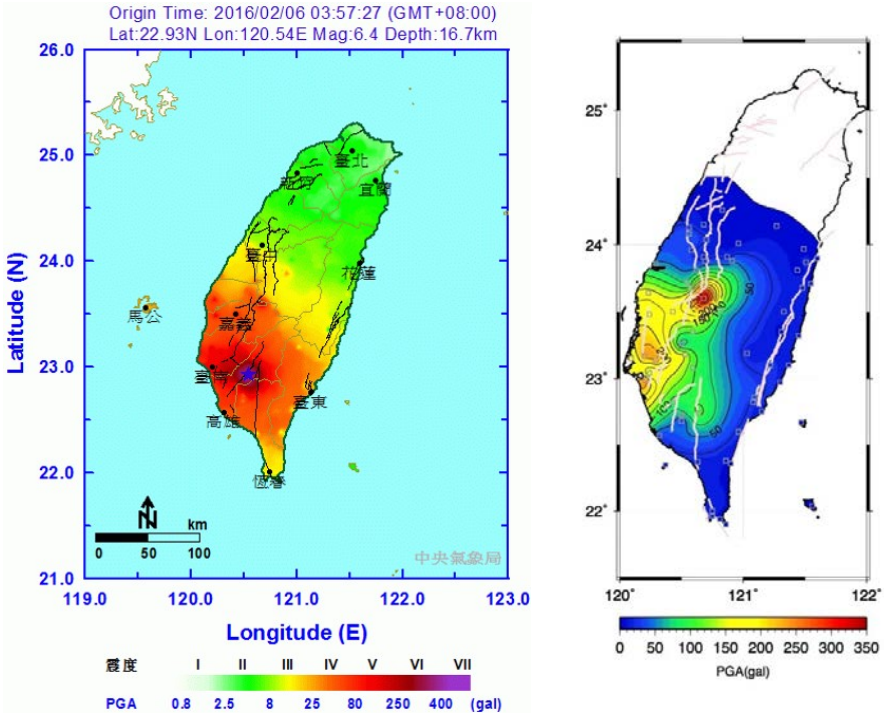

Figure 3-3: Intensity map from Central Weather Bureau and PGA contours from real-time strong motion stations

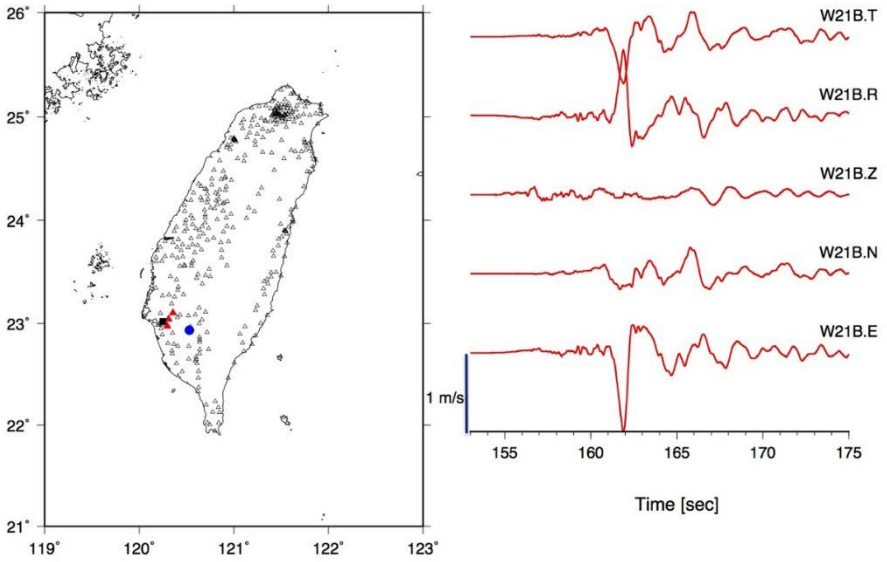

Figure 3-4: Earthquake Early Warning (EEW), P alert instrument and station distribution, and the velocity waveforms at station W21B. Please note that the polarity of P alert waveform needs further calibration (Yih-Ming Wu, personal communication).

3.4 Focal mechanism, Rupture direction and aftershocks

The focal mechanism determined from different agencies and different methods are shown in Figure 3-5. The focal mechanism is quite consistent with similar mechanisms between the different agencies. The focal mechanism is mainly a strike-slip with an oblique thrust component. The BATS solution is as strike=288.4, dip=51.02, and rake=19.8. The methods in determination of the focal mechanisms are described through BATS quick CMTs (http://bats.earth.sinica.edu.tw/Quick_CMT/cmtQ.html), cut and paste method of gCap solution (http://tecdc.earth.sinica.edu.tw/gcap/index_main.php), and real-time moment tensor (RMT) (http://rmt.earth.sinica.edu.tw/, Lee et al., 2013).

From the temporal shaking map of P alert, and first couple hours of the aftershocks distribution, the earthquake was identified as a rupture from east to west direction as seen from the real-time shaking map. However, this earthquake has not yet been clearly resolved due to its source complexity as well as the wide spread clusters of aftershocks. Figure 3-6 shows the aftershock distribution for nearly 120 hours after the mainshock. The aftershocks were clustered in two zones. One cluster gathered close to the epicenter, the other cluster located about 25 km west of the mainshock. A further extension to the north of the first cluster appeared several days after the mainshock. Figure 3-6 also shows the profiles across the aftershock clusters, the profiles actually show little consistency to the mainshock focal mechanism. The profile A-A' shows two distinct clusters of aftershocks. The aftershock cluster to the west of the mainshock tends to be at a deeper depth of around 20-30 km, while the first cluster, close to the mainshock, is around the depth of 10-20km and closer to the mainshock. The vertical profile C-C' across the mainshock shows a near-vertical distribution of the aftershocks rather than the northern dipping feature suggested from the western rupture direction from the EW strike focal mechanism. The northern cluster shows the aftershocks are at shallower depths comparing to other clusters. The vertical profile B-B' across the western cluster shows a gathered cluster without clear dipping, the near EW profile from A-A' in the section across the western cluster shows a possible tendency of the aftershocks along a plane dipping to the west.

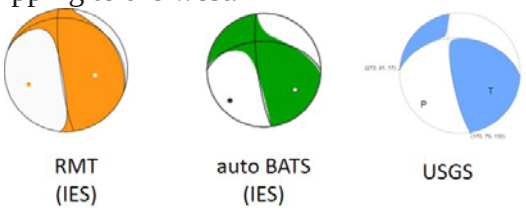

Source	Depth	Magnitude
CWB	16.7km	ML=6.4
RMT	22 km	Mw=6.2
Auto BATS	23 km	Mw=6.3
CWB CMT	26km	Mw=6.3
GCAP	22km	Mw=6.3
USGS	20km	Mwb=6.2

Figure 3-5: Focal mechanism solutions from different agencies and methods (http://tesis.earth.sinica.edu.tw, http://earthquake.usgs.gov).

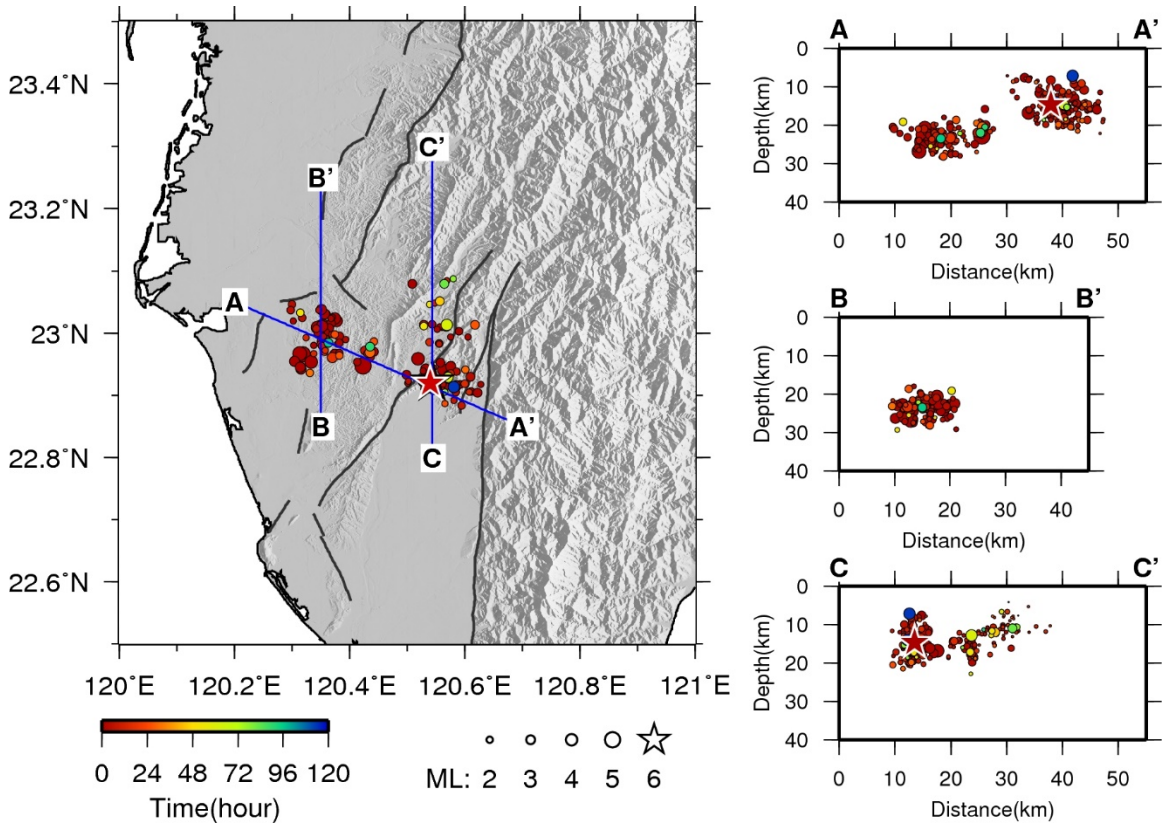

Figure 3-6: Aftershocks distributions and associated profiles

These complex distributions of the aftershocks along with the observed long period velocity pulse, which brought the damage to Tainan region, suggest this earthquake might have resulted from a complex earthquake mechanism rather than a more typical Mw 6.3 earthquake. Current studies suggest that this earthquake might start with a relative smaller event (asperity) following by a larger event (asperity) to the east of the Tainan region and with a rupture toward the northwest. The large PGA and PGV velocity pulse observed in Tainan region are mainly caused by this source mechanism with directivity effect. Further studies from teleseismic waveform analysis and source deconvolution from teleseismic to regional reveal another source time function about 20 sec after the mainshock. This event, immediately after the mainshock, may have a different focal mechanism than the previous two asperities. We suspect this unidentified event might be related to the distinct vertical deformation lineament observed in GPS and InSAR data near Guanmiao. This event may be related to a back-thrust (westerly dipping) mechanism or mud intrusion feature. However, more studies are still needed to understand the overall mechanism which should help to explain the observed deformation and ground effects.

4. GROUND RESPONSE FROM THE MEINONG EARTHQUAKE IN THE TAINAN AREA

Figure 4-1 shows the shaking intensity (Modified Mercalli Intensity Scale) estimated by USGS for this earthquake[3]. The highest intensity was VI, which occurred in Tainan City, about 40 km from the epicenter. A total of just over 50 free field ground motion instrumentation stations operated by Taiwan CWB were triggered by the earthquake with its locations and peak recorded values listed in Table (4-1).

Near the epicenter, five stations within a radius of 35 km from the epicenter recorded a PGA at or below 0.1g. The ground motion intensity increases to 0.24g in Tainan City, a local population center. The largest PGA recorded for this event was 0.35 g at Caoling located 72 km from the epicenter. Figure 4-2 shows the PGA contour map by USGS with the instrumentation stations shown as small triangles color-coded by intensity. In addition to the CWB's free field seismic stations, the National Center for Research in Earthquake Engineering (NCREE) has a less sophisticated real time early warning system (P alert), which also monitors ground motions in real time as described in Chapter 3. These sensors were usually mounted on simple structures and thus maybe do not truly represent the free field. Table 4-2 lists the NCREE P alert stations that recorded the Meinong earthquake. The highest recording from P alert was 0.41g at Nanhua site (A730) located 21.5 km form the epicenter. Figure 4-3 shows the estimated PGA, spectral acceleration (Sa) at 0.3 sec, and 1.0 sec from NCREE using both the CWA and P alert system with the gray circles representing the CWB stations and the black circles representing the NCREE stations. The USGS developed similar spectral acceleration maps. However, since NCREE used more stations in development of its maps, theirs is selected for this report.

The largest Peak Ground Velocity (PGV) of 35 cm/sec was also recorded at Caoling with the CWB sensors. Within Tainan City, the largest PGV recorded was just below 30 cm/sec. Most of the city experienced a PGV between 18 cm/sec and 22 cm/sec as shown in Figure 4-4. The PGA and PGV attenuation relationships, Figure 4-5 and Figure 4-6, respectively, were made in comparison to the Ground Motion Prediction Equation (GMPE) from a general understanding of the earthquake by USGS.

Figure 4-7 show the location of stations in the Tainan area along with their recorded PGA and PGV. This figure includes the highest recordings from NCREE at Nanhua (Station A730), which recorded a PGA of 0.41g. Figure 4-8 through Figure 4-12 show the recorded time histories and response spectra for some of the stations shown in Figure 4-7. It can be seen from Figure 4-12 that Nanhua station (A730) has a ground shaking duration of about 5 seconds and the peak spectral acceleration occurred at 0.2 to 0.3 seconds suggesting this is a rock site. In Tainan city (Figure 4-9), the strong ground shaking duration increased to 15 to 20 seconds likely due to site response. Note that the response spectra are showing a site period between 0.8 and 0.9 seconds. Jiali (Figure 4-

[3] See http://earthquake.usgs.gov/earthquakes/eventpage/us20004y6h#general_region

10) and Shanhua (Figure 4-11) both are on alluvial soils in Tainan City. Spectra from these recordings indicate a site period of about 0.6 seconds. At the Caoling site (Figure 4-8), the long distance from the epicenter caused most of the high frequency motions to be damped out. In addition, the duration of strong shaking at this site was short likely due to lack for near surface soil response.

It is also worthwhile to note that at most locations (except Jiali and Nanhua), the EW component of shaking is much stronger that the NS component especially in the 0.5 seconds to 1.5 second range in Tainan (Figure 4-9). The latter is close to the estimated period of one of the collapsed buildings from this event (Weiguan building); in this case the long axis of the building aligns with the NS direction and is located about 5km form this recording station. All of the records show a long period spectral peak at 0.7 seconds, regardless of the site condition and epicentral distance. This abnormal spectral peak may be related to the velocity pulse described in Chapter 3.

Due to the ground acceleration described above, the soil sites in Tainan city experienced significant shaking with PGAs ranging from about 0.15 to 0.2, and some slightly higher, with a ground shaking duration in excess of 15 seconds, which is higher than that expected of a Mw 6.3 earthquake. This ground motion excitation, the sandy native soil characteristics of this area, a high ground water table in this low lying area, and poor backfill practices associated with build activities over old fish ponds in the city over 30 years ago, all contributed to liquefaction that was observed in pockets of the City in this earthquake.

The sites that experienced liquefaction in the Meinong earthquake around Tainan can be grouped into three categories: (1) liquefaction developed in residential areas where ground liquefaction occurred in maturely developed sectors of the city, (2) liquefaction developed in open fields where surface manifestation is not obstructed by manmade improvements, and (3) liquefaction triggered lateral spreading along river banks. Description of categories (1) and (2) failures and performances are presented in Chapter 7, and liquefaction induced lateral spreading sites are covered in Chapter 8.

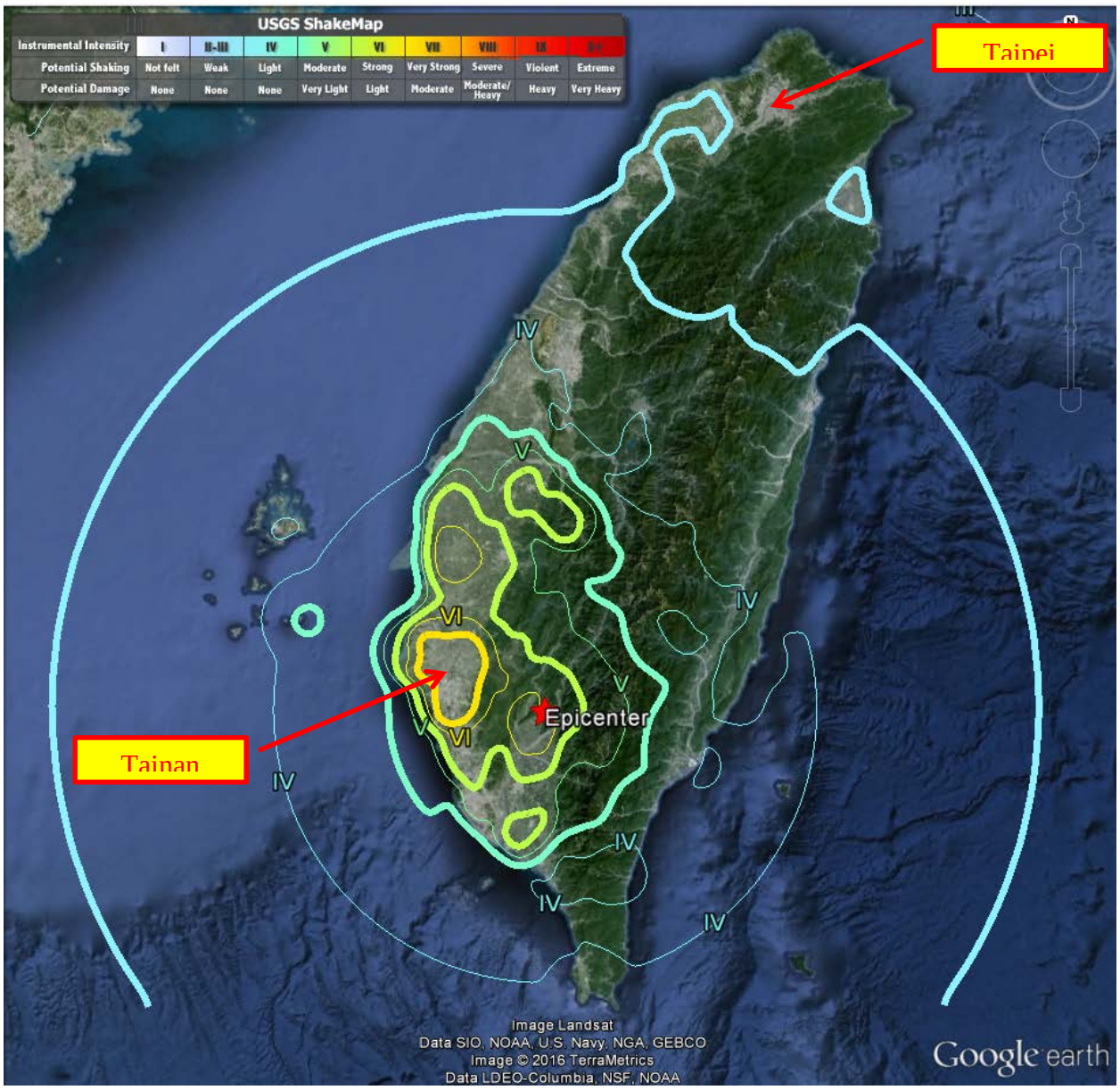

Figure 4-1: MMI Intensity from Meinong Earthquake (http://earthquake.usgs.gov/earthquakes/eventpage/us20004y6h#general_region).

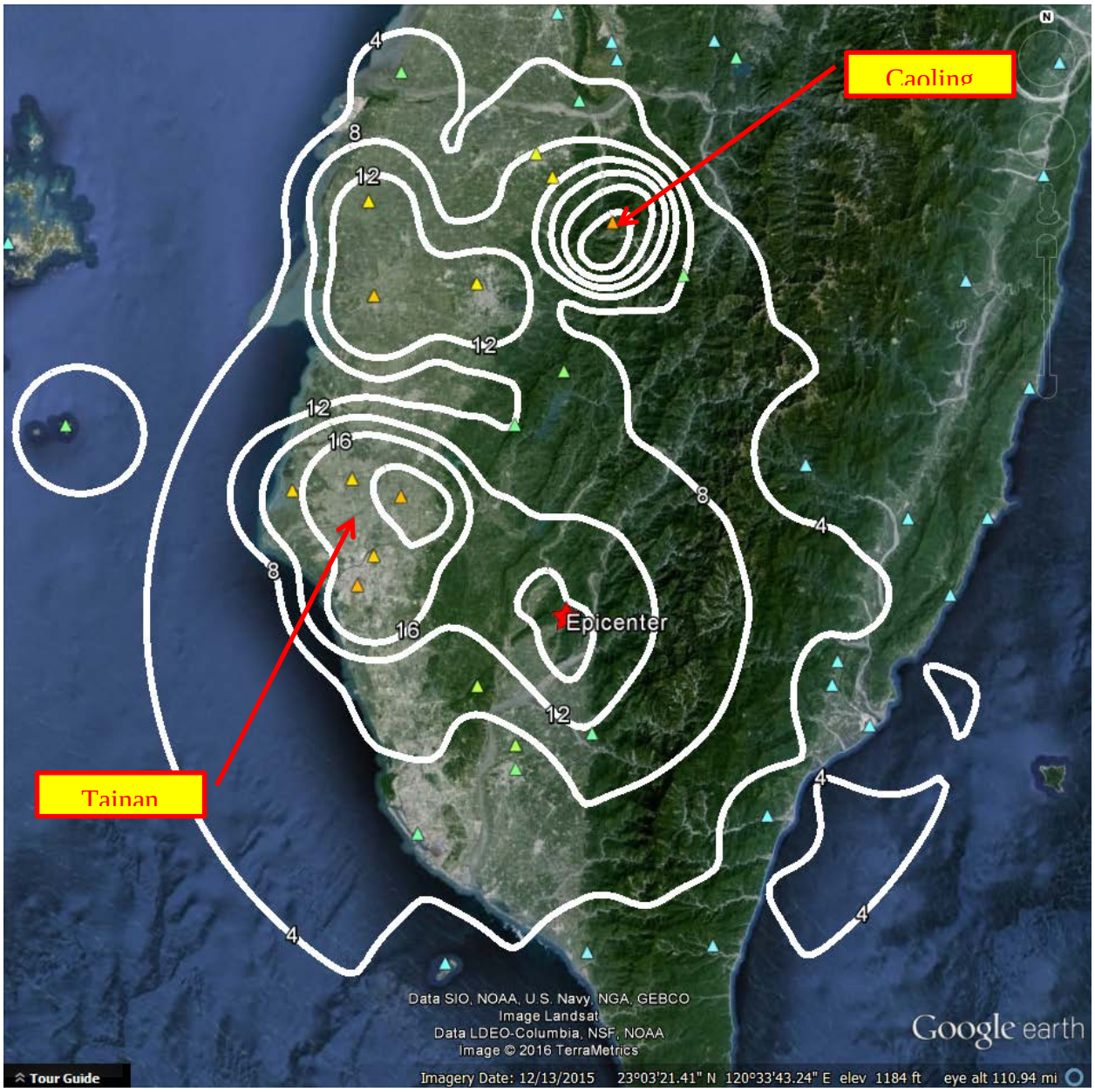

Figure 4-2: PGA (%g) estimated by USGS.
(http://earthquake.usgs.gov/earthquakes/eventpage/us20004y6h#general_region).

實測紀錄之地震動分佈圖

使用CWB 即時網測站與國震中心即時監測站

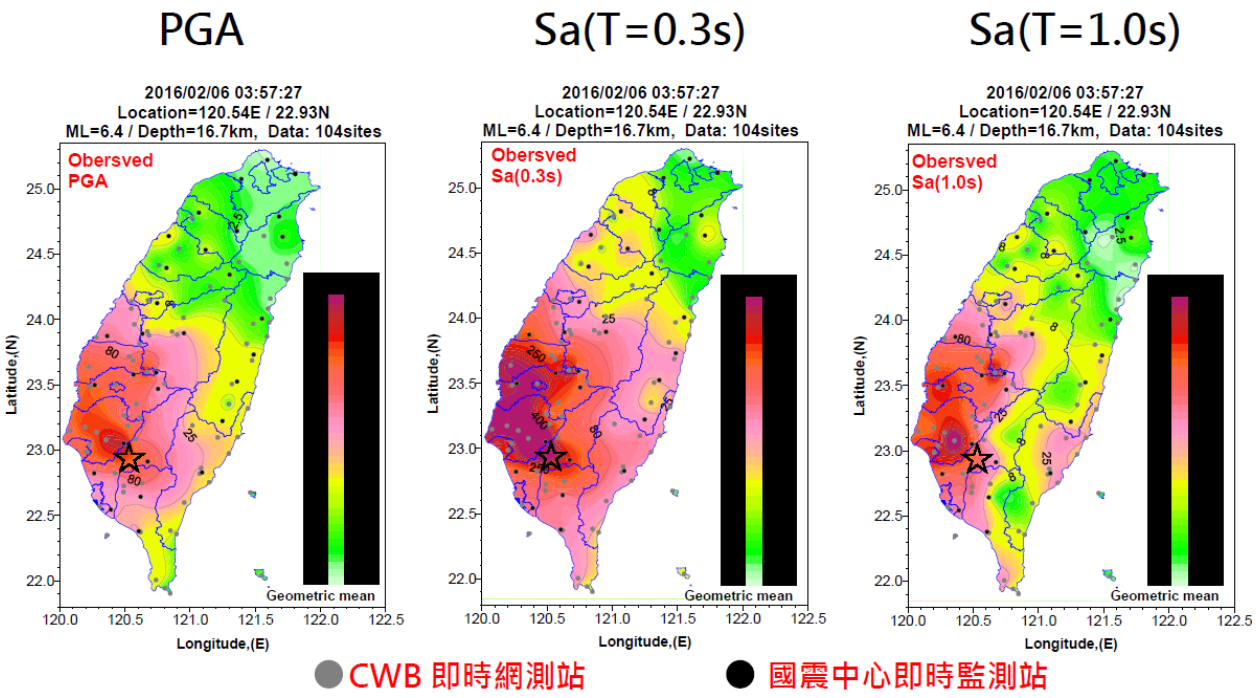

Figure 4-3: PGA and Spectral Acceleration Estimated by NCREE.

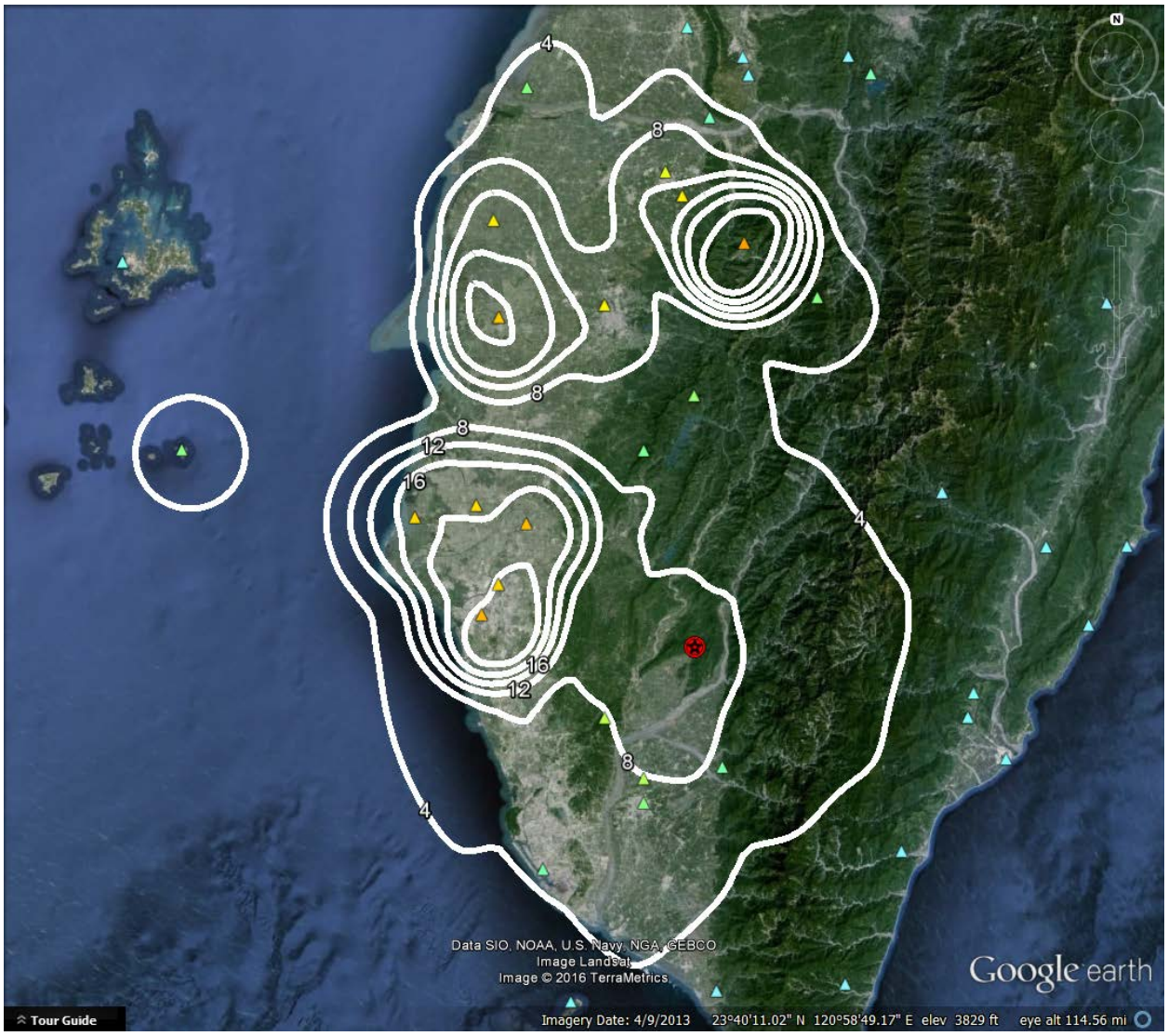

Figure 4-4: PGV (cm/sec) Estimated by USGS (http://earthquake.usgs.gov/earthquakes/eventpage/us20004y6h#general_region).

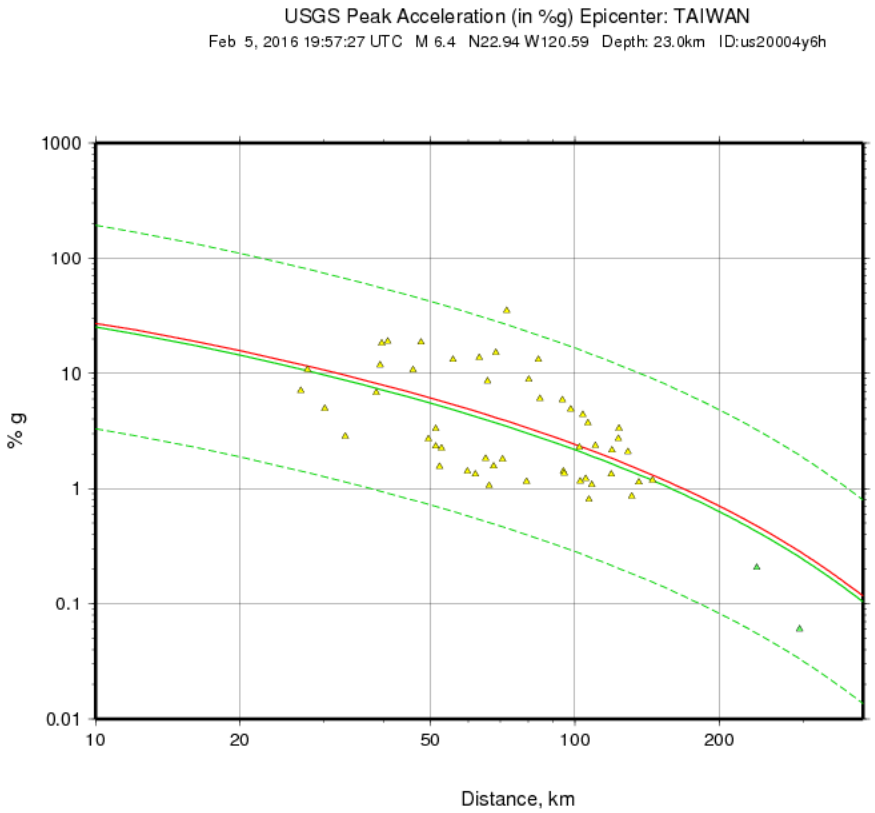

Figure 4-5: Attenuation of Peak Ground Acceleration (PGA) with Distance (from USGS).

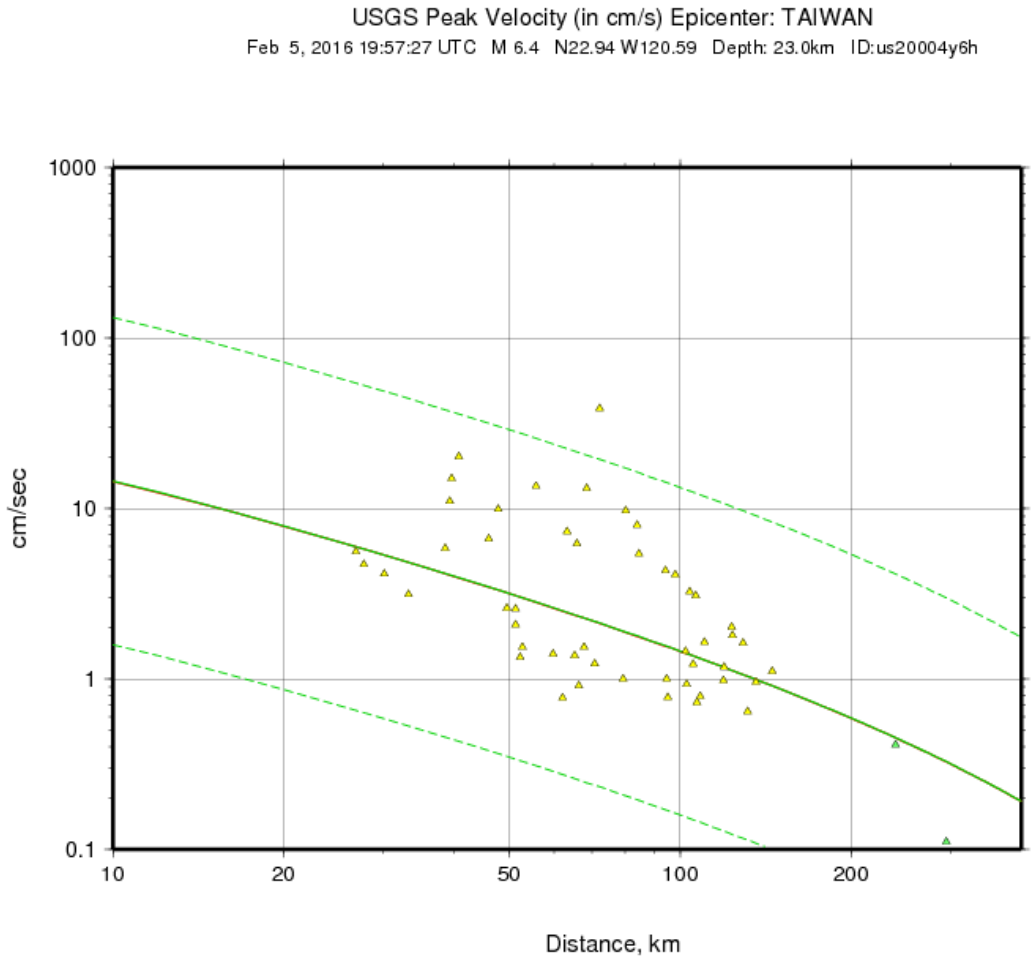

Figure 4-6: Attenuation of Peak Ground Velocity (PGV) with Distance (from USGS).

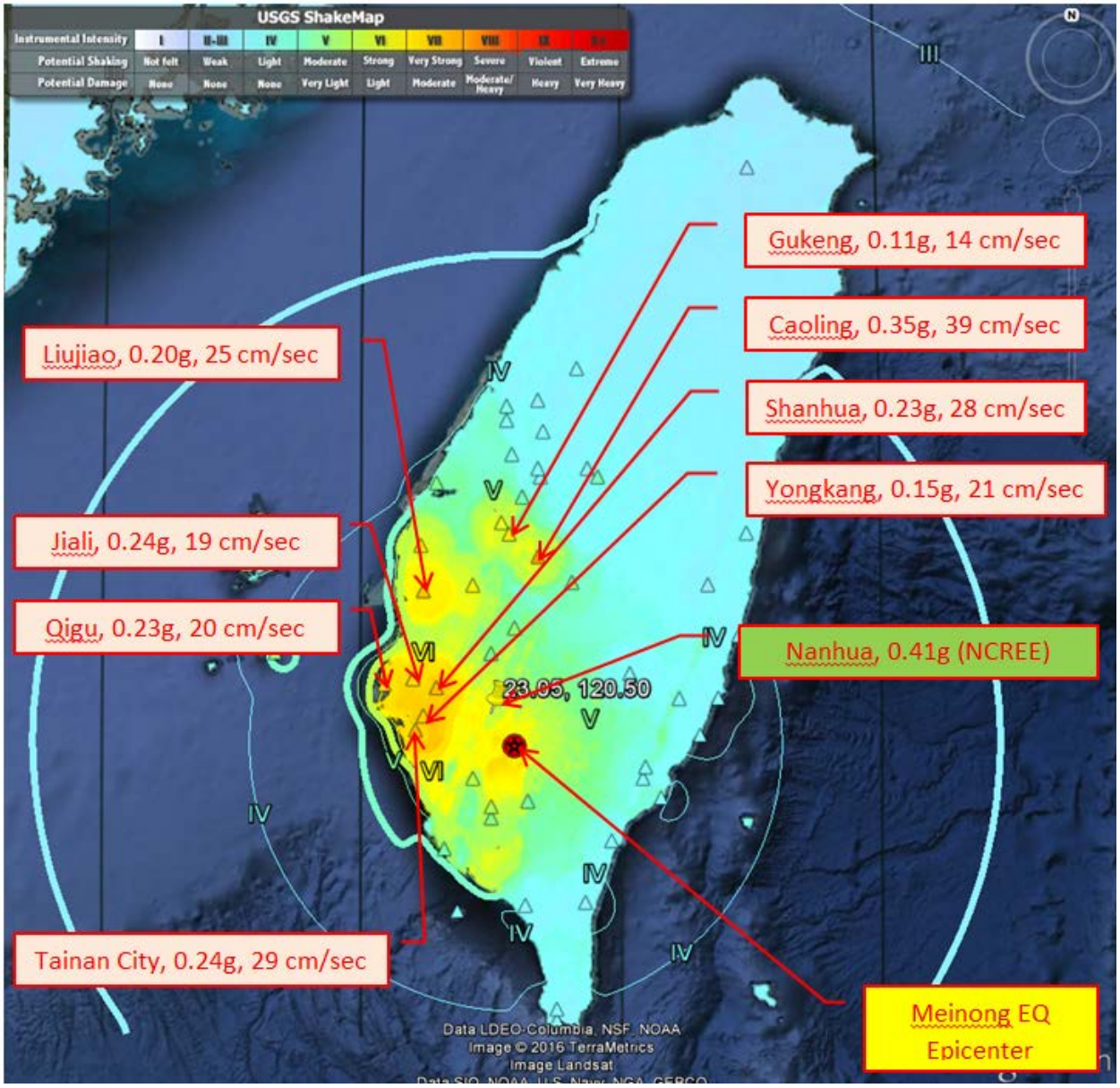

Figure 4-7: CWB and NCREE Stations in the Vicinity of Tainan (MMI Intensity in Background).

CHN5 (草嶺)

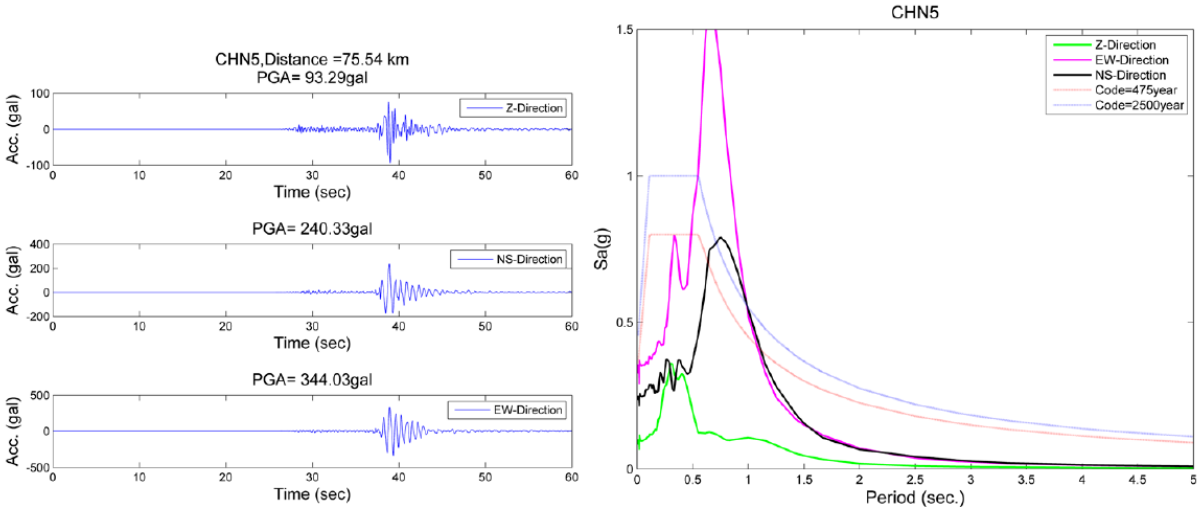

Figure 4-8: CWB Ground Motion Recorded in Caoling (from NCREE).

TAI (臺南市)

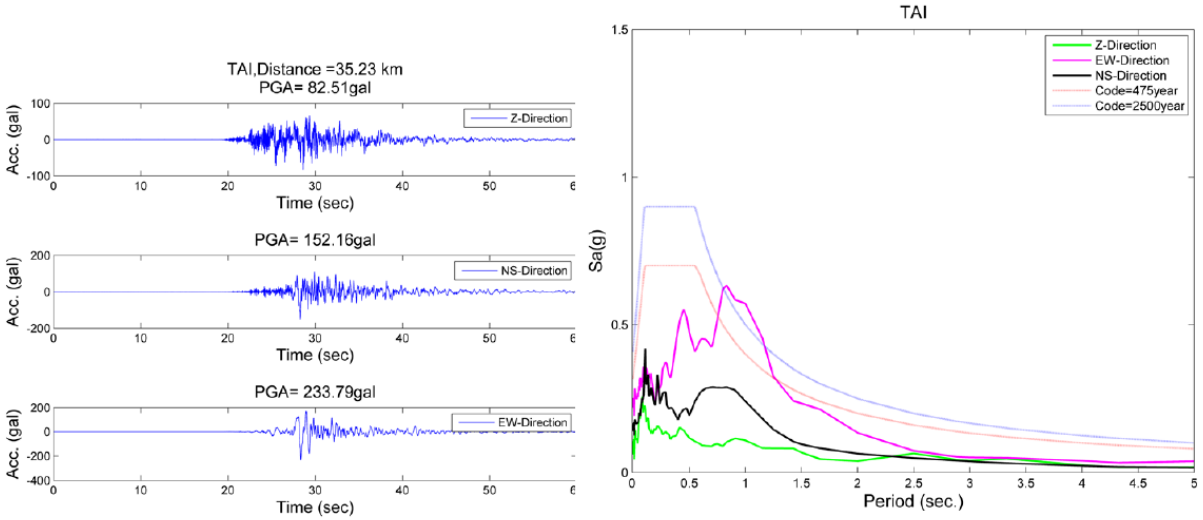

Figure 4-9: CWB Ground Motion Recorded in Tainan City (from NCREE).

SCL(佳里)

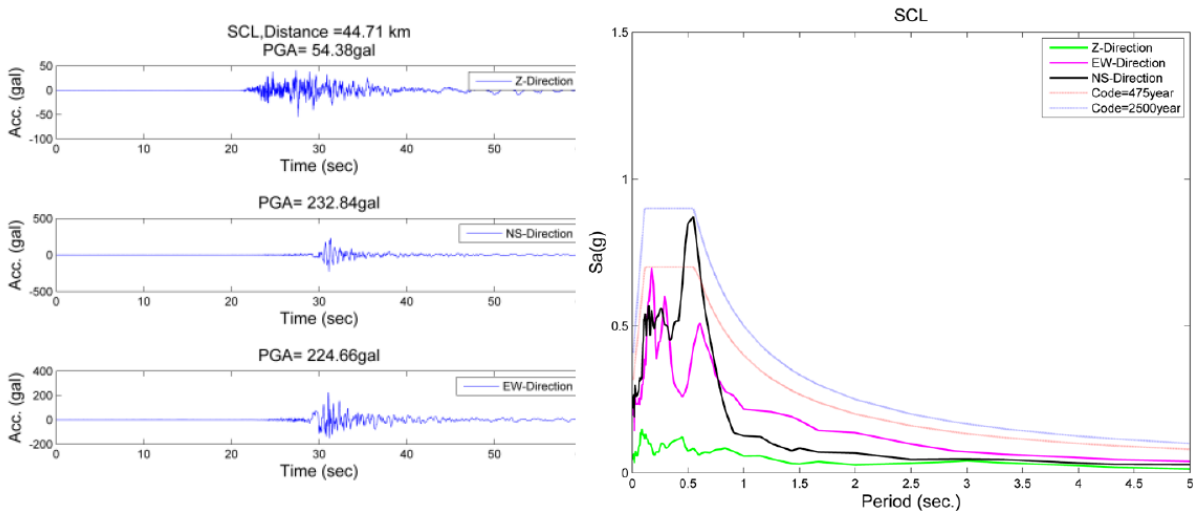

Figure 4-10: CWB Ground Motion Recorded in Jiali (from NCREE).

SSH (善化)

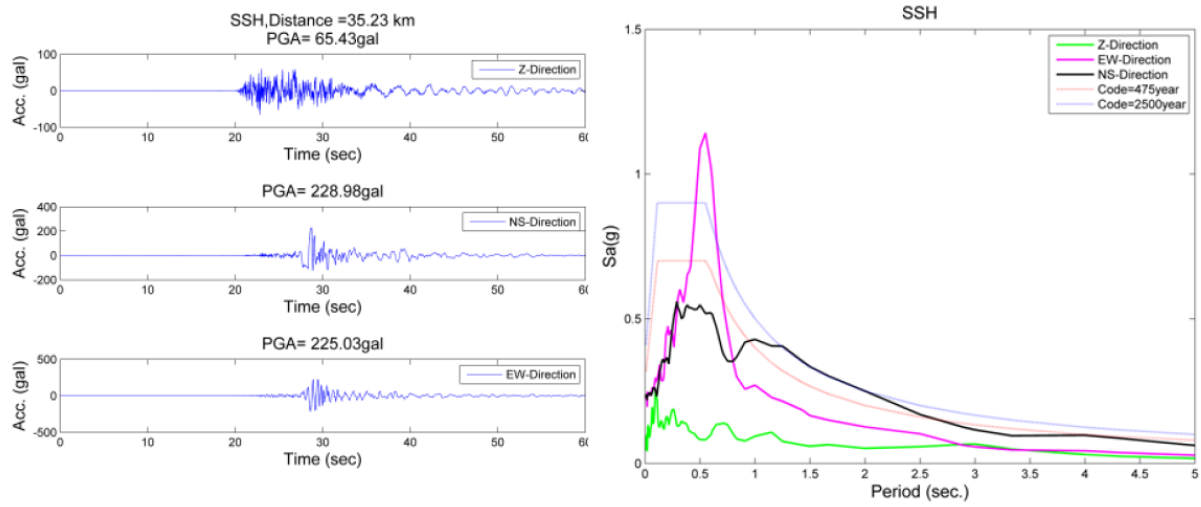

Figure 4-11: CWB Ground Motion Recorded in Shanhua (from NCREE).

A730(南化埔仔)

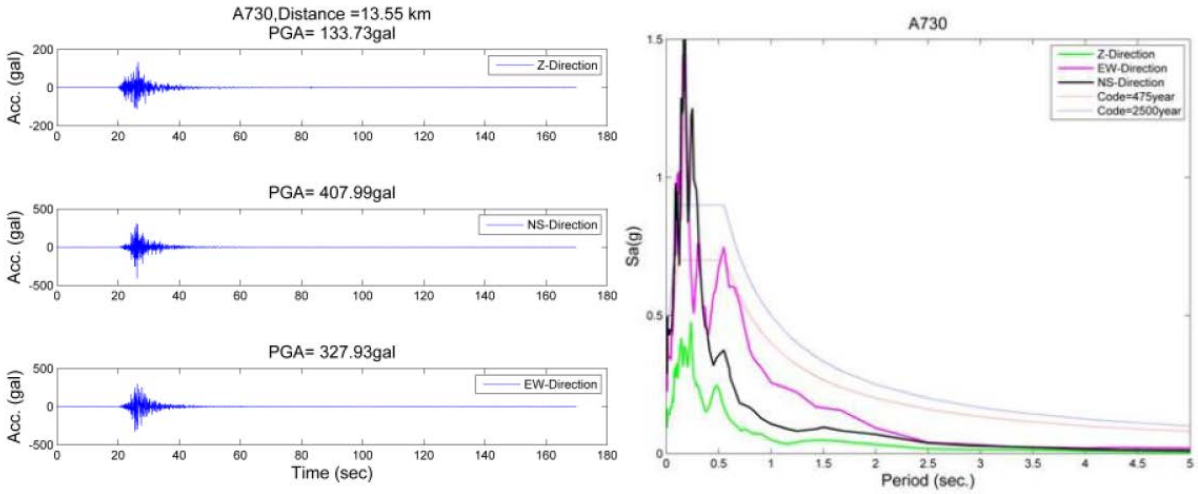

Figure 4-12: NCREE Station Recorded Ground Motion in Nanhua (from NCREE).

Station ID	Location	Lat	Long	Dist (km)	PGA (%g)	PGV (cm/sec)
CWB.ALS	Alishan	23.51	120.81	66	8.567	6.22
CWB.CHK	Chenggong	23.1	121.37	79	1.458	1.46
CWB.CHN4:	Caoshan	23.35	120.59	46	10.671	6.64
CWB.CHN5	Caoling	23.6	120.68	72	35.079	38.67
CWB.CHN7	Liujiao	23.48	120.24	68	19.451	24.53
CWB.CHY	Chiayi City	23.5	120.43	63	17.469	13.71
CWB.EAS	Anshuo	22.38	120.86	66	1.055	0.91
CWB.ECB	Changbin	23.32	121.45	95	1.781	1.46
CWB.ECL	Taimali	22.6	120.96	53	2.238	1.54
CWB.ECS	Chishang	23.1	121.22	65	2.299	2.00
CWB.ECU	Chulu	22.86	121.09	51	3.299	2.58
CWB.EDH	Donghe	22.97	121.3	71	1.799	1.23
CWB.EGF	Guangfu	23.68	121.48	119	1.677	1.43
CWB.EHY	Hongye	23.5	121.33	95	1.360	0.78
CWB.ELD	Lidao	23.19	121.03	52	1.555	1.34
CWB.ESF	Shoufeng	23.87	121.51	136	1.439	1.40
CWB.HEN	Hengchun	22	120.75	103	1.476	1.75

Station ID	Location	Lat	Long	Dist (km)	PGA (%g)	PGV (cm/sec)
CWB.KAU	Kaohsiung City	22.57	120.32	49	3.433	4.87
CWB.PNG	Magong City	23.57	119.56	123	3.439	2.94
CWB.SCK	Qigu	23.15	120.09	56	16.634	19.65
CWB.SCL	Jiali	23.17	120.2	48	23.744	18.55
CWB.SCZ	Fangliao	22.37	120.63	62	1.683	1.13
CWB.SGL	Jiuru	22.72	120.5	30	6.317	7.75
CWB.SML	Sun Moon Lake	23.88	120.91	106	4.695	4.50
CWB.SNW	Nanwan	21.96	120.75	107	1.018	1.06
CWB.SPT	Pingtung City	22.68	120.5	33	3.616	5.88
CWB.SSD	Sandimen	22.74	120.64	28	10.750	4.69
CWB.SSH	Shanhua	23.14	120.29	40	23.348	28.15
CWB.TAI	Tainan City	22.99	120.21	41	23.835	29.40
CWB.TAI1	Yongkang	23.04	120.24	39	15.121	20.70
CWB.TCU	Taichung City	24.15	120.68	131	1.086	0.94
CWB.TTN	Taitung City	22.75	121.15	60	1.775	2.04
CWB.TWG	Beinan	22.82	121.08	51	2.317	2.08
CWB.TWL	Dongshan	23.26	120.5	39	6.811	5.84
CWB.TWM1	Qishan	22.82	120.43	27	8.963	8.14
CWB.TYC	Yuchi	23.91	120.87	109	1.366	1.15
CWB.WCH	Changhua City	24.08	120.56	124	4.189	2.62
CWB.WDD	Dadu	24.13	120.56	129	2.640	2.37
CWB.WDG	Dongjidao	23.26	119.67	98	6.158	5.96
CWB.WDL	Douliu City	23.72	120.54	85	7.683	10.12
CWB.WDS	Dongshi	24.26	120.83	145	1.488	1.61
CWB.WES	Ershui	23.81	120.62	94	5.872	4.33
CWB.WGK	Gukeng	23.68	120.57	80	11.158	14.15
CWB.WLC	Liuqiu	22.35	120.37	68	1.969	2.24
CWB.WNT	Mingjian	23.88	120.69	102	2.884	2.11
CWB.WNT1	Nantou City	23.91	120.68	105	1.542	1.77
CWB.WSF	Sihu	23.64	120.23	84	16.786	14.96
CWB.WTC	Dacheng	23.86	120.29	104	5.597	6.08
CWB.WWF	Wufeng	24.04	120.7	120	2.714	1.71
CWB.WYL	Yuanlin	23.96	120.58	110	2.994	3.08
IU.TATO	Taipei, Taiwan	24.97	121.50	240	0.206	0.41

Table 4-1: Seismic Instrument Recordings Summary – Meinong Earthquake.

NCREE Real-Time Seismic Monitoring Network

- Stations observing PGA>20gal

Re = 21.5km

Station	Name	E	N	PGA_U,gal	PGA_N,gal	PGA_E,gal
A730	南化埔仔	120.50	23.05	133.732	407.994	327.928
A800	茂林萬山	120.68	22.91	65.438	158.471	101.689
A660	六腳溪厝	120.28	23.50	36.330	138.891	184.579
A620	梅山圳北	120.57	23.58	31.837	79.585	96.053
A590	二林香田	120.37	23.87	24.072	60.057	72.547
A771	路竹北嶺	120.27	22.82	28.233	50.669	59.984
A601	豐山	120.75	23.59	17.975	39.016	42.083
A600	達邦特富野	120.76	23.47	24.155	33.905	35.178
A770	大寮林園	120.40	22.54	13.807	28.637	28.800
A530	魚池東光	120.96	23.89	9.855	28.097	23.062
A810	瑪家佳義	120.63	22.64	19.682	27.570	33.943
A560	南投永興	120.64	23.89	12.969	27.446	26.643
A860	枋寮瓦磘	120.61	22.38	13.049	25.783	29.582

Table 4-2: Instrumentation from NCREE P alert Stations.

4.1 Regional Site Effects

Tainan, Gangshan, and Pingtung are three cities with similar distances to the epicenter of the Meinong earthquake. However, Tainan City recorded comparatively larger peak ground accelerations and most of the damage caused by the earthquake was located in Tainan. Such a pattern raises the possibility of site amplification in the Tainan area. Data collected from H/V measurements and borehole seismic measurements of the southwest region of Taiwan are discussed in this section to examine the possibility of site effects due to site resonance or soft ground conditions.

Between 2002 and 2008, Prof. Wen's research group at the National Central University conducted a thorough site effect study for Taiwan Island (Huang, 2009). H/V measurements were conducted at 5 km spacing grid points. Based on results from these measurements, contour plots of dominant frequencies and H/V amplitudes at the dominant frequencies of the southwest region of Taiwan are generated and presented in Figures 4-13 and 4-14, respectively. In general, surface waves dominate the H/V response. Dominant frequencies obtained from H/V measurements correspond to the site natural frequency (Nakamura, 1989). The H/V amplitude at the dominant frequency is not equal to the site amplification factor. It is corresponded to the impendence contract

between the top soil layer and the underlay stiffer layer (Foti et al., 2014). In other words, a large H/V amplitude at the dominate frequency indicates a clear soil-bedrock boundary. It should be noted that an H/V amplitude greater than 2 at the dominant frequency is required to fulfill the clear peak criteria for the measured dominant frequency (SESAME, 2004).

Locations of the epicenter and collapsed buildings are also provided in Figures 4-13 and 4-15. As shown in these figures, the collapsed buildings are mostly located in regions with a dominant frequency between 1.0 and 2.0 Hz and an H/V amplitude at the dominant frequency between 3.0 and 4.0. Similar observations can be found in Gangshan and Pingtung Cities, but no buildings collapsed in these regions. There are no clear features in these two figures that distinctly explain the higher recorded peak ground accelerations in Tainan.

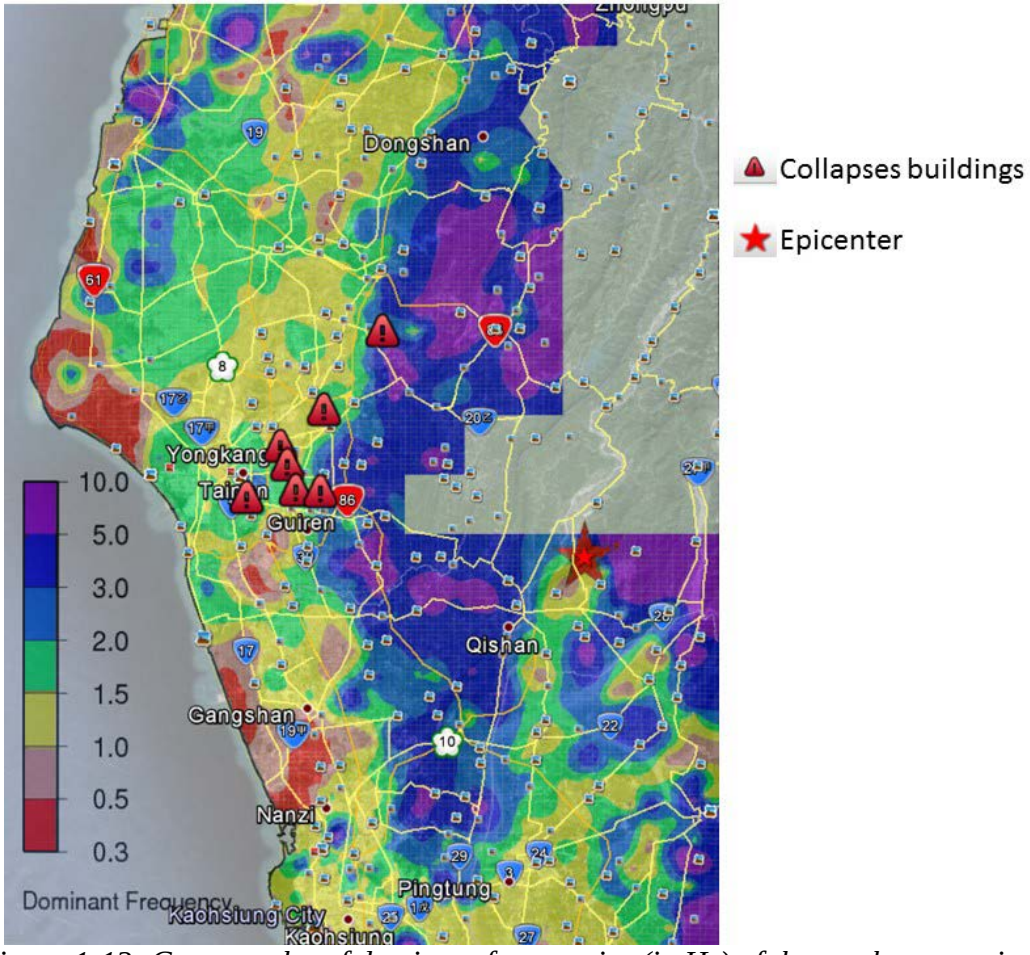

Figure 1-13: Contour plot of dominant frequencies (in Hz) of the southwest region of Taiwan.

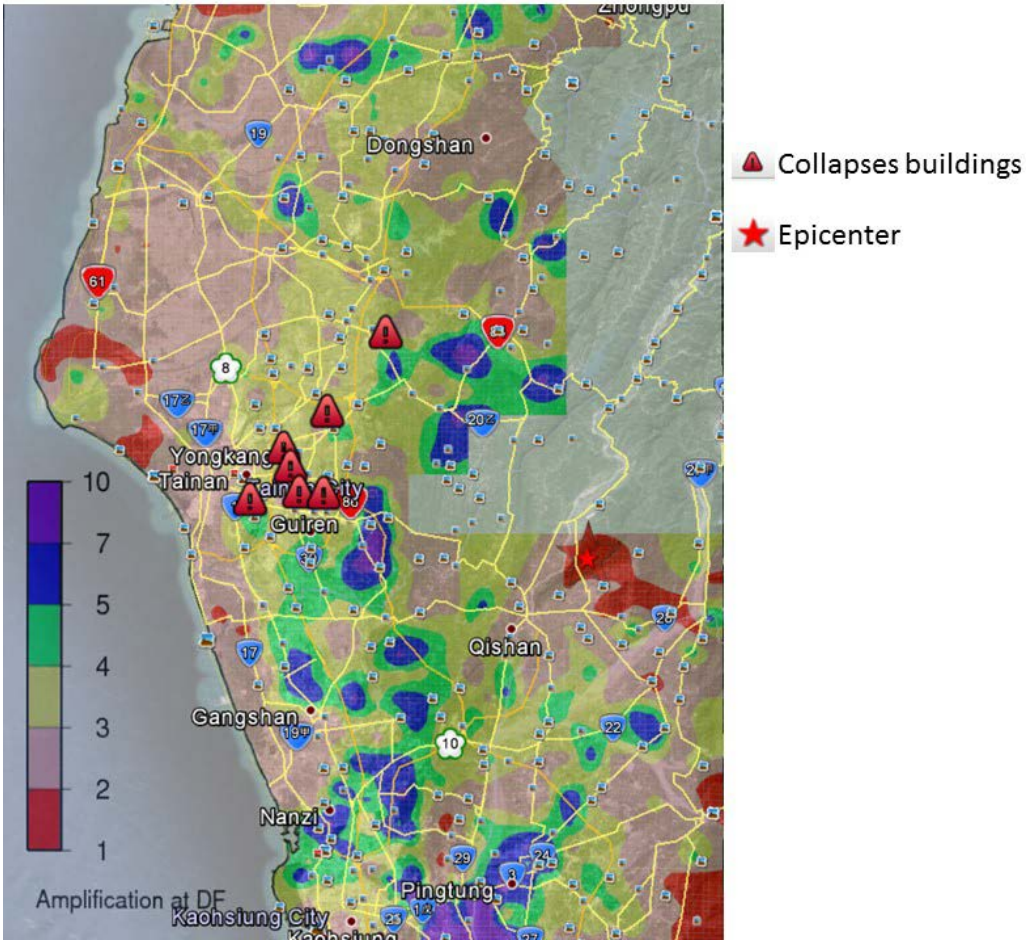

Figure 4-14: Contour plots of the H/V amplitude at the dominant frequency of the southwest region of Taiwan.

The values of Vs30 of the southwest region of Taiwan were provided by the National Center for Research on Earthquake Engineering (Kuo et al., 2011 and Kuo et al., 2012). The National Center for Research on Earthquake Engineering and the Central Weather Bureau in Taiwan has constructed an engineering geological database for the Taiwan Strong Motion Instrumentation Program. This database contains engineering geological measurements at 469 strong motion stations. Of these stations, 385 have a shear velocity profile extended to a depth greater than 30 m. From this database, a contour plot of the Vs30 values for the southwest region of Taiwan was constructed (Figure 4-15). It should be noted that locations of Vs30 measurements are much less than those of H/V measurements. As shown in Figure 4-15, collapsed buildings are mostly located in the region with a Vs30 value varying between 180 and 300 m/s. This is not too different from those in the areas of Gangshan and Pingtung Cities.

Based on the contour plots of the dominant frequency and the distribution of Vs30 locally, the larger peak ground accelerations recorded in Tainan City are likely not caused by site resonance or soft ground conditions.

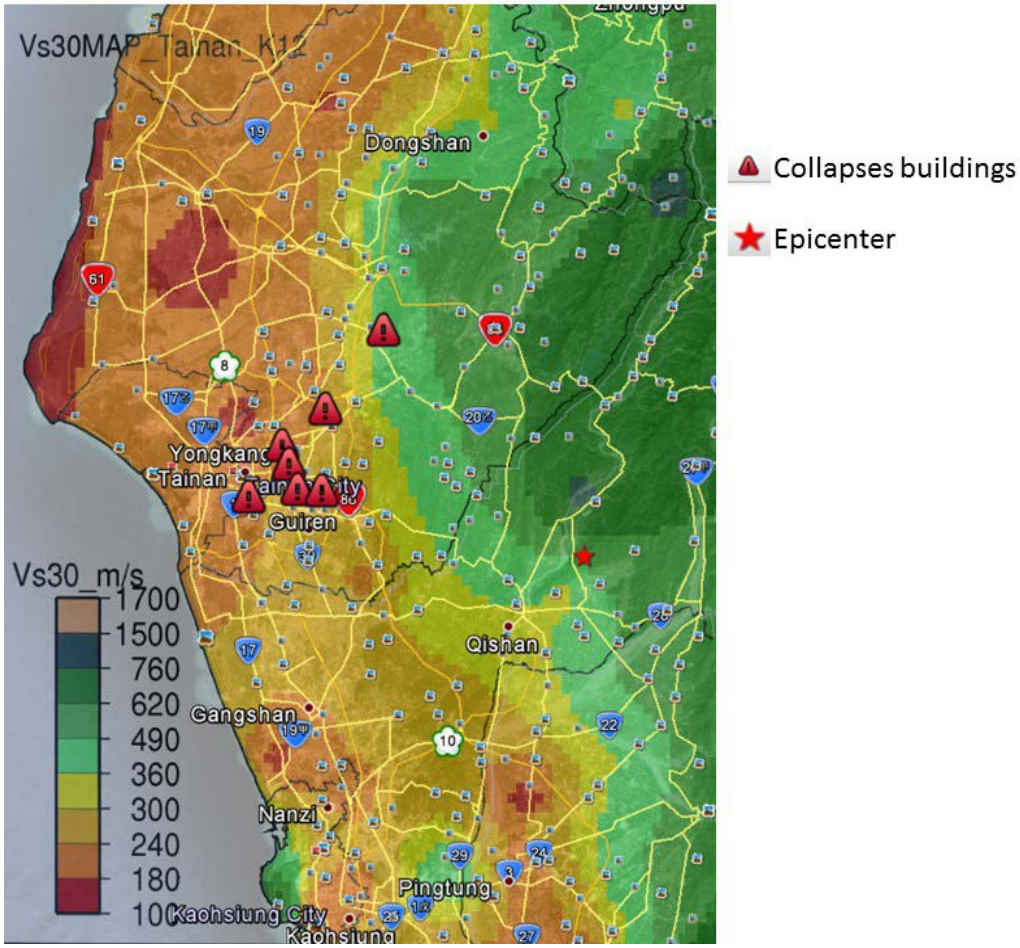

Figure 4-15: Contour plot of Vs30 of the southwest region of Taiwan.

5. STRUCTURAL DAMAGE - BUILDINGS

5.1 Inventory, Regional characteristics, and Relevant Building Codes/Practices

Tainan city includes 742,256 private buildings, with nearly half (46%) constructed between 1983 and 1997, and a third (33%) constructed prior to 1982 (Figure 5-1a). A large majority of the total number of buildings (~75%) are between 1-3 stories, with half of those buildings constructed of either reinforced concrete or concrete masonry (total ~50%) (Figure 5-1b). Almost 20% of buildings are constructed of unreinforced masonry. The number of mid-rise buildings in Tainan is quite small (~1%), with most constructed of reinforced concrete frame or wall-braced systems.

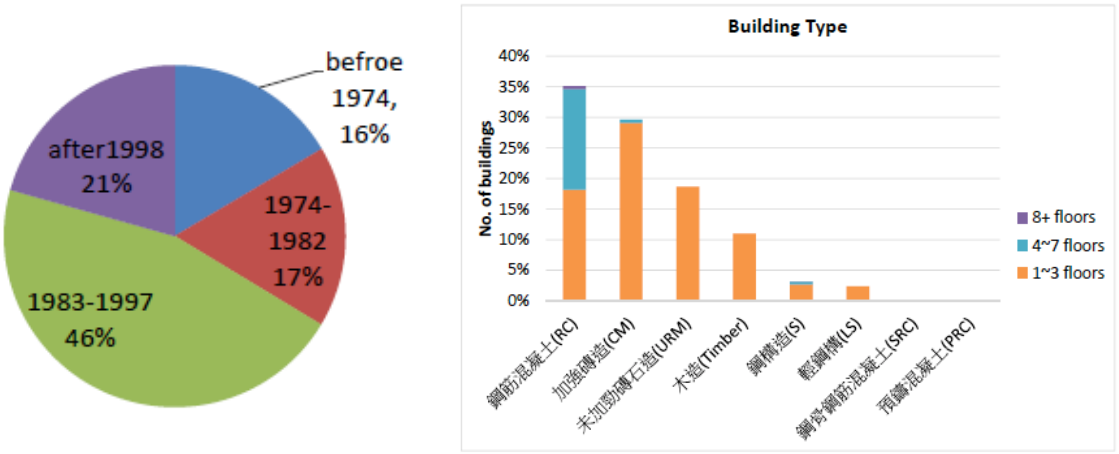

(a) (b)

Figure 5-1: Distribution of private buildings in Tainan City: (a) by age of construction and (b) by construction type (courtesy of NCREE, 2016a).

Seismic code	RC Building code	ACI code
1974 (民63)	CE401-59 (WSD)	318-63
1982 (民71)	CE401-68 (USD)	318-77
1989 (民78)	CE401-80 (USD, 1.4E)	318-89
1997 (民86)	CE401-84 (USD, 1.4E)	318-89
1999 (民88)	CE401-86a (USD, 1.4E)	318-95
2005 (民94)	CE401-93 (USD, 1.4E)	318-02
2011 (民100)	CE401-96aUSD, 1.0E	318-05

Table 5-1: Timeline of the adoption of U.S. seismic and concrete building design codes in Taiwanese practice (courtesy of NCREE, 2016a).

Taiwanese practice generally follows U.S. seismic design, adopting the 1963 Uniform Building Code by 1974 (Table 5-1). At that time, ACI 318-63 was also adopted for reinforced concrete building design. In 1982, the Taiwanese design seismic design code

was updated to UBC 1976, and in 1988 amplification effects for Taipei Basin were included. In 1997, separate provisions for seismic design were provided by a Building Seismic Design Code. This effort included introducing ductility factors for individual building systems (similar to the UBC), consideration of liquefaction, base isolation and energy dissipation systems. Seismic zonation was revised after the September 21, 1999 event; and in 2006 micro zonation was implemented. Since 2009, the Taiwan government has invested billions of dollars in the evaluation and retrofit of elementary schools, high schools and public buildings. The performance of these buildings during the present event was generally good. In Tainan City, a few of the buildings that were part of this retrofit program were damaged during the 2016 event. One of the 151 buildings that passed this evaluation (the Yuh-Ching junior high school (玉井國中)) was damaged to an extent that will likely lead to demolition, however this building did not collapse. This junior high school is located 22km from the epicenter. The Yuh-Ching elementary school (玉井國小), located about 1.2km from this high school, was also retrofit according to the recent program. Despite the relatively large shaking intensity at the elementary school of PGA = 445gal; no damage was observed at the elementary school.

5.2 Building Collapse Statistics

In totality, 8 buildings, ranging in height from 2-16 stories, suffered complete collapse (Table 5-2, Figure 5-2). These structures were mostly constructed of reinforced concrete, concrete masonry block and unreinforced masonry infill. Most appeared to have frame or wall-bracing. Related reports by NCREE, EERI, and U.S. structural engineers (see blogs by Degenkolb and SGH, 2016) provide additional discussion of the characteristics of these failures. However, it was noted that structural irregularities (vertical and/or plan) and/or lack of modern seismic detailing likely precipitated the collapse of these buildings. In addition, some demolition activities at collapsed building sites uncovered weak concrete and construction defects that likely contributed to the collapse of select buildings.

5.3 Overall Building Damage Statistics

According to Tainan Government statistics, provided as of March 2, 2016; 283 buildings were red-tagged and 19 buildings were yellow tagged (Figure 5-2). Some buildings exhibited column shear failures, exposing relatively large diameter conduit within the confined concrete core. Most columns appeared to be inadequately detailed to resist combined shear and axial demand, while maintaining adequate confinement. A few column failures showed adequate cross ties and confining steel to vertical steel ratios. Reports of other field teams will summarize other structural features that contributed to observed damage in a wide range of buildings. However, due to their prominence in this event and to facilitate comparison, the Weiguan Jinlong Complex (維冠金龍大樓), the King's Town Bank (京城銀行), the Wanglin Hotel (旺林飯店歸仁館), and a street building in the Gueiren District (歸仁區信義路大仁街口) are discussed in the following

sections. The GEER team visited these sites to understand if site amplification, excessive foundation movement or liquefaction played a role in the failures.

Figure 5-2: Google Earth image locating collapsed buildings (see Table 5-2).

No.	Location of Collapsed Buildings	Category	Year of Const.	Long.	Lat.	PGA (gal)	Sa(T=0.3s) (gal)	Sa(T=1.0s) (gal)
1	Weiguan Jinlong Complex (維冠金龍大樓), Yongkang District, Tainan City	Residential and commercial building, 16 floors	1992-1995	120.261	23.005	117.0	261.8	128.7
2	King's Town Bank (京城銀行), Sinhua District, Tainan City	Commercial building, 10 floors	1996	120.301	23.036	141.5	294.6	115.1
3	Dachih Market Place (大智市場), East District, Tainan City	Residential building and public market, 4 floors	-	120.231	22.962	132.8	341.5	407.4
4	Shanshang District Pubic Market (山上區公有菜市場), Tainan City	Residential building and public market, 2 floors	1983	120.355	23.101	176.3	404.8	236.4
5	Nanhua District Pubic Market (南化區公有菜市場)	Residential building and public market, 2 floors	-	120.477	23.042	312.8	662.6	169.9
6	Xinyi N. Rd. & Daren St., Gueiren District, (歸仁區信義路大仁街口), Tainan City	Street house, 6 floors	-	120.298	22.967	182.3	398.3	198.9
7	Lane 101, Taizi Rd. Rende District, (仁德區太子路) Tainan City	Street house, 3 floors	1980	120.267	22.989	123.3	285.2	163.9
8	Wanglin Hotel – Guiren (旺林飯店歸仁館)	Commercial building, 10 floors	1996	120.275	22.969	-	-	-

Table 5-2: Building collapse statistics (data provided by NCREE).

(2) King's Town Bank (京城銀行), Sinhua District, Tainan City

(3) Dachih Market Place (大智市場), East District, Tainan City

(4) Shanshang District Pubic Market (山上區公有菜市場), Tainan City.

(5) Nanhua District Pubic Market (南化區公有菜市場)

Figure 5-3: Images of collapsed buildings sans the Weiguan Jinlong Complex(維冠金龍大樓) and Wanglin Hotel – Guiren (旺林飯店歸仁館), which are discussed in a subsequent section (organization following Table 5-2).

(6) Xinyi N. Rd. & Daren St., Gueiren District (歸仁區信義路大仁街口), Tainan City

(7) Lane 101, Taizi Rd. Rende District (仁德區太子路), Tainan City

Figure 5-3 (continued): Images of collapsed buildings sans the Weiguan Jinlong Complex(維冠金龍大樓) and Wanglin Hotel – Guiren (旺林飯店歸仁館), which are discussed in a subsequent section (organization following Table 5-2).

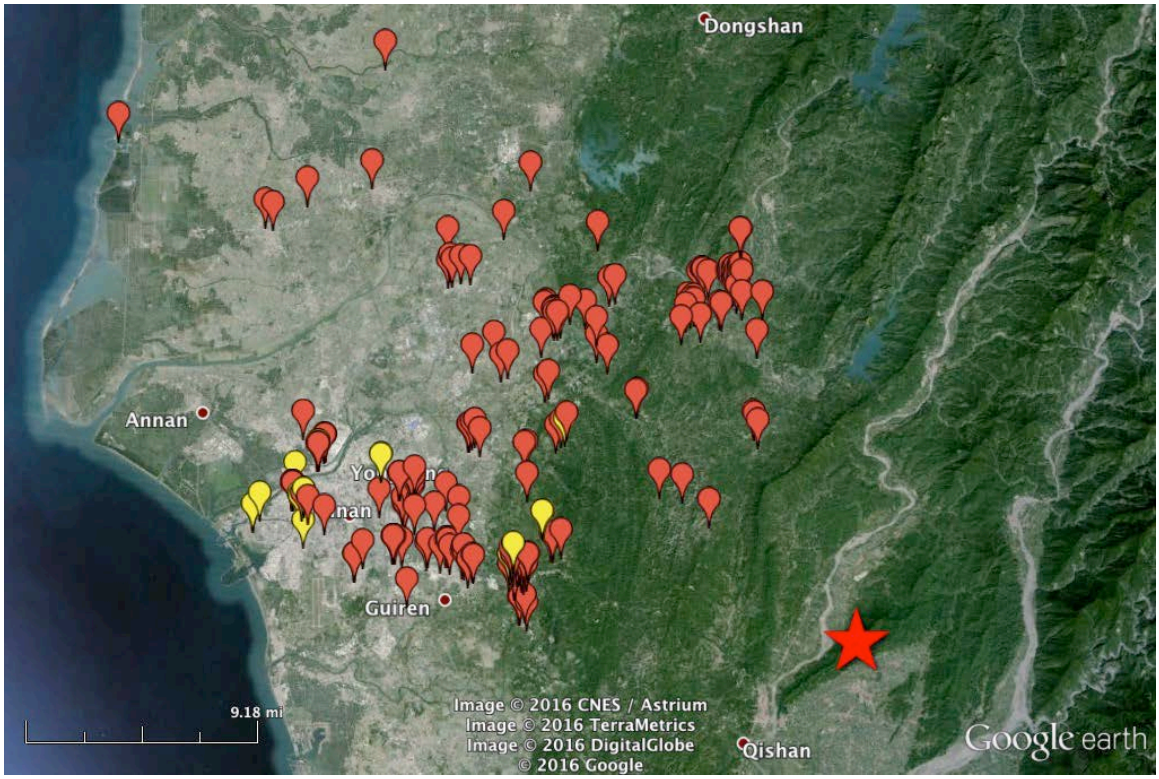

Figure 5-4: Google Earth image of yellow and red-tagged buildings (data from Tainan Government statistics as of March 2, 2016; input by Kuo-Fong Ma).

5.3.1 Weiguan Jinlong Complex (維冠金龍大樓), Yongkang District, Tainan City (120.261,23.0052)

The collapse of the Weiguan Jinlong Complex (Figure 5-5) in Yongkang district resulted in the loss of 114 lives. This building was a 16-story reinforced concrete structure constructed between 1992-1995 (Figure 5-6), thus it likely followed reinforcing detail provisions comparable to ACI 318-89 (Table 5-1). According to Mr. Justin Shih, who performed an extensive analysis of this building post-event, the structure was designed for a minimum horizontal shear force of V = 0.062W, with an estimated period (for an h_n = 52.5m) of 1.17s. Modal analysis by Mr. Shih identifies this period as the torsional mode; and review of field measurements during the 2016 event at station TAI in Tainan city indicates large spectral accelerations at about 1s (Figure 5-7). Due to its vintage, this building was also subjected to the Sept 21, 1999 event (921 earthquake), however suffered no damage. Seismic stations TAI1 and TAI2 were the closest to this building at 4.4 and 5.7km away respectively; and for comparison station TAI1 recorded peak accelerations of 105 and 148gals, whereas these values were about half this amplitude at 44gals and 87gals in the NS and EW directions respectively, during the 921 earthquake (Figure 5-8). In addition to the much larger amplitude ground shaking at periods closer to those of the building, importantly, several structural features likely contributed to the collapse of this building. These include its irregular floor plan and elevation and poor (non-ductile) detailing practices. Standing more than 50-m tall, the building's first floor height vertical irregularity of 5.5m compared to the uniform floor height of the remainder of the building (3.2m), was more than 1.5 times greater. Non-ductile detailing practices included the use of short 90-degree hooks (rather than 135 degree hooks), insufficient beam-column confinement, and the use of inadequate coupler splices at column rebar (particularly notable in the first floor columns (Figure 5-9b).

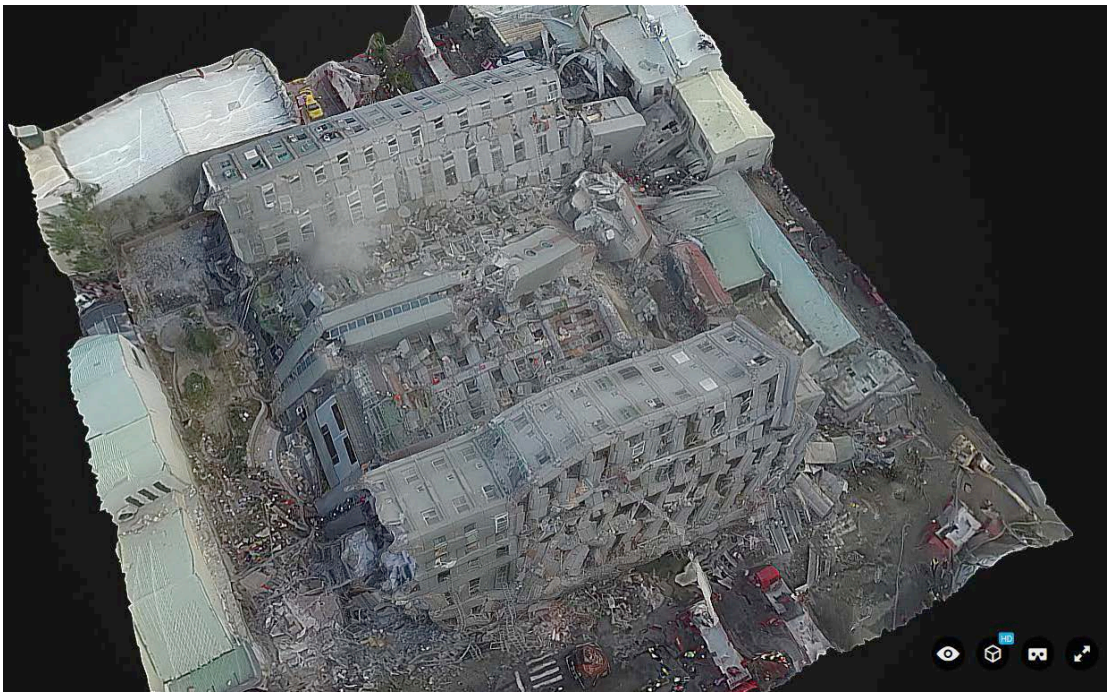

Figure 5-5: Aerial model generated with a UAV flight over the collapsed Weiguan Jinlong Complex (120.261,23.0052) (Created by the Department of Geomatics, NCKU, Tainan, Taiwan).

Figure 5-6: (a) Southeast perspective rendering of the Weiguan Jinlong Complex (rendering courtesy of Mr. Justin Shih) and (b) google streetview of the complex (original view). (120.261,23.0052).

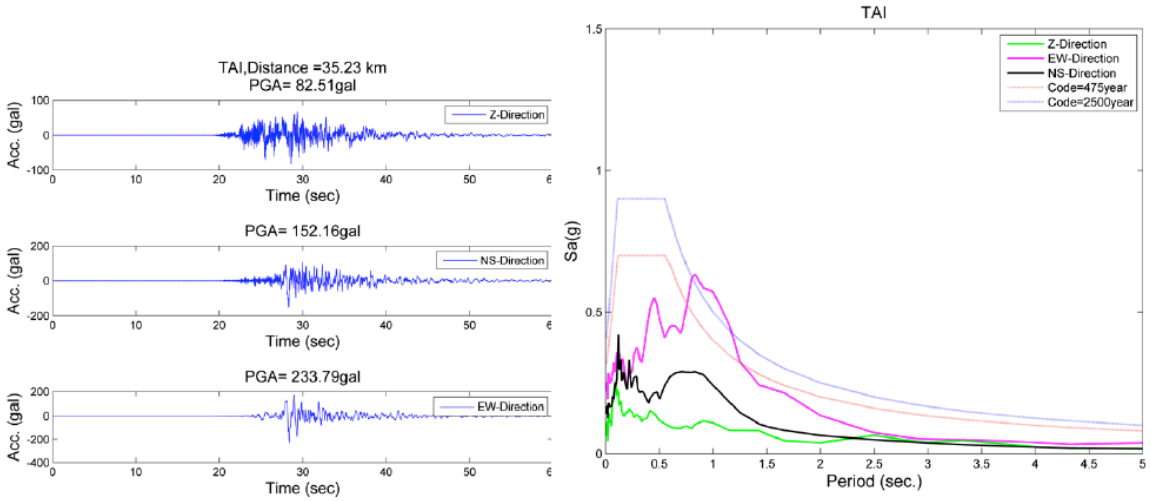

Figure 5-7: (left) Acceleration measurements of station TAI (120.21, 22.99) (vertical, N-S, and E-W components, respectively) and (right) elastic spectral accelerations (courtesy of NCREE, 2016b).

2016206美濃地震(1.7倍九二一)

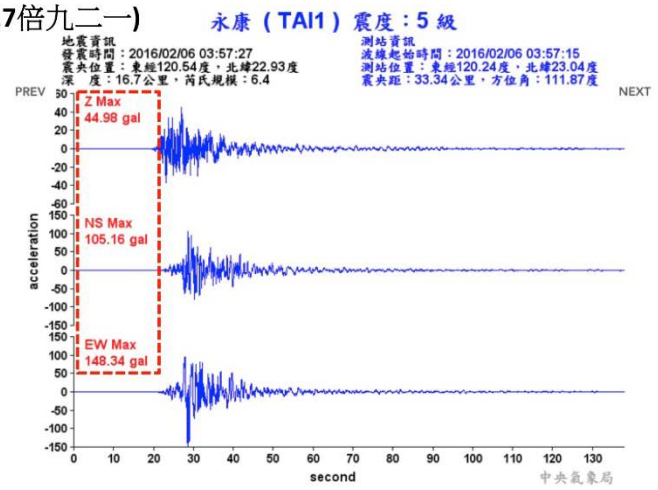

19990921九二一地震

::: 個案地震報導 ..>19990921集集地震 ..>各地震度原始資料(ASCII)..>

19990921集集地震(震度分級表)

測站代碼	測站名稱	震度值 (連結震波圖)	震央距 (Km)	垂直向 (gal)	南北向 (gal)	東西向 (gal)	縣市	鄉鎮	TWD97經緯度 (連結地圖)	ASCII 檔案下載
CHY057	鳴頭國小	4	88.16	21.18	52.70	38.64	台南縣	大內鄉	120.42E,23.15N	
CHY078	永康氣象站	5	108.14	20.94	43.84	86.92	台南縣	永康市	120.24E,23.04N	
TAI1	永康氣象站	5	108.14	20.58	44.50	87.57	台南縣	永康市	120.24E,23.04N	
CHY062	玉井國小	4	88.90	19.26	48.68	59.22	台南縣	玉井鄉	120.46E,23.12N	

Figure 5-8: Comparison of accelerations measured at station TA1 (4.4km from the Weiguan Jinlong Complex (120.24, 23.04)) during the 2016 and 1999 events (courtesy of Mr. Justin Shih).

(a) *(b)*

Figure 5-9: Weiguan Jinlong complex (120.261,23.0052): (a) North column damage to building and (b) close-up of building column reinforcement, which directly pulled out at the first floor. (images courtesy of Justin Shih).

5.3.2 King's Town Bank (京城銀行), Sinhua District, Tainan City (23.036, 120.301)

The King's Town bank was a 10-story mixed use (retail/residential) building in Sinhua District that collapsed at its lower floors (Figures 5-10 and 5-11). The ground floor of this building was notably taller than the uniform floor height over floors 2 through 10. Because of a substantial wall located at the rear of the building compared in contrast to the large open walkway in at its

front, it is likely that the primary response of the building was torsional, resulting in large displacement demands on the singular frame at the front of the building. Two mid-rise residential structures approximately, 100-m from this building, suffered minor damage during the earthquake, without impact to their continued use after the earthquake (Figure 5-12).

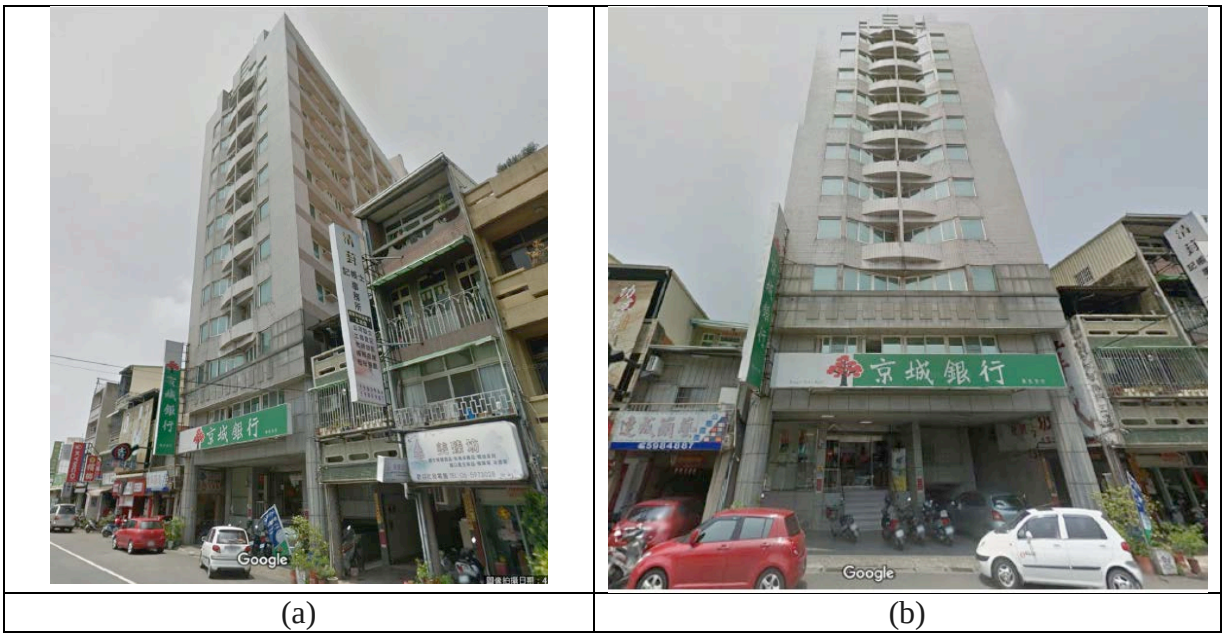

(a) (b)

Figure 5-10: King's Town Bank Google street view images before the earthquake (23.036, 120.301).

(a) (b)

Figure 5-11: King's Town Bank (a) prior to earthquake and (b) during demolition (Febuary 18, 2016) – both views looking East (23.036, 120.301).

Figure 5-12: Pair of 10 and 12 story buildings about 100m from the King's Town Bank (23.0363, 120.300) – the building on the right suffered minor damage. Both were operational after the earthquake.

5.3.3 Wanglin Hotel, Guiren (旺林飯店歸仁館) (22.968,120.275)

The Wanglin Hotel - Guiren (旺林飯店歸仁館) collapsed during the Meinong earthquake (Figure 5-13). This building was a 10-story plant office building completed in 1996. However, this building had not been not occupied for the past 20 years. In 2014, Wanglin Hotel (旺林飯店) purchased the building and began remodeling the building to serve as a hotel. The online announcements provided by the new owner, Wanglin Hotel, indicated that the remodel was non-structural. A photograph from Google Street View taken in March 2015 before the earthquake and a photograph taken by the GEER team on February 19th, 2016 are shown in Figure 5-13. After the earthquake, the lower 5 stories collapsed on the west side and the lower 6 stories collapsed on the east side. As a result, the building leans toward the east at a 15 degree angle. No evidence of soil liquefaction or movement of the foundation were noted at this site. For safety concerns, the GEER team did not conduct observations inside of the building. However, damaged columns in this building exhibited evidence of nonductile detailing. The lateral force resisting system appeared to be unbalanced, most likely causing a torsional response to the earthquake motion, imposing large displacement demands on tall first story columns. The common locally adopted style of leaving a walkway in the front area of buildings rendered a major shortcoming to this and other buildings, resulting limited lateral load resistance and precipitating a torsional problem. In this particular building, vertical and plan structural irregularities also appeared to significantly contribute to its collapse.

(a) March 2015 | (b) February 19th, 2015

Figure 5-13: Photographs of the Wanglin Hotel, Guiren (旺林飯店歸仁館) before and after the earthquake.

5.3.4 Street Building at Xinyi N. Rd. & Daren St., Gueiren District, (歸仁區信義路大仁街口) (22.968,120.298)

The street building at the intersection of Xinyi N. Rd. & Daren St., in Gueiren District, Tainan was a 6-story building with residential occupancy. A photograph of the building before the earthquake from Google Earth street view is shown in Figure 5-14a. The street side of this building was constructed without walls to allow a pedestrian sidewalk of about 3 meters width. This is a common architecture feature called騎樓 (veranda) in Taiwan. A photograph of a nearby 4-story building is also evident in the right side of Figure 5-14a. This 4-story building was not damaged by the earthquake. Columns in the veranda area of the building that collapsed failed during the earthquake, and the building tilted toward the street following the earthquake. This building was under demolition during the GEER team visit (Figure 5-14b). However, the team noted no evidence of soil liquefaction or manifestations of movement of the buildings foundation at this site.

(a) March 2015

(b) February 17th, 2015

Figure 5-14: The Street Building at Xinyi N. Rd. & Daren St., Gueiren District, (歸仁區信義路大仁街口) before and after the earthquake

5.4 Microtremor Response

The GEER team brought two sets of seismometers to Tainan to conduct microtremor measurements and calculate horizontal-to-vertical (H/V) spectral ratios using Nakamura's technique, referred to herein as H/V measurements. Studies have shown that the H/V spectral ratio at a site provides an estimate of the site frequency between the ground surface and bedrock at a site (Nakamura, 1989). Because this method does not require a borehole, it is a convenient and inexpensive method to estimate the site resonant frequency. In total, 10 sites where structure, foundation, or slope damage from the Meinong earthquake was observed were measured.

The two sets of the seismometers utilized by the GEER team were provided by the Natural Hazards Engineering Research Infrastructure Equipment Facility at the University of Texas at Austin (NHERI@UTexas, https://utexas.designsafe-ci.org/). Each set of equipment consists of a Trillium Compact broadband seismometer and a Taurus data logger. Both the seismometer and the data logger are manufactured by Nanometrics Inc. GPS coordinates, dominant frequencies, and amplification factors at the dominant frequencies of the measured locations near collapsed buildings are presented in Table 5-3. It should be noted that an H/V amplitude greater than 2 at the dominant frequency is required to fulfill the clear peak criteria for measuring the dominant frequency (SESAME, 2004).

In addition to the two seismometers provided by NHERI@UTexas, another two sets of seismometers (VSE-311C seismometers with SAMTAC-801B data loggers, made by Tokyo Sokushin Co., Ltd) provided by Prof. Wen's research group from the National Central University (NCU, http://www.gep.ncu.edu.tw/en/) were also utilized in the H/V measurements. A photograph of the equipment provided by each of NHERI@UTexas and NCU are presented in Figure 5-15.

Comparison between measured dominant frequencies and estimated resonant frequencies of the collapsed buildings are shown in Table 5-4. The estimated building resonant frequency, f, is calculated as:

$$f = {}^{10}/_{Number\ of\ stories}$$

As shown in Table 5-4, natural frequencies of the King's Town Bank, Wanglin Hotel, and Guiren Xinyi Residential Building are near the site natural frequencies. It should be noted that there are three buildings near King's Town Bank that are as tall as King's Town Bank. These three buildings only observed minor cosmetic damage from the earthquake. Thus, site amplification is likely not the main cause of the collapse of the King's Town Bank building. On the other hand, the Wanglin Hotel and Guiren Xinyi Residential Buildings are the only tall buildings in their vicinity. It is possible that site effects played a role in the collapse of these two buildings. However, additional studies are needed to further characterize site amplification at these locations.

Site Name	GPS coordinates	Dominant Frequency (DF), Hz	Amplitude at DF	Sensor Type
Weiguan Building				
	23.00530°,120.26060°	1.13	2.1	Trillium Compact
	23.00582°,120.26087°	1.32	3.0	VSE-311C
	23.00496°,120.26041°	1.22	3.0	VSE-311C
	Average	1.22	2.7	
King's Town Bank				
	23.03642°,120.30085°	1.16	3.3	Trillium Compact
	23.03667°,120.30027°	1.19	2.3	Trillium Compact
	23.05143°,120.28980°	1.16	4.4	Trillium Compact
	23.03643°,120.29996°	1.19	2.3	Trillium Compact
	23.03640°,120.30051°	1.28	5.5	VSE-311C
	Average	1.19	3.6	
Wanglin Hotel - Guiren				
	22.96856°,120.27531°	1.32	2.9	Trillium Compact
Guanmiao Dongxing				
	23.00530°,120.26059°	1.59	5.2	Trillium Compact
	22.95536°,120.33477°	1.68	5.2	VSE-311C
	22.95595°,120.33461°	1.70	5.7	VSE-311C
	22.95587°,120.33505°	1.68	6.5	VSE-311C
	Average	1.67	5.6	
Dachih Market Place				
	22.96252°,120.23010°	1.04	5.6	VSE-311C
Xinyi-Daren Residential Building				
	22.96722°,120.29780°	1.62	4.3	VSE-311C
Lane 101 Taizi Rd Residential Building				
	22.98975°,120.26740°	1.49	3.0	VSE-311C

Table 5-3: GPS coordinates, dominant frequencies, and amplification factors at the dominant frequencies at locations of collapses buildings.

Figure 5-15: Photograph of a seismometer and data recorder provided by NHERI-EF@UTexas and a seismometer and data recorder provided by NCU.

Building Name	Number of floors	Estimated resonant frequency	Dominant Frequency (DF), Hz	Amplitude at DF
Weiguan Building	16	0.6	1.22	2.7
King's Town Bank	10	1.0	1.19	3.6
Wanglin Hotel - Guiren	10	1.0	1.32	2.9
Guanmiao Dongxing	1	10.0	1.67	5.6
Dachih Market Place	4	2.5	1.04	5.6
Guiren Xinyi Residential Building	7	1.4	1.62	4.3
Lane 101 Taizi Rd Residential Building	3	3.3	1.49	3.0

Table 5-4: Comparison of measured site frequencies from H/V and estimated resonant frequencies of the collapsed buildings.

Acknowledgements

The GEER team appreciates the input of the U.S. structural engineering teams of Degenkolb and SGH, led by Mr. Daniel Zapeda and Mr. Kevin Moore, respectively; for their reviews of this chapter. The GEER team also would like to thank the U. S. National Science Foundation for the support of the NHERI@UTexas seismometers under grants CMMI-1520808.

6. PERFORMANCE OF OTHER STRUCTURES

6.1 Bridge Performance

Bridges in the region impacted by the earthquake generally performed well. Nearly all bridges were functioning following the main event, although several were noted to have sustained at least minor cosmetic damage. The only bridge not functioning was the East-bound direction of elevated, provincial highway 86 bridge #24 (22.9258, 120.5380), which was closed to traffic immediately after the earthquake. NARLabs surveyed this bridge and presented its findings during an NCREE briefing which the GEER team attended. What follows is a summary of their observations (Liu, 2016). Bridge #24 along highway 86 is approximately 29 km west of the epicenter, and was constructed in 1996. Teles predicted the PGA near the site was 0.25g. Constructed with a single cell box girder superstructure supported on 13 piers, which are each in turn carried by a pile group, the East-bound direction of this structure spans 555 m. Failure of the bridge manifested due to the unseating of spans RP5-RP9, which were supported on either hinged or movable bearing types. NARLabs reports a maximum residual gap between the West and East bound spans as 59 cm (Liu, 2016) (Fig 6-1).

The maximum separation of 59 cm between the east and west-bound directions reportedly included outward displacement of the east-bound direction of over 40 cm and over 10 cm of displacement of the west-bound direction. The reported maximum permitted displacement of the bridge is 70 cm. The bridge was closed for repair during the GEER reconnaissance and repair construction was proceeding (Fig 6-2).

(a) (b)

Figure 6-1: Provincial highway 86 bridge # 24: (a) separation of east and west bound elevations and (b) failure of hinge bearing at RP9. (Images courtesy of Dr. Kuang-Yen Liu, NARLabs).

(a) (b)

Figure 6-2: Provincial highway 86 bridge # 24: (a) east bound direction support repair (note separation of drainage lines and sheared hinges) and (b) failure of hinge and concrete support for west bound direction.

6.2 Lifeline Damage

During the Meinong earthquake, the most severely damaged lifeline system was the water supply system, which impacted 400,300 customers and caused a shortage of water that lasted just over 2 weeks. The repair effort was partly hindered by the rescue and recovery effort of the collapsed Weiguan building where the collapsed building damaged and buried the main water supply line. Information presented in this section was obtained from a briefing by the Taiwan Water Corporation (TWC) on February 9, 2016, National Science and Technology Center for Disaster Reduction (NCDR) of Taiwan (http://www.ncdr.nat.gov.tw), Central Emergency Operation Center (CEO) of Taiwan (www.nfa.gov.tw), and local media sources.

6.2.1 Water Supply

The earthquake damaged numerous transmission and distribution waterlines in the City and caused about 400,300 customers to lose water supply. It is fortunate that the earthquake did not trigger any major fires, as propane tanks are still being used as household fuels by a significant portion of the population.

Based on the information provided by Taiwan Water Corporation, 26 damage locations were identified in pipelines with diameters of 300 mm or greater with the largest damaged pipe being 2,400 mm in diameter. Figure 6-3 shows 18 of the 26 locations reported. Pipeline materials that experienced damage

included pre-stressed concrete pipes, ductile iron pipes, steel pipes and PVC pipes. Table 6-1 summarizes the damage statistics in terms of pipe sizes. Three days after the earthquake, 20 of the 26 damaged pipe locations were repaired. Table 6-2 summarizes the recovery status through 2/13/2016.

Pipe Diameter (mm)	No. of Reported Failures
300 - 400	8
400 – 600	3
800	3
900	1
1200	2
1500	3
1750	1
2000	3
2400	1
Unknown	1

Table 6-1: Waterline Damage Statistics (Taiwan Water Corporation).

Date	Repaired Services	Outage Customer
Earthquake	-	403,000
2016/2/6	150,300	250,000
2016/2/7	350,300	50,000
2016/2/10	348,800	48,200
2016/2/11	370,300	30,000
2016/2/13	395,300	5,000
2016/2/21	403,000	0

Table 6-2: Water Supply Recovery Status (from NCRD and CEO).

Figure 6-4 shows a damaged steel transmission waterline crossing a river. The damage likely resulted from ground shaking and/or differential movement between the abutments. Figure 6-5 shows the repair of a steel pipeline damaged by the collapsed structure which supplies water to area south of Tseng-Wen River. To temporarily bypass another heavily buried water main in the Hsinghua Distinct, an above ground pipeline was constructed (Figure 6-6).

6.2.2 Natural Gas

Likely because propane tanks are still being used as the predominate fuel locally; natural gas pipelines are not extensively used in the City. This combined with the fact that plastic pipelines were used for gas distribution, which performed extremely well in the Chi-Chi earthquake, resulted in limited distribution to gas customers (1,241 reported). Table 6-3 summarizes the recovery progress for natural gas.

Date	Repaired Services	No. of Customer outages
Earthquake	-	1,241
2016/2/6	950	291
2016/2/7	1,034	207*

*Not repairable (building collapsed)

Table 6-3: Natural Gas Recovery Status (from NCRD and CEO).

6.2.3 Electricity

No major damage was reported for electric transmission and distribution system. However, immediately after the earthquake, 173,084 services were temporarily interrupted and most of them (166,362) were restored the same day. By the second day (2/7/2016), 172,644 were restored. The remaining 420 that could not be restored were due to collapsed structures (Based on report from NCRD and CEO).

6.2.4 Communication

Minor damage to local landline communication systems was reported with 1,248 customer's service temporarily interrupted by the earthquake. All interrupted services were restored by the following day (2/7/2016). A total of 131 cell phone transmission facilities experienced interruption or suffered damage after the earthquake. Later in the evening of 2/6/2016, most were restored and only 20 sites remained to be serviced. By late evening of 2/8/2016, all cell phone facilities were restored. Prior to the full restoration, the City of Tainan mobilized 8 mobile cell sites to the earthquake damaged area. The above information was based on NCRD.

6.2.5 Transportation

Tai-3 highway near Sta. 369K, pavement bulged 20 cm from earthquake (Figure 6-7). At the Don-Shi-Pu (東勢埔) bridge, differential movement of 10 cm occurred across the bridge deck. The road was closed as a precautionary measure. The Taiwan High Speed Rail (bullet train) suspended service to 30 km north of Tainan city. After a mandatory post-earthquake inspection, full service was restored by 2/7/2015 17:00. The Taiwan Rail Corporation reported minor distress of rails north of Tainan near Chia-Yi. Train operation was not suspended but operated at a reduced speed in the distressed zone. This repair was completed on 2/17/2016 and the train restored to normal operation at 19:00. There was no reported impact to air traffic.

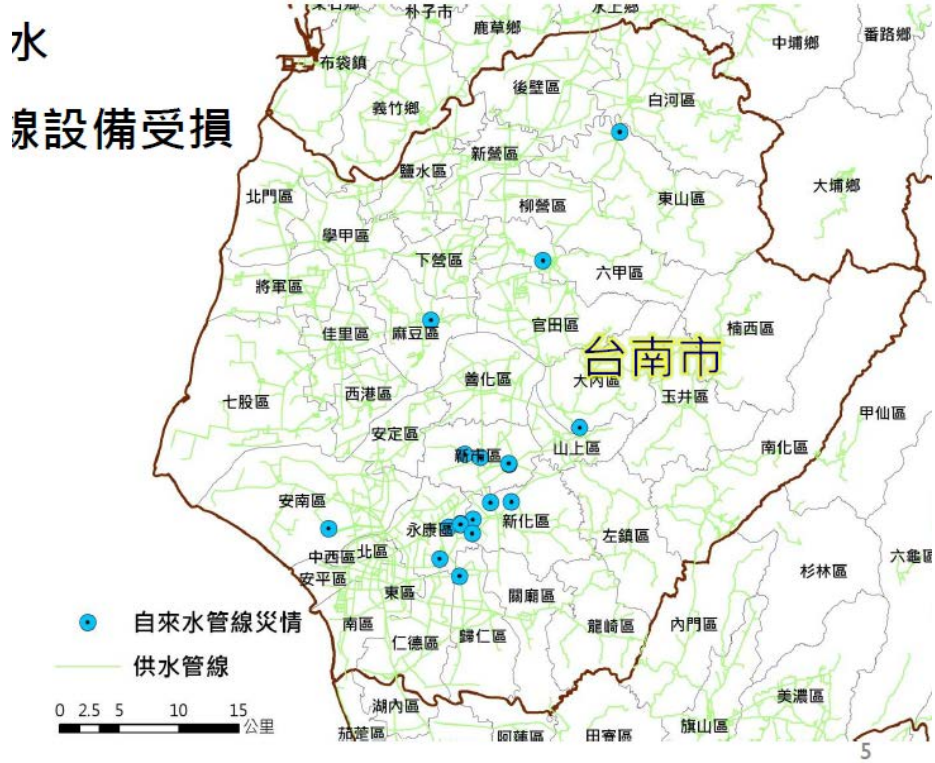

Figure 6-3: Location of Damaged Waterline (from NCDR).

Figure 6-4: Damaged 2000 mm Water Pipeline near Bridge in Yung Kang District (開運橋頭永康側) (23.034244, 120.286719).

Figure 6-5: Repair of Damage Water Main (image Courtesy of Liberty Times) (23.005214, 120.261222).

.

Figure 6-6: Emergency Bypass Water Supply Pipeline (Courtesy of CRNTT).

Figure 6-7: Pavement and Bridge Deck Distress along Tai-3 Highway.

6.3 Emergency Response

Taiwan media reported that the response by hospitals, fire departments, and other emergency operations was not significantly hindered following the earthquake. While the GEER team did not visit emergency facilities during its efforts, U.S. engineers from Degenkolb did; therefore, what follows is a summary of their findings. Degenkolb engineers visited two hospitals while in Tainan: the NCKU University hospital (成功大學醫院) and the 1200 Bed Chi-Mei Hospital (奇美醫院). The Chi-Mei Hospital was closest to the damage sites therefore received the most casualties. This hospital (Figure 6-8) consists of two main bed towers with a connecting tower structure, with a total of 1200 beds (mostly 4 beds per room). Each of the three buildings is seismically separated from the other. The towers are 12 stories above ground. One tower has two stories below grade, and the other has four stories below grade. The first tower was constructed in the 1980's and the other in 1992. From the exterior of this structure, removed brick veneer removed from a number of wall piers/columns was visible. Hospital staff indicated that the veneer had been removed to avoid falling hazards. Review by local engineers indicated that cracks to the concrete core of the building were small; and that the veneer was the most significant damage to this building. The lone nonstructural failure highlighted by hospital staff was the failure of a 10-12" chilled water pipe near the 11 and 12th floors. After the earthquake, this hospital received approximately 100 patients, mostly with minor injuries. No disruption of service occurred to this hospital. The NCKU hospital (成功大學醫院) observed very minor damage in the form cracking of brick veneer, however very little concrete cracking underneath.

Figure 6-8: 1200 Bed Chi-Mei Hospital (奇美醫院) (23.02095, 120.22206) (image courtesy of Degenkolb).

7. PERFORMANCE OF LIQUEFACTION SITES

7.1 Summary of Liquefaction Observations

The sites that experienced liquefaction in the Meinong earthquake around Tainan can be grouped into three categories: (1) liquefaction developed in residential areas where ground liquefaction occurred in maturely developed sectors of the city, (2) liquefaction developed in open fields where surface manifestation is not obstructed by manmade improvements, and (3) liquefaction triggered lateral spreading along river banks. This section covers categories (1) and (2) and liquefaction induced lateral spreading sites are covered in Chapter 8. Four specific sites that experienced liquefaction are discussed in this section. They include, the Annan (安南區) Wenhe (文和街), Xinshi (新市), and Xinhua (新化) areas, with the first three sites located in developed residential areas and the fourth site located in an open field. Assessment of ground failure at these sites were evaluated using the Ground Failure Index presented Table 7-1 (Bray and Stewart, 2000); while assessment of structural damage utilized the indices presented in Table 7-2; (modification adopted by Bray and Stewart, 2000; of work by Coburn and Spence, 1992). This chapter focuses on the geotechnical, foundation, and building performance aspect of the liquefied sites.

Index	Description	Interpretation
GF0	No Observable Ground Failure	No settlement, tilt, lateral movement, or sediment ejecta
GF1	Minor Ground Failure	Settlement, D < 10 cm; Tilt < 1 degree; no lateral movements
GF2	Moderate Ground Failure	10 cm < D < 25 cm; Tilt of 1-3 degrees; small lateral movements (< 10 cm)
GF3	Significant Ground Failure	D > 25 cm; Tilt of > 3 degrees; Lateral movement > 25 cm

Table 7-1: Ground Failure Index (after Bray and Stewart, 2000)

Index	Description	Interpretation
D0	No Observable Damage	No cracking, broken glass, etc.
D1	Light damage	Cosmetic cracking, no observable distress to load-bearing structural elements
D2	Moderate Damage	Cracking in load-bearing elements, but no significant displacements across these cracks
D3	Heavy Damage	Cracking in load-bearing elements with significant deformations across the cracks
D4	Partial Collapse	Collapse of a portion of the building in plan view (i.e., a corner or a wing of the building)
D5	Collapse	Collapse of the complete structure or loss of a floor

Table 7-2: Structural damage index (modified from Coburn and Spence, 1992; as used by Bray and Stewart, 2000)

Samples of ejected material were taken at all 4 sites and tested for their physical properties. Table 7-3 summarizes the grain size, plasticity, and USCS soil classification. Figure 7-1 presents the grain size distribution curves. Test results indicate that the ejected materials are predominantly poorly-graded fine sands (SP) and silty fine sands (SM) with fine contents ranging from 6 to 30%. The grain size distribution curves indicate that the ejected soils all have very uniform gradation with C_u (D_{60}/D_{10}) varying between 1 to 3, especially between the 80% and 20% passing range where the curves show very steep slopes. It is recognized that some fines may have been lost during the ejection process, and thus the reported fines may be less than the in-place soils before they were ejected.

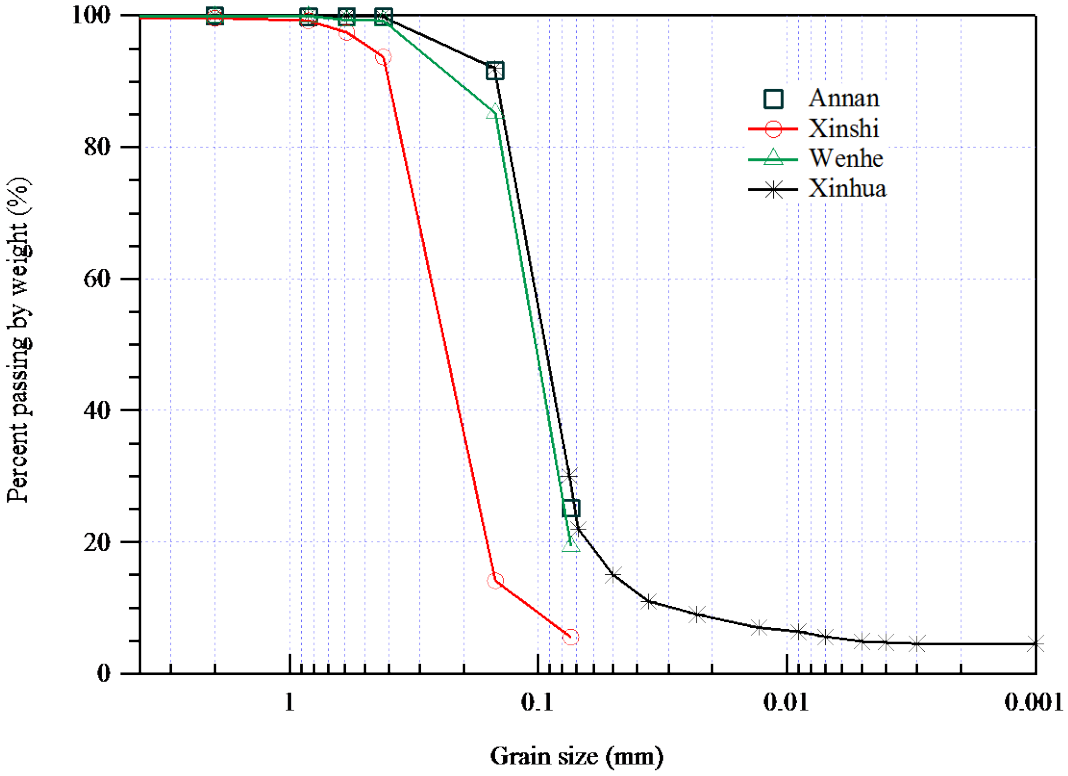

Figure 7-1: Grain size distribution of ejected soils from the 4 sites.

By comparing the liquefied residential sites with the historical pre-development map prepared in 1898 (http://gissrv4.sinica.edu.tw/gis/twhgis/), all three sites are located in areas previously mapped as fish ponds. These ponds were backfilled in the 1970s to 1980s during a rapid economic growth period of Taiwan. The ponds were backfilled at different times, by different developers, and likely using different construction means and materials. While it might be anticipated that during strong shaking each of these sites may liquefy due to their poor quality, the seismic performance of individual backfilled ponds is expected to behave differently during moderate ground shaking. The reduced quality of backfill of these fish ponds is likely responsible for the liquefaction in the residential areas. The areas that experienced liquefaction during the Meinong earthquake are generally isolated and limited to less than 0.05 km^2.

Detailed shear wave velocity profiles were collected using multi-channel analysis of surface waves (MASW) in both liquefied and adjacent non-liquefied areas. The simplified procedure

using V_s correlation by Andrus and Stokoe (2000) is used to identify the liquefied layer. The preliminary results show that the liquefied layers are located at depths of 2 to 6 m below grade, which is the general depth of commercial fish ponds in this area corresponding to the depth ranges of the loose backfill. This is also in agreement with observations discussed herein, which indicate that new buildings constructed with a deeper basement performed well in areas where adjacent older structures without a basement suffered liquefaction induced settlement and associated structural distress.

An emerging issue recognized by this reconnaissance is the need to identify potential liquefiable zones in residential areas. While available geologic and historical planning maps are both good references to help identify potential liquefaction areas, they nevertheless are not accurate enough to describe the liquefaction potential at a small enough scale for an individual property owner. Based on observations from this earthquake reconnaissance, Vs profiling techniques (MASW) provide good data for estimating liquefaction potential. In other words, it can be considered an inexpensive screening tool to delineate areas that need more detailed geotechnical investigations. This method, in conjunction with conventional geotechnical investigations, may be a powerful screening and investigation tool to prepare high resolution liquefaction potential maps in the metropolitan area.

Site	Gravel (%)	Sand (%)	Fines (%)	LL	PI	USCS
Annan	0	75	25	--	NP	SM
Wenhe	0	81	19	26	NP	SM
Xinshi	0	94	6	--	NP	SP
Xinhua	0	70	30	--	NP	SM

Table 7-3: General properties of ejected soils

7.2 Annan Site

The Annan site is located in the Dinshi community of Annan district, Tainan city. Based on the distribution of sand boils and building settlement, the zone of liquefaction of the Annan site is outlined in Figure 7-2. Overlapping the current and the 1898 maps in Figure 7-3, clearly indicates that the liquefaction occurred in the area mapped as an old fish pond, with the two sides of the liquefied boundaries located along the mapped old dike. Field reconnaissance identified differential settlement along the dike as high as 50 cm in some locations.

Figure 7-2: Liquefied zone of the Annan site (23.025585°, 120.207441°).

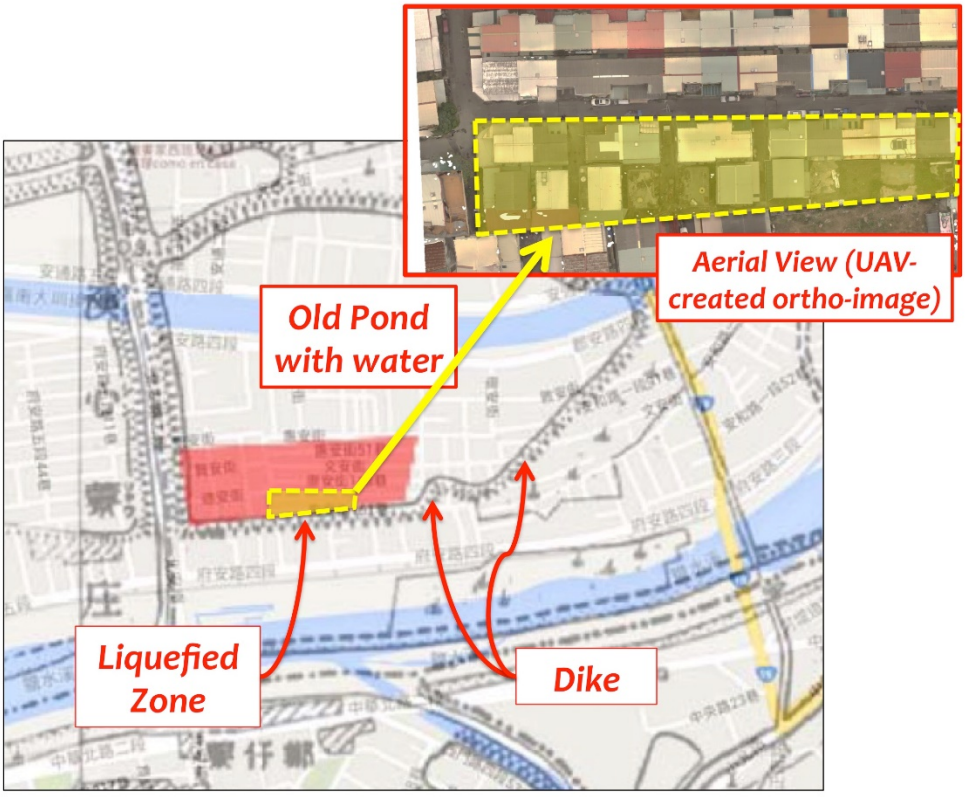

Figure 7-3: Overlap of 1898 map and current Google map at the Annan site (inset denotes location of region presented in damage mapping in Figure 7-6) (1898 map source: http://gissrv4.sinica.edu.tw/gis/tainan_en_us.aspx)

Exterior hardscape evidence of damage was readily visible in the form of pavement cracking; sand boils, and disconnected water supply lines (e.g. Figure 7-4). Liquefaction in this developed area is generally manifest at the surface in several ways: sand ejection along structural perimeter boundaries and along utility lines, building tilting and/or settlement resulting from liquefied foundation soils, and sand ejection along edges of the interior slab (Figure 7-5).

Figure 7-4: Typical failure patterns of pavement crack, breakage of water pipe, and foundation settlement in the Annan district.

Figure 7-6 adapts the ground failure-structural damage mapping used in Bray and Stewart (2000) with a simple color-coding overlaid on individual buildings in a local region most heavily damaged. This map is useful as it provides context to the extent of ground failure as contextualized with foundation damage and its link with physical damage state of buildings in the region. To interpret the map, note that ground failure is delineated via color-coding of the border of individual buildings; while structural damage is delineated via color-coding of the fill used within the building outline.

Several important aspects can be investigated in the context of Figure 7-6. Beginning with the highly dominant blue shading at the exterior building, these long buildings consistently observe little to no structural damage as graded with a structural damage index between D0 and D1; despite the presence of ground failure features, though graded as minor GF1. The pair of photos shown in Figure 7-7 articulates an example of a nominal ground failure graded as GF1, where settlement of the structure is observed; yet at most damage to the structure is only cosmetic in nature (graded as D1); despite the manifestation of settlement, the lack of significant structural damage is likely due to the well connected and continuous foundation of this building. Moreover, no building extensions were noted in these buildings. In contrast, structures within the interior of the damage map shown in Figure 7-7 demonstrate significant structural damage (graded as yellow through red or D3->D5), these excessive structural damage regions of the district were mostly associated buildings with structural discontinuities primarily at the foundation, and often associated with light-weight single story addition regions.

Figure 7-5: Liquefaction surface manisfestation in the Annan District (23.025697, 120.207138).

Figure 7-6: Assessment of ground failure – structural damage index (A, B, C denote images shown in Figures 7-7, 7-8, and 7-9, respectivley). (center of region at: 23.0254°, 120.2074°).

Figure 7-8 provides a perspective view from the southeast looking onto several buildings where clear evidence of liquefaction in the field is noted as visible in the bulging of exterior slabs (center of image) and rotation of light-weight screen fences (left of image), surface sand boils (in field and elsewhere). The pair of buildings on the left of this image observed ground failure features at their exterior classified as moderate to severe (GF2-GF3; while their resulting structural damage was graded as heavy (D3; significant damage to load bearing elements); as is evident from views on the opposing side (not shown here); in stark contrast, the long building on the right, likely of similar weight, and with surrounding ground failure characterized as minor, observed only very minor cosmetic damage. Its foundation and structural system were continuous and no additions were observed along the exterior of this building, which may be why this building suffered no damage despite the visible surrounding ground failure.

Figure 7-7: Example of mapping GF1-D0 (or GF1-D1). (23.025561°, 120.207827°).

Figure 7-8: Example of mapping GF1 through GF3; demonstrating various structural damage states. (23.025409°, 120.207565°).

The sequence of images in Figure 7-9 articulates severe ground failure and corresponding structural collapse. For reference, a pre-earthquake image obtained from Google streetview is shown in Figure 7-10. This alleyway, though narrow; provides a perspective of a number of important features. In Figure 7-9, to the left an excessively tilting and settling building, within the middle a single story (high-bay) addition is visible. The middle single story (high-bay) addition is attached to a 3-story structure on the right, which suffered excessive settlement on the

order of more than 30cm. The lightweight single story high-bay structure, which shows significant distortion, is subject to significant shear strain imposed due to its attachment to the main residence to the right, which is clearly at a state of collapse; as is the building suffering excessive rotation (~5 degrees to the West and ~3 degrees to the South). The building on the left in this image sequence experienced differential settlement between the perimeter footing and outside pavement greater than 75 cm (see right image in Figure 7-9). The alley generally heaved about 30cm between the settling buildings on either side. To gain perspective on this scene, a suite of LiDAR scans was collected at this site (near the image denoted as C in Figure 7-6); the 3D model generated from these scans may be found in Report Part 2 documenting this event.

Figure 7-9: Example of mapping worse case ground and structural damage combination (GF3-DF5). (23.025442°, 120.207400°; Lane 161, Hui'an St)

Figure 7-10: 2014 Pre-earthquake street view from Google. (view shown of Alley structures of Figure 7-9; 23.025442°, 120.207400°)

A common theme in this region and others impacted by liquefaction is that, perimeter footings, if continually connected, performed well even though the building experienced significant

differential movement as manifest in observations of the surrounding soils (e.g. Figure 7-11). In contrast, unreinforced slabs not tied to the foundation heaved and suffered complete disconnection in some cases in response to surrounding liquefaction (Figure 7-12). Perimeter footings connected with adequately reinforced grade beams generally performed well, even with structures that experienced significant displacement. Figure 7-11 shows that although the ground heaved more than 30 cm outside of the front door of this residence, no structural cracks were observed on the interior walls nor distorted window frames. In this situation, settlement of the building was fairly uniform, rendering very little to no differential displacement onto the structure. Meanwhile ejected sand was observed along slab edges.

Figure 7-11: Building that survived liquefaction-induced settlement and ground heave (23°01'31.5"N 120°12'25.8"E).

Figure 7-12: Damaged unreinforced slab in liquefied soil of the illegal expansion behind the building shown in the left portion of Figure 7-9 (23.0253°, 120.2074°).

MASW surveys were conducted on 2016/02/24 along Lane 161, Hui'an St. The V_s profiles are measured near the building in Figure 7-9 and along the outside of the East boundary of the liquefied zone shown in Figure 7-2. These Vs profiles, along with the liquefaction analysis using the Vs correlation are shown in Figure 7-13. Note that the ground water table is estimated at the depth of 2.3 m below the surface; as inferred from the Vs profile and confirmed by local residents. A peak ground acceleration (PGA) of 0.18g and M_w of 6.4 are used in this analysis. These results indicate that the liquefied layer is located at depths from 2.3 to 6 m. The non-liquefied zone has ample factor of safety over 1.0 at all depths. These results agree with the performance of subsoils and the history of the site.

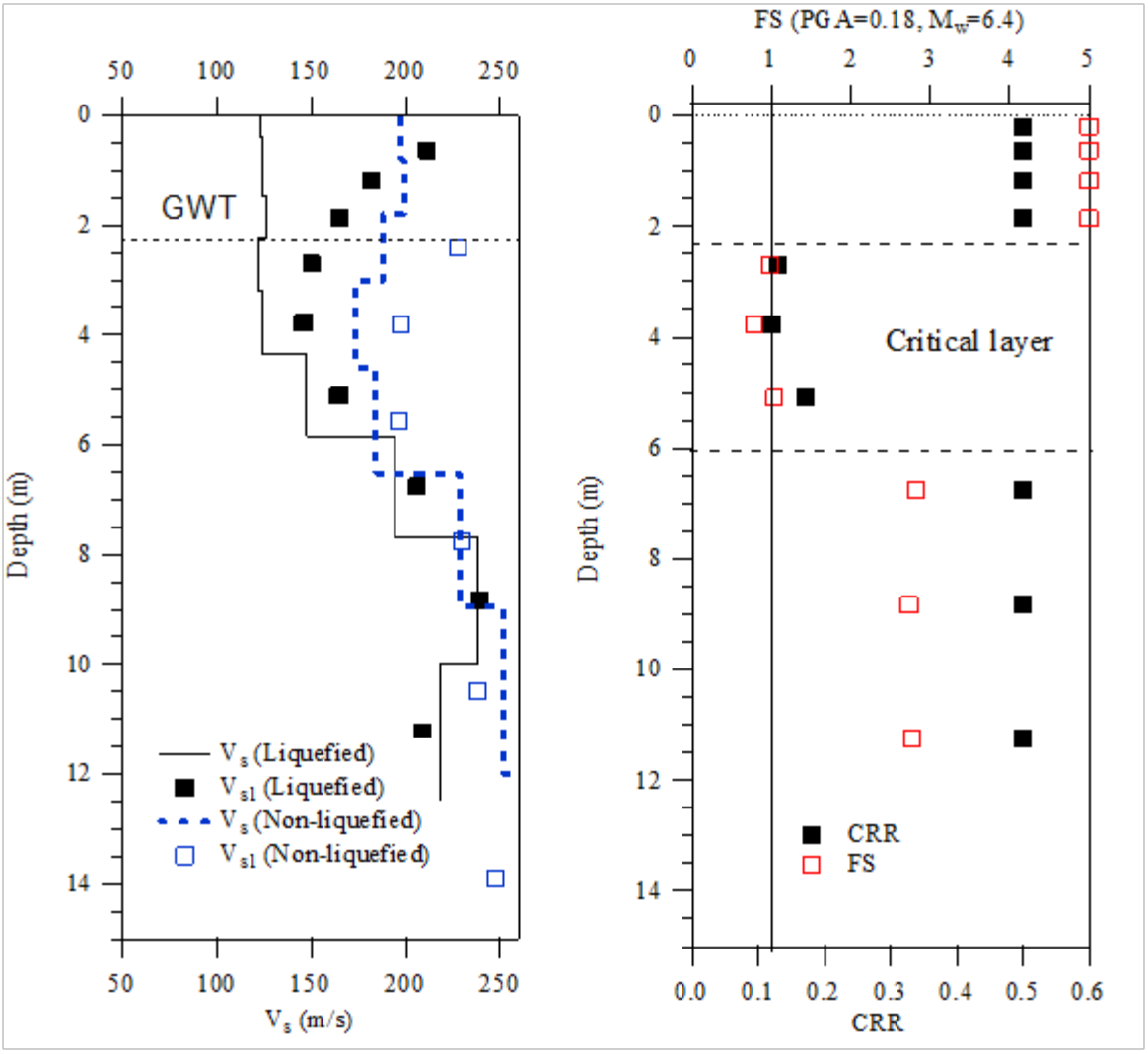

Figure 7-13: Vs profiles and liquefaction analysis of Annan site.

7.3 Wenhe Site

The Wenhe site is located in the Wenxian community of central-west district, Tainan city. The liquefied zone of the Wenhe site is marked in Figure 7-14. Figure 7-15 shows the area overlain by the 1898 map clearly indicates that the liquefaction occurred in the old pond/ water area and the two sides of liquefied boundaries coincide with the old dikes. Field reconnaissance shows that the differential settlement along the dike could be up to 40 cm. The most severe damage occurred at No. 88 and 84 of Wenhe St. A total of 10 older, generally brick or concrete wall-type construction buildings and one reinforced 3-story residential structure suffered severe damage and as shown in Figures 7-16 and 7-17. The differential settlement along the liquefied boundaries was noted to be as large as 30 cm at the corner of the 3-story red building near the steps as shown on Figure 7-17. Figure 7-18 shows that the 3-story building in Figure 7-17 tilted approximately 4 degrees as a pronounced structural hinge developed vertically along the buildings 3-story to 2-story (newer to older) interface. While the most severe damaged area is relatively compact and in close proximity to the location where Figures 7-16 through 7-18 are

shown, the general neighborhood showed evidence of cleaned up sand ejection along the perimeter of many buildings with minor differential settlement between the pavement and the edge of the building (usually less than 1 to 2 cm).

Figure 7-14: Liquefied zone of Wenhe site.

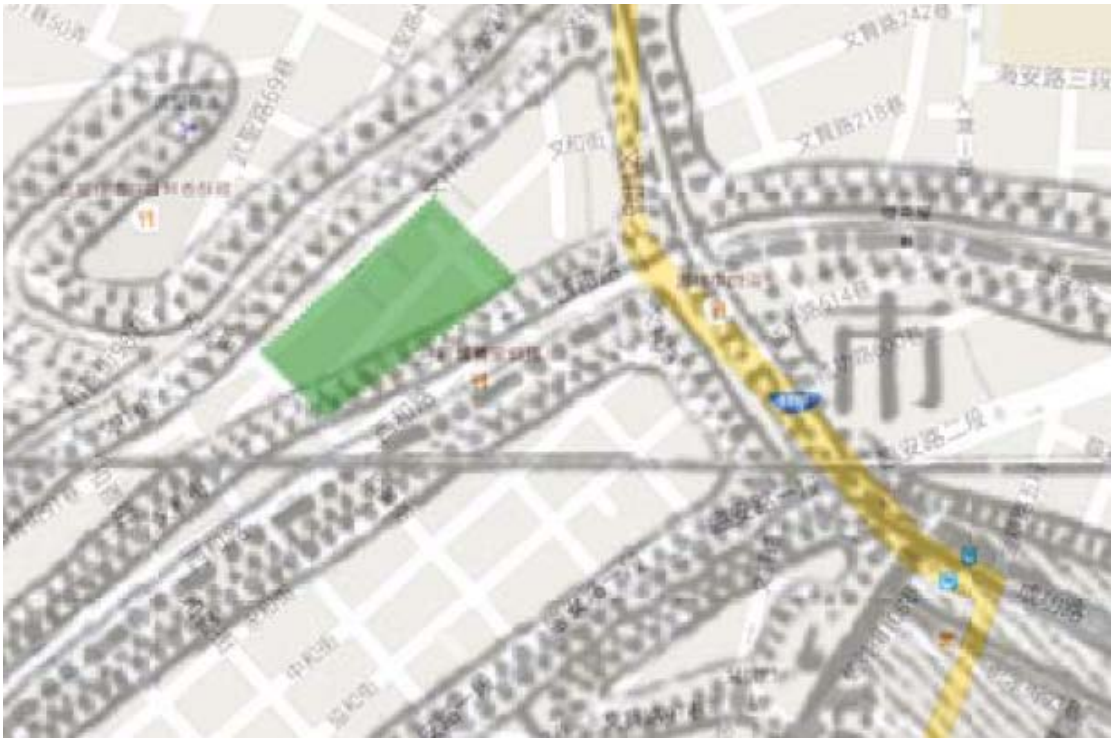

Figure 7-15: Overlap of 1898 Map and Google Map at Wenhe site (source: http://gissrv4.sinica.edu.tw/gis/tainan_en_us.aspx).

An MASW survey was conducted on February 27, 2016 along Wenhe St. at an interval of 40 m distance. The Vs profiles at locations marked on Figure 7-14 are shown in Figure 7-19. The Vs profile shows a test site in the liquefied zone (point No. 88 on Figure 7-14) and another test site located outside the liquefied east boundary (Figure 7-14). The ground water table as inferred from the Vs profile and confirmed by local residents, is estimated to be at depth of 1.0m. A PGA of 0.18g and M_w of 6.4 are used in the liquefaction analysis. For the Wenhe site, the liquefied layer is identified at depths from 5 to 8 m. The liquefied layer becomes deeper toward the east. Tests performed at non-liquefied sites also have a low shear wave velocity layer from 8 to 11 m deep with factors of safety against liquefaction close to 1.0. The effect of building rocking on the manifestation of liquefaction at borderline liquefaction sites is possible but needs further investigation.

Figure 7-16: Damage features at the Wenhe site (23°00'12.7"N 120°11'30.5"E).

Figure 7-17: Severely tilted building in Wenhe Street and adjacent alley with significant expression of hardscape liquefaction features (23°00'12.7"N 120°11'30.5"E).

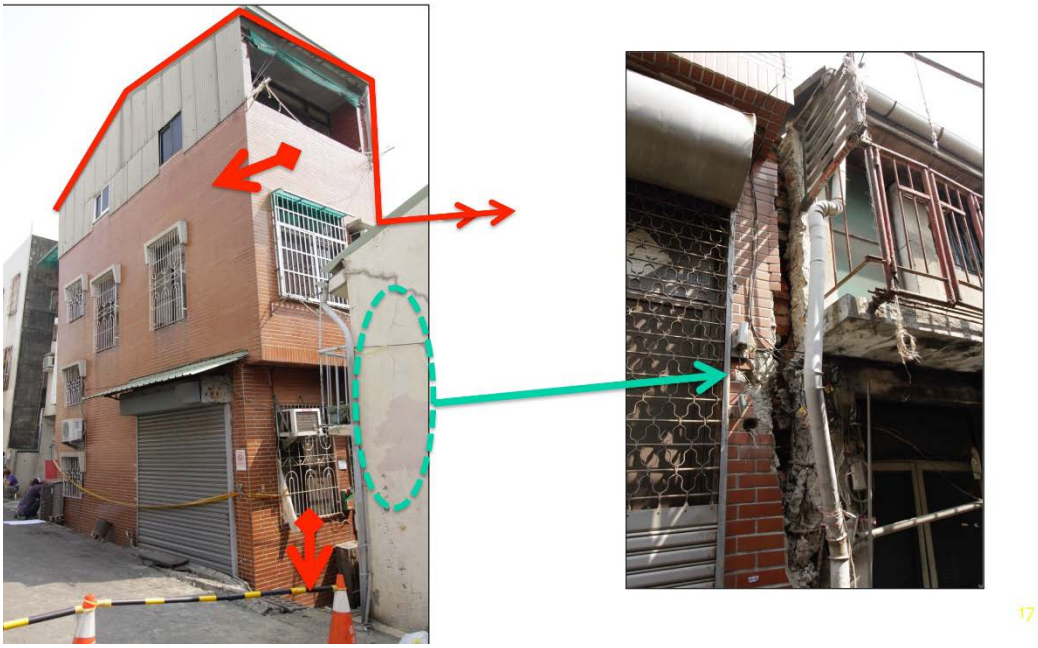

Figure 7-18: Approximately orthogonal perspective and local view (left and right respectively) of the damaged building shown in Figure 7-17; note the well delineated structural hinge that developed along the brick-concrete interface of the right image (older portion of structure on right). The green denotes that the image on the right is taken behind the building. (23.003471°,

120.191852°).

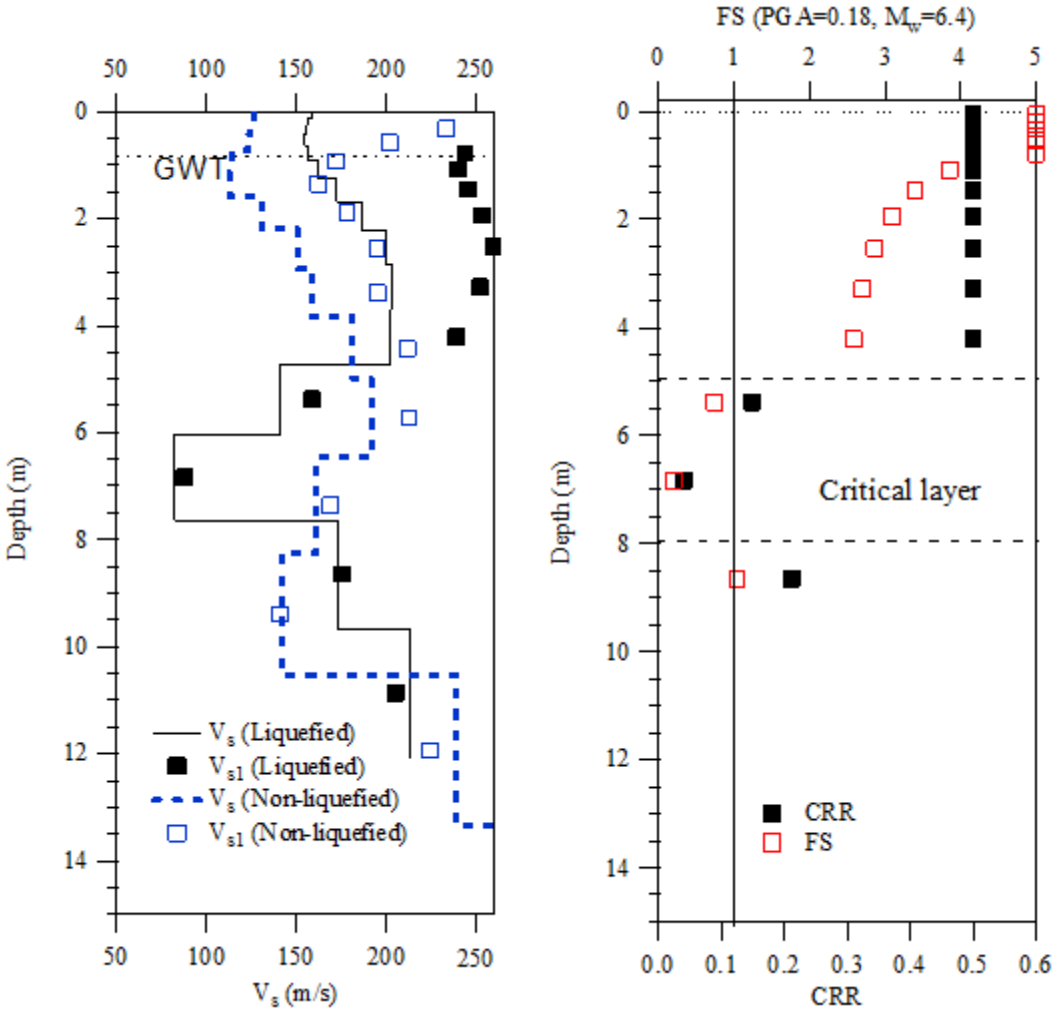
GWT
Depth (m)
V_s (m/s)
V_s (Liquefied)
V_{s1} (Liquefied)
V_s (Non-liquefied)
V_{s1} (Non-liquefied)
FS (PGA=0.18, M_w=6.4)
Critical layer
CRR
FS

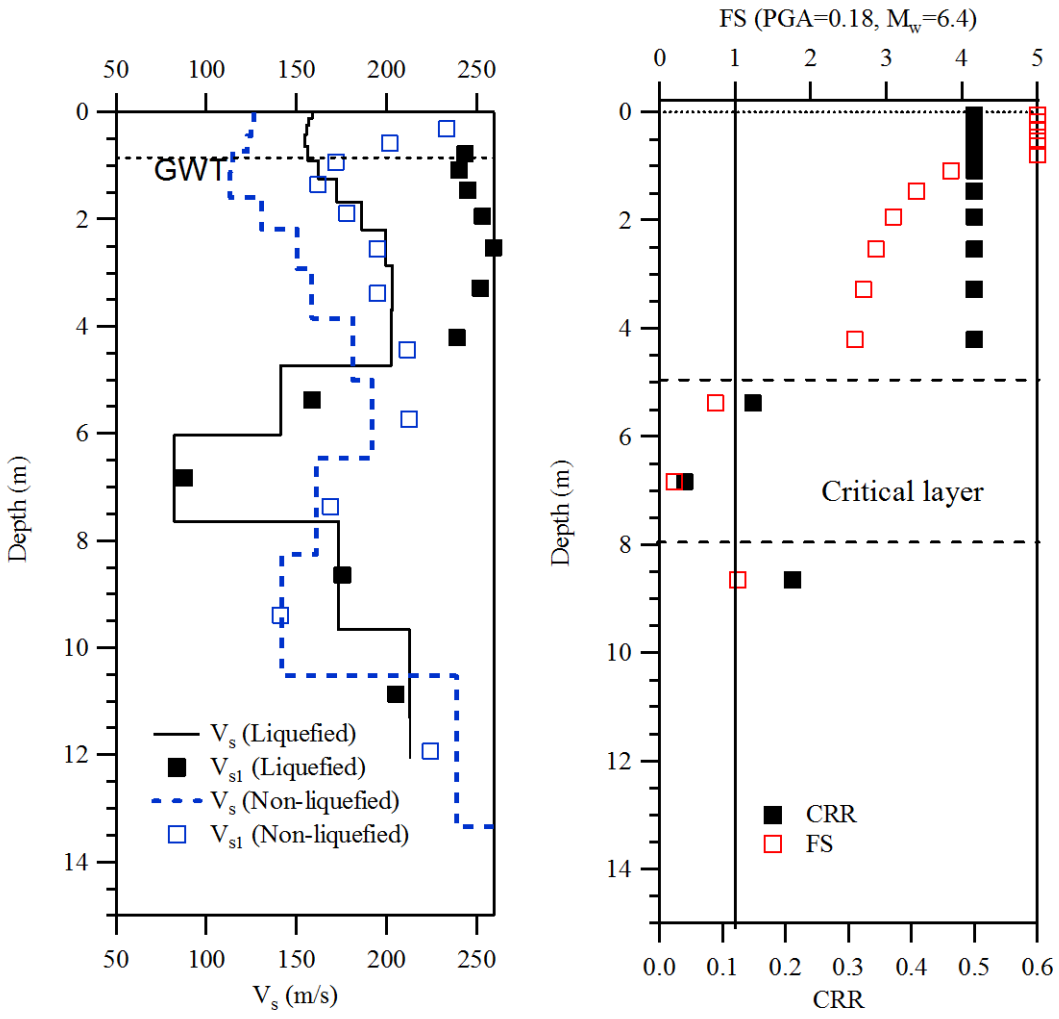

Figure 7-19: Vs profiles and liquefaction analysis at the Wenhe site.

7.4 Xinshi Site

The Xinshi site is located in Lane 50, Sanmin St. of Xinshi district, Tainan City. The liquefied zone of the Xinshi site is marked as shown in Figure 7-20. Figure 7-21 shows this region with a 1921 map. It can be see that the liquefied zone occurred in a triangular shaped area of an old pond/ water area and the two sides of liquefied boundaries coincide with the old dike. Field reconnaissance shows that the differential settlement along the dike could up to 30 cm. All of the buildings within this triangle zone were constructed by the same company in 1989 with spread footings connected with perimeter grade beams as foundation. According to one of the building owners, the triangle area was a fish pond before it was backfilled for residential development.

Figure 7-20: Approximate liquefied zone of the Xinshi site.

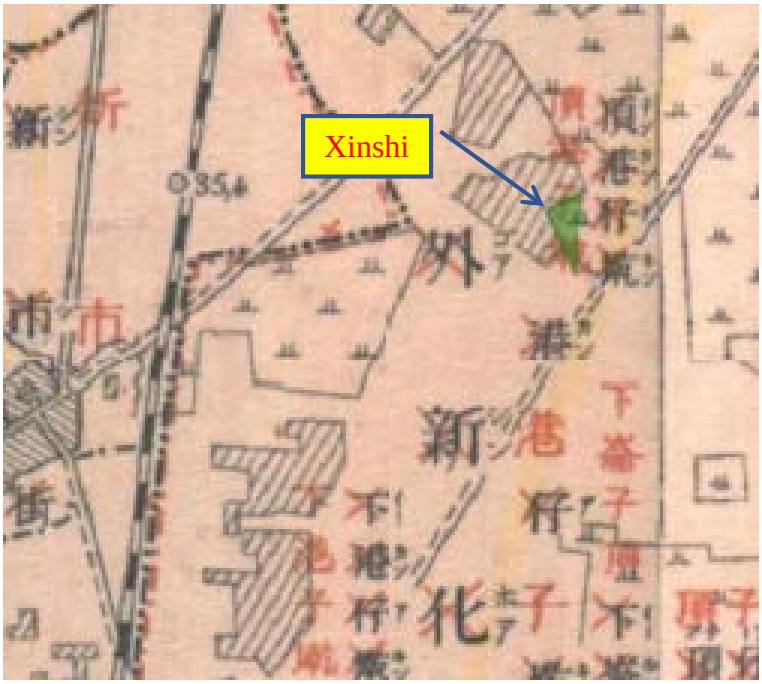

Figure 7-21: 1921 map at the Xinshi site (source: http://gissrv4.sinica.edu.tw/gis/tainan_en_us.aspx).

Liquefaction in this area was widely evident, with building settlement and extensive pavement heave both within garage/carports and along exterior hardscape/pavement. The average differential displacement was about 60 cm within the entire triangular region. The boundaries of the old pond can be located at the fire lane and the garage along Alley 10 of Lane 50 (Figure 7-22). Differential settlement along the fire lane was measured to be about 25-30 cm. Most of the ejected sands had been removed when the team arrived, however ground settlement was estimated from ground heave (Figure 7-23) and differential settlement along the edges of buildings. While most of the multi-story residential buildings were constructed in a modern era, illegal add-ons were common. In this neighborhood, additions consisted primarily of carports or front porches added to the front of the buildings or kitchen extensions added towards the back. These add-ons usually are not structurally connected to the main building and thus suffered greatly from differential ground movement resulting from liquefaction even through the buildings sustained only minor and repairable damages (Figures 7-24 and 7-25). The excessive moment of unconnected foundations at this site resulted in large strains induced in supporting beams of the carport and other structures; as shown in Figure 7-26. This form of damage necessitated the demolition of the extensions. At the time of the GEER team visit, demolition of one of the car ports columns was being conducted, and it was noted that the column supporting the car port lacked a foundation and structural connection to any adjacent foundations (Figure 7-26).

Most of the main building structures performed well and were occupied at the time of the teams visit, although the area suffered from extensive liquefaction. The most obvious damage occurred at the car port area were the unreinforced slabs covering the car port heaved and cracked (Figure 7-27) yet the main structure connected to this damaged car port suffer only minor damage and the building itself only tilting about 0.5 degrees. In a building the team was able to enter, the 4-in-thick unreinforced slab heaved over 60 cm (Figure 7-28). It is worthwhile to note that in Figure 7-28, despite the building settlement and heaved ground, the perimeter grade beam connected shallow footing apparently performed well and held the main building structure together with no visible cracking expressed on the brittle brick infill walls nor broken windows or jammed doors.

Figure 7-22: Damage to buildings at the Xinshi site (left: fire lane with expressed surface manifestation and building settlement and right: garage expressing significant hardscape damage).

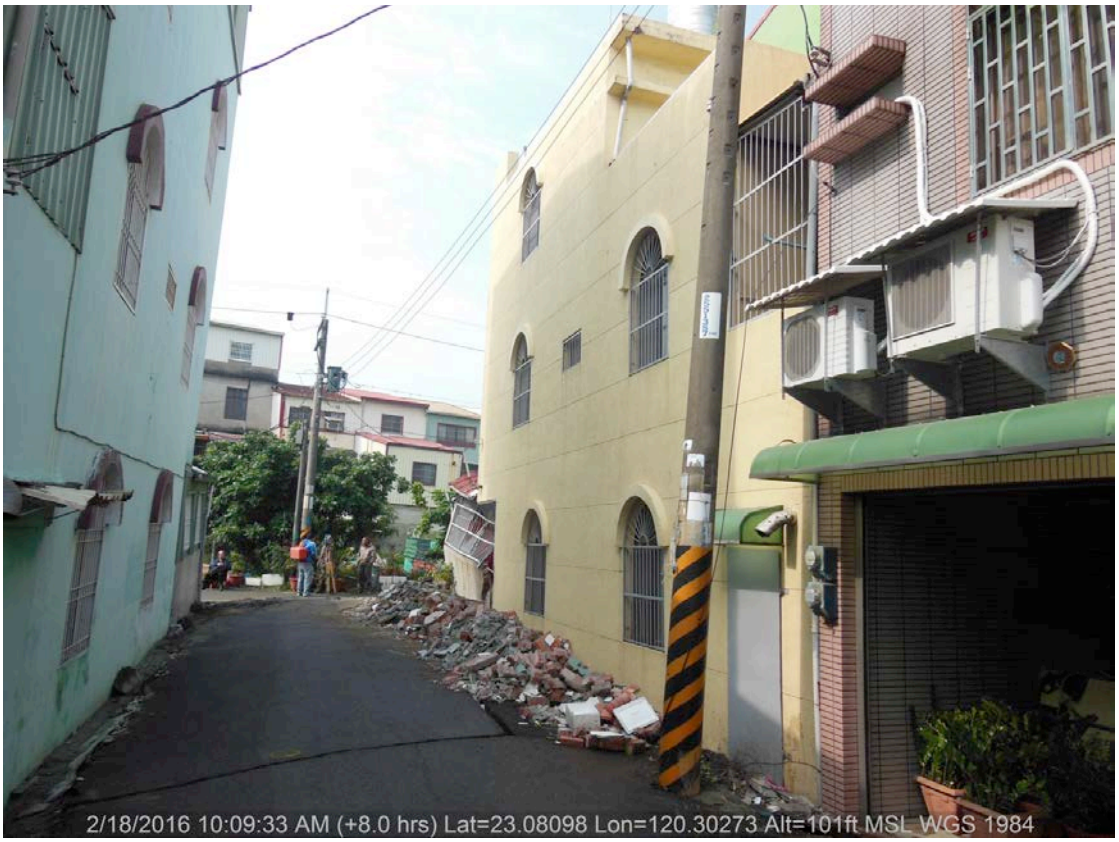

Figure 7-23: Ground heave along an alley between two settling buildings (23.08098, 120.30237).

Figure 7-24 Damage to illegal add-on car port (23.08096, 120.30258).

Figure 7-25: Structural hinge mechanism developed due to movement of unconnected foundations at carport add-ons at the Xinshi site. (23.08096, 120.30258).

Figure 7-26: Structural column at the interior of a garage, note the lack of foundation support (23.08096, 120.30258).

Figure 7-27: Damaged unreinforced car port slab due to ground heave (23.08099, 120.30241).

Figure 7-28: Heaving of Unreinforced Interor Slab (23.08135, 120.30233).

The ground failure index assessment for this region is shown on Figure 7-29. The GF3 zone is controlled by total settlement. In the surrounding area, no visible signs of liquefaction were observed.

Figure 7-29: Ground failure index assessment of Xinshi site (By C.C. Tsai).

An MASW survey was conducted on February 27, 2016 at the center of the triangular area and along Alley 10 (Figure 7-23) with the exact test locations shown on Figure 7-20. The measured Vs profiles at the 2 marked locations are shown on Figure 7-30. Two low Vs layers were detected in the upper 20 meters. The ground water table at this site is 1.0 m below the ground surface. The first low Vs layer is located at depths between 2 to 5 m and most likely represents the loose backfill zone that is very susceptible to liquefaction. The other low Vs layer was identified at depths between 7 to 10 m. However, MASW is incapable of differentiating material property; the low Vs may represent a clayey soil layer according to the regional geologic well log not drilled at the same location. Whether the deeper low Vs is a loose sand layer susceptible to liquefaction or a soft clay layer not susceptible to liquefaction can only be confirmed with a tradition geotechnical investigation to be performed at a later date.

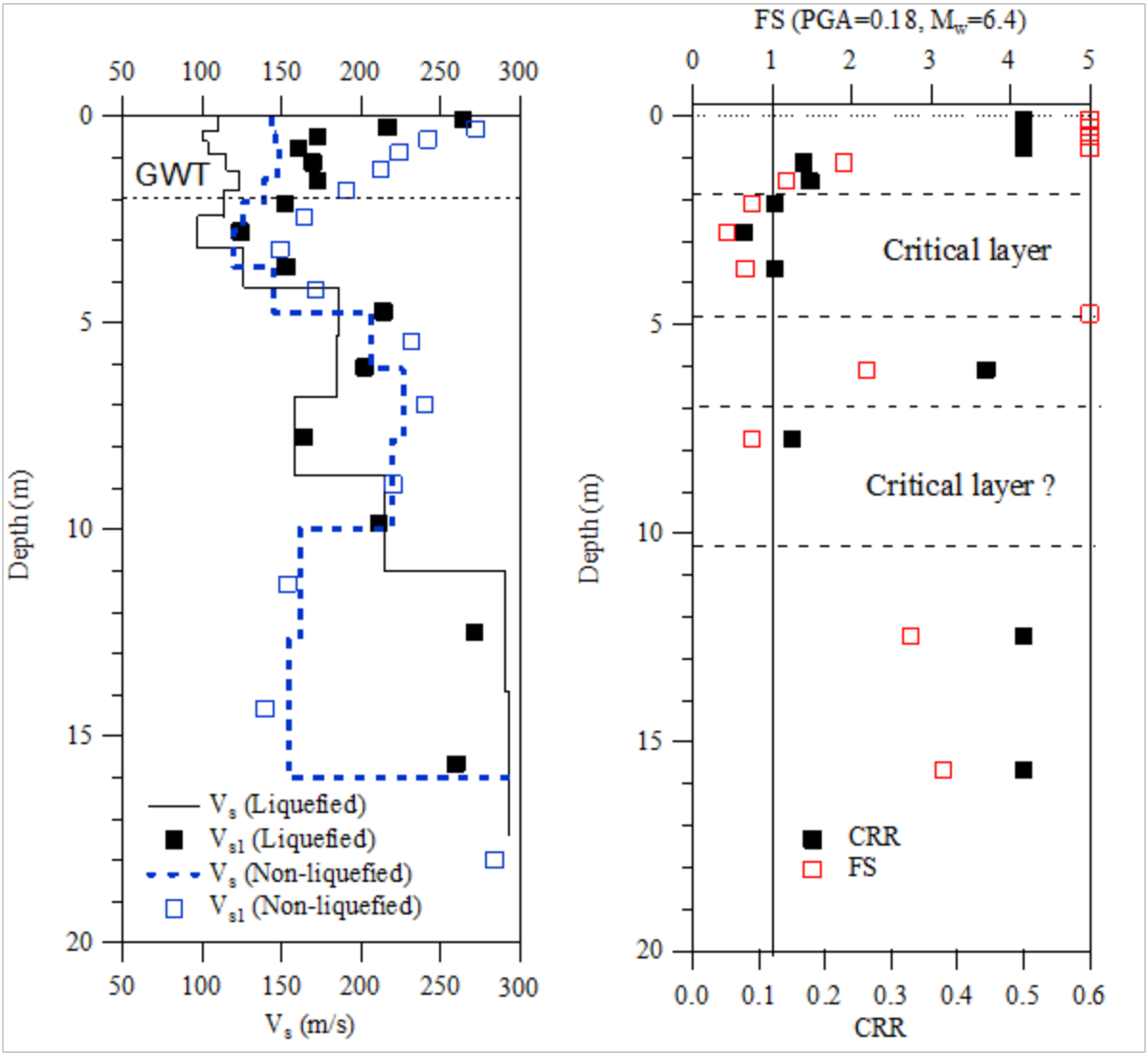

Figure 7-30: Vs profiles and liquefaction analysis of Xinshi site.

7.5 Xinhua site

The Xinhua site is located at Beishi village, Xinhua district, Tainan city. According to Chang et al. (2011), this site liquefied in the 1946 Xinhua earthquake, and the 2010 Jiasian earthquake (Figure 7-31). This same area liquefied again in the Meinong earthquake in 2016 for the third time in documented history. Sand boil crests were randomly spread within a 500 m long and 250 m wide paddy and sweet potato field. The closest distance of observable sand boiling crests to the viaduct of the Taiwan high-speed railway (THSR) was only 50 m (Figure 7-32). Although sand boiling crests were discovered on both sides of the THSR, the close distance was no less than 50 m from the viaduct, which was supported by pile groups, with piles extending to 60 m below the ground surface. This site would be an ideal study location for investigating soil-pile interaction in liquefiable soil stratum.

Due to its wide-open nature and limited infrastructure, this area observed quite distinctly visible surface manifestation of sand boils following this earthquake. Within the open field at least 20 major sand boils with diameters in excess of 1 meter were visible (Figures 7-33 and 4-34). One of the sand boils suggests multiple ejecta, likely manifest from aftershocks (Figure 7-35).

Detailed soil conditions at the Xinhua site can be found in Chang et al. (2011). The groundwater table in this area is about 1.3 m below grade. The liquefiable layer is located between 3 to 9 m deep in a silty fine sand (SM) layer with fines content from 15 to 80% (Figure 7-36). The near surface non-liquefiable silty clay cap contributed the near perfect sand boils manifestation in this area. Liquefaction analyses using SPT-N values, CPT-qc and Vs are shown in Figure 7-37. This will be a good site to install a downhole array for studying the effects of fines content on liquefaction triggering and boundary effects of pore pressure accumulation.

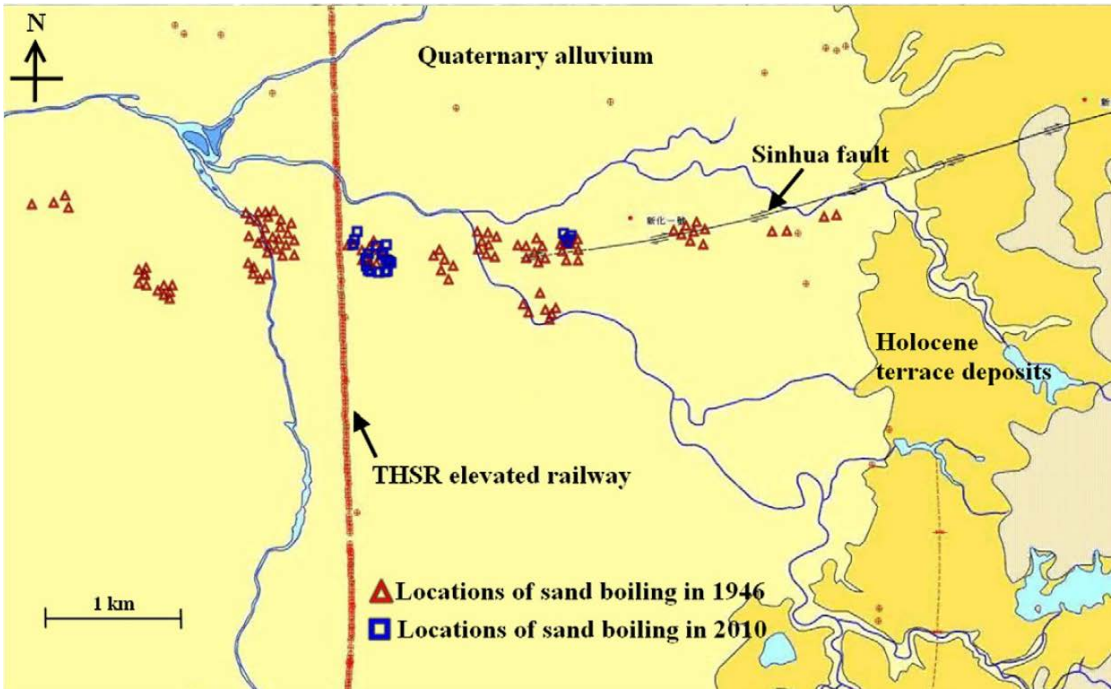

Figure 7-31: Geologic setting and sand boil locations of 1946 and 2010 earthquakes (Chang et al. 2011).

Figure 7-32: Open Field Liquefaction in Xinghus (THSR Viaduct in Background) (23.05081, 120.29111).

Figure 7-33: Sand Boil in Xinhua (23.05007, 120.29082).

Figure 7-34: Sand Boil in Xinhua (23.04999, 120.29081).

Figure 7-35: San Boil in Xinhua (23.04971, 120.29091).

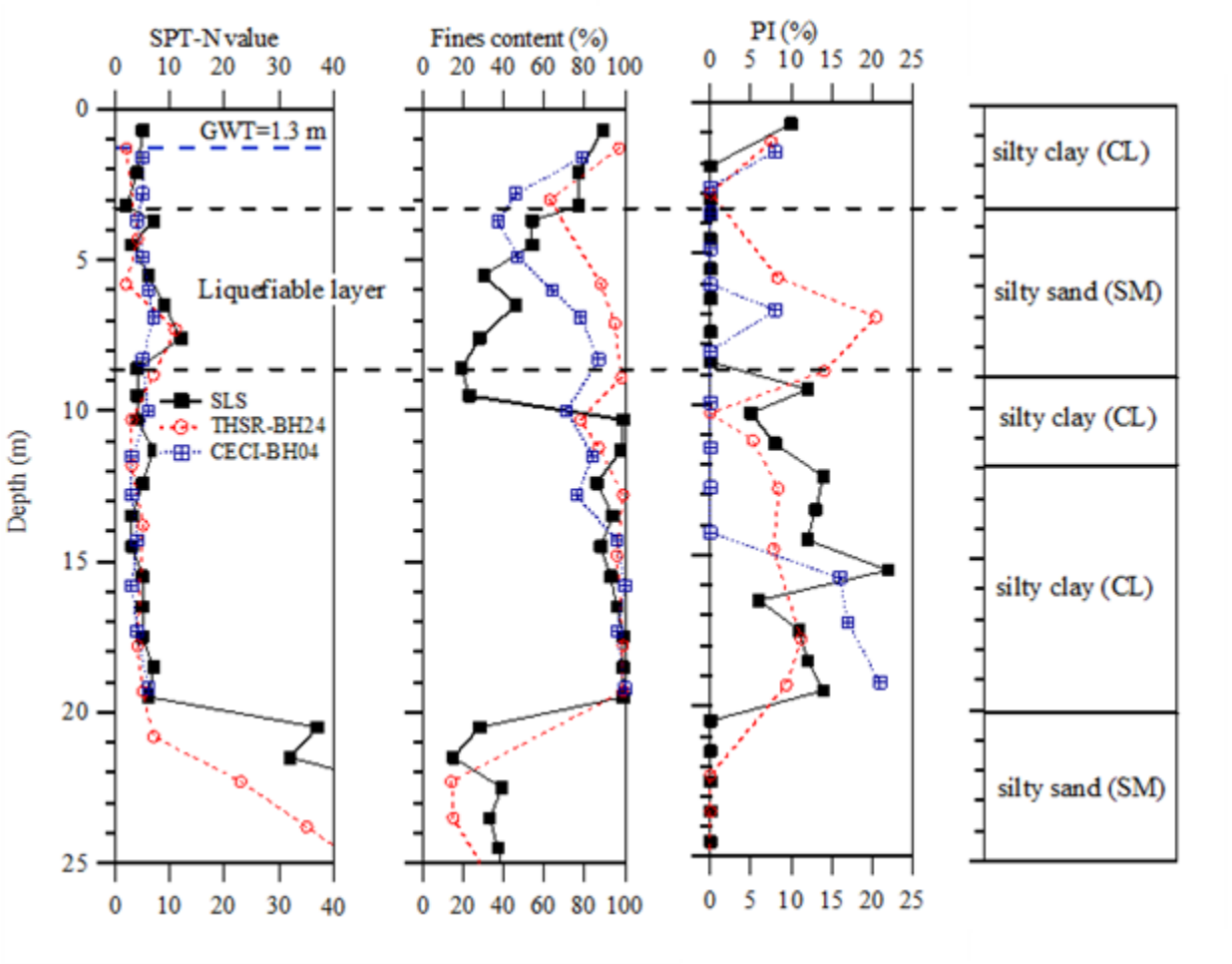

Figure 7-36: Compiled Borehole Logs and Soil Layers (Chang et al. 2011).

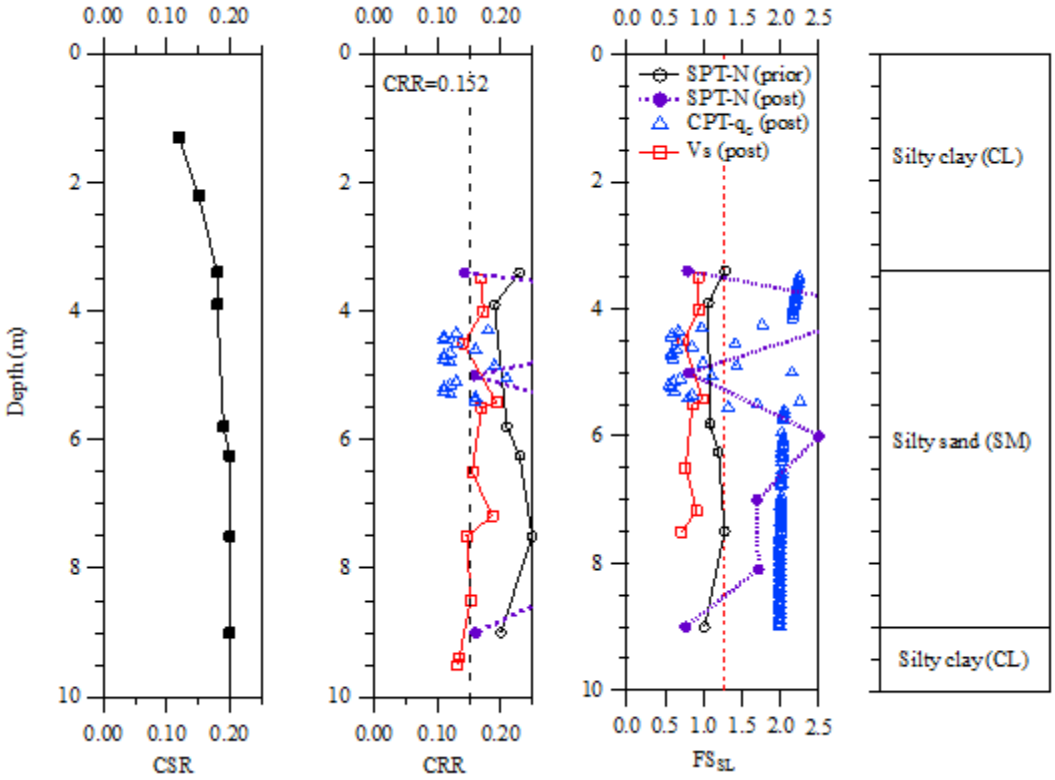

Figure 7-37: Liquefaction Analysis of Xinhua Site.

8. PERFORMANCE OF SLOPES

Slopes generally performed well during the February 6, 2016, Meinong earthquake, however, several large slope failures did occur including, four along the Tsengwen river and one at the Nanbao golf course. Three of the four failures along the Tsengwen river bank occurred along the northern designed Rixin levee with the fourth failure occurring upstream (north-northwest) of ErXi bridge. Two of these failures occurred in areas protected by concrete facing and two occurred along graded slopes. The post failure appearance and configuration indicate these river bank failures had large lateral displacements, a blocky non-liquefied soil cap over a saturated and seeping base, and very gently dipping slide planes, all of which are characteristics of liquefaction induced lateral spread failure. The failure at the Nanbao golf course, on the contrary, shows the slide mass moved in a more coherent manner without much internal deformation of the slide mass. The slide mass failed toward a creek bank without much translational movement but as a more traditional rotational slope failure.

8.1 Rixin Levee Failures (日新堤岸滑移破壞)

During the February 6, 2016 Meinong earthquake, three sections of the Rixin levee (日新堤岸) along the northern bank of Tseng-Wen river failed along a 800-m stretch near where the river crosses under the Freeway No.3 bridge in Guantian (官田區) District, Tainan (23° 9'12.40", 120°20'37.68"). All three failures lie on the erosional bank (active margin) of the meandering river that is contained by the Rixin Levee. Two of the three failures have either partial or complete concrete slab slope protection and the third failure had no concrete slope protection. In this report, the three failures are numbered Nos.1, 2, and 3 from north-west to south-east or in the upstream direction as shown in Figure 8-1. The height of the levee is estimated to be about 5~7 meters measuring from the levee crest to the toe of the failed surface. Aerial photo comparisons of the levee before and after the earthquake are shown in Figure 8-2.

8.1.1 Rixin Levee Failure No. 1

Failure No. 1 occurred in a graded levee embankment about 70 meters downstream from the Freeway No. 3 bridge crossing (Figures 8-3 and 8-4), at: Lat: 23° 9'13.23", Long: 120°20'34.98". The failure width measured along the scarp is about 135 meters (Figures 8-5 and 8-6). The run-out distance (top of levee scarp to the toe of the sliding body) is about 135 meters (Figure 8-5). The landslide toe blocked the 50 m wide actively flowing river, and temporarily formed a debris dam.

Soil boring information was made available to the GEER team for a pipeline river crossing located about 500 m downstream (northwest) of failure No. 1. This borehole is located on the northeast side of the pipe crossing (closest to failure 1) and its log (Figure 8-6) shows that the subsurface soils consists of loose brown silty fine sand with uncorrected blowcounts varying between 6 and 9 extending to 5.5-m deep followed by a firm to stiff gray silty clay layer interlayered with medium dense to dense fine sands (Figure 8-7).

Near the base of the slide, within the scarp, an elevated water table was observed with water actively seeping at the contact with the dark grey firm to stiff clayey silt and the levee fill. The

discharged water created a small depositional fan at its discharge point (Figure 8-8). It is believed that failure of the levee originated from liquefaction of the saturated material along this contact.

The southeast margin of the head scarp is influenced by the presence of the bridge piers, which prevented the failure from extending further to the southeast (Figure 8-9). However, in the vicinity of the bridge piers, we did notice arcuate cracks extending to the bridge pier (Figure 8-10) and behind the piers (Figure 8-11). Settlement of the soil around the piers measured 4 to 5 inches (Figure 8-12). Minor sub horizontal shear cracks were notice on both piers but the cracks appear to be dull and filled and thus may not be related to the earthquake.

8.1.2 Rixin Levee Failure No. 2

Failure No. 2 is located about 400 meters upstream of the Freeway No. 3 bridge (23° 9'3.26", 120°20'47.59"). The width of the landslide along the head scarp is about 160 meters and the landslide length is 109 meters from scarp to toe (Figure 8-13). The landslide mass also temporarily blocked the river forming a landslide dam (Figures 8-13 and Figure 8-15). The levee fill material is mainly a mixture of predominantly loose silty sand with gravel. An unreinforced concrete slab protected the embankment prior to failure and is visible as detached blocks near the landslide toe (Figures 8-14 through 8-17). Near the levee toe, the slope is generally flat at 5:1 (H:V) to 10:1 (Figure 8-17).

Based on a review of Google Earth historical photos (Figure 8-18 through 8-23) it appears that the area close to failure No. 2 has experienced multiple slope failures and multiple repairs in the past. We confirmed with the local engineer that prior to the earthquake; this section of the levee failed during a heavy storm event in June 2012 and was later repaired.

At the time of our visit the GEER team noted an emergency repair was made by dumping sandy fill from the levee crest without compaction (Figure 8-24). If the original construction was performed similar to the emergency repair, such construction methods produce very loose fill that are easily erodible, susceptible to liquefaction during earthquakes and even to a static failure during extreme storms amidst increase groundwater levels in the levee fill.

On the outside margin of the levee, the ground elevation is closer to the levee crest and heavy irrigation water is used for farming. This elevated high water table forces a positive seepage to flow through the levee's sandy fill, saturating the base of the fill because the dark grey clayey silt below the fill serves as the aquitard that prevents the groundwater from infiltrating further into the ground. This saturated zone of sandy fill is susceptible to liquefaction and will have lower strengths when the water table in the fill is high during storms. The source of past performance issues are due to extreme storms and earthquake triggered liquefaction lateral spread.

A pile foundation was installed at the toe of the levee between Failure 1 and 2 to protect the water conservancy facilities and the factory behind the levee. This pile enhanced section of the levee survived the earthquake with only minor damage.

8.1.3 Rixin Levee Failure No. 3

Failure No. 3 occurred in an unprotected levee about 670 meters upstream from the Freeway No. 3 bridge crossing (Figure 8-26, location: 23° 8'55.24", 120°20'52.46"). The width of the landslide measured along the levee crest is about 96 meters and the length of the landslide is 92 meters measured from scarp to toe. The slide mass also blocked the river and temporarily formed a small debris dam (Figure 8-27). Levee materials observed here are artificial fill composed of alluvial gravel, sand and clay. The road behind the landslide crown was not damaged and the scarp is about 2 meters in height. Within the slide mass, seepage flow and ponding was noticed indicative of a high ground water level behind the levee (Figure 8-28).

8.1.4 Rixin Levee Conclusion of Observation

All three failures did not appear to be conventional slump type slope failures characterized by a toe bulge with limited lateral movement. The failures observed at all three levee sites appear to be caused by movement on a very weak layer that liquefied during the Meinong earthquake. The basal failure plane was very gently dipping but produced large lateral displacements of between 30 to 60 meters. The damage and displacement pattern is in agreement with a liquefaction triggered lateral spread observed in past earthquakes. Failure of all three levee embankments likely took place along the saturated contact between the base of the fill and the underlying dark grey impervious silty clay.

The adverse condition could be resolved if extended retrofit and drainage control is performed for the levee embankment. One example successfully used along this section is by installing piles at the waterside levee toe (Figure 8-29).

8.2 ErXi Bridge Levee Lateral Movement (二溪橋堤岸側移)

On the right (west) bank of YenSwei River approximately 770 m upstream (north northwest) of ErXi bridge in Danei District (大內區), liquefaction likely contributed to the distress of a section of concrete slab levee protection (Figure 8-30). Location of this distressed zone is approximately Lat: 23.120964, Long: 120.379392. The total distressed zone measures about 120 meters measured along a previously repaired section of the levee with added riprap protecting the toe. The concrete slab distress occurred along the contact between the horizontal slab protecting the crest and the slab protecting the embankment. The horizontal separation is about 30 cm (Figure 8-31). Some of the separation occurred along a newly replaced section where limited re-bar can be seen to connect the horizontal and inclined slabs. Observation of the rebar indicates that it does not have adequate bond length (less than 5 cm) and wa pulled from the inclined slab. In some areas, there was no rebar connecting the horizontal and inclined slabs. Minor buckling and shear cracking was also observed on the newly placed inclined slab (Figure 8-32 and 8-33) as well as fresh distress along old repairs (Figure 8-34). The concrete slab also broke at the toe of the levee (Figure 8-35). Patches of sand deposits can be seen on the bench where concrete cracking exists (Figure 8-36), however, there is no clear evidence to indicate that these sand deposits liquefied.

The distress mostly occurred on a more recently repaired section (newer concrete). This suggests the repaired section has previously experienced some distress either from ground movement or erosion of the toe. These observations suggest there may be some differential movements of the soil supporting the slabs or the slab responded differently from the subgrade during the earthquake.

On the landslide of the aforementioned slab distress zone, evidence of minor liquefaction in the nearby farm field was observed (Figure 8-37). The sand boils ejected less than about 5 cubic feet of sand and silt but the manifestation of liquefaction occurred in a fairly small farm field measuring 20 m by 40 m. The levee road south of the distressed area undulates in excess of 30 cm, which suggests unstable subgrade but the movement of the supporting soil is limited and did not damage the pavement but nevertheless may have undermined the slab (Figure 8-38). Along this stretch of the levee, NCREE reconnaissance observed cracking of the embankment toe (Figure 8-39).

8.3 Slope Failure at Nanbao Golf Course (南寶高爾夫球場邊坡滑動)

The Nanbao golf course is located in the Danei district of Tainan city. The PGA at the site is estimated to be about 250 to 400 gal in the east-west direction and 2/3 of that in the north-south direction during the Meinong earthquake. The strong ground shaking caused a golf fairway fill slope to fail towards a nearby creek (Figure 8-40). The coherent soil block moved northwest toward the creek with the largest vertical displacement at the southern end of about 2.5 m (Figure 8-41). The landslide headscarp extends about 100-m in a direction subparallel to the creek (Figure 8-40) and the scarp height diminishes toward the north (Figure 8-42). Limited by accessibility to the river, no obvious toe heave was observed from the crest of the block. The failure was repaired soon after the Chinese New Year holiday or shortly after the earthquake.

Based on the information provided by the manager of this course, the subsurface soil along the rupture is in a backfill zone, which was constructed using material excavated from the hill to the east side in a balanced cut/fill grading operation used to create the level fairway. The pond on the north-east side is designed to store the water pumped from the creek and to be used for irrigation of the golf course. The layered backfill is comprised of mudstone intermixed with silty clay as shown in Figure 8-41.

The consistency of the fill allowed the scarp to stand vertically for several days after the earthquake. Regular watering of the golf course and potential leakage from the pond allowed the near surface soil in the slide mass to be in a moist condition but far from saturation. Because February is the dry season in southern Taiwan and no evidence of groundwater was noticed in the scarp area nor observed in the deep cracks, the subsurface compacted fill material materials is believed to be unsaturated. The groundwater table is estimated to be at a level similar to creek (estimated to be no less than 8 m from the crest). Several PVC pipes buried below the surface in the fill (used for water pumping and irrigation for the maintenance of the course) were ruptured by the slide as shown in Figure 8-43. A 30 cm drainage pipe passed through the mid-section of the rupture and was broken after the failure. The water caved around the drainage pipe indicating that the soil has low permeability and the sliding surface has healed after the sliding.

Based on field observation of the rupture pattern, the location of water table, the consistency of the compacted fill material, and water cave around the drainage pipe several days after the earthquake, the slope failure is considered to be the result of movement of a coherent block of compacted fill triggered by the inertial forces from the earthquake during ground shaking.

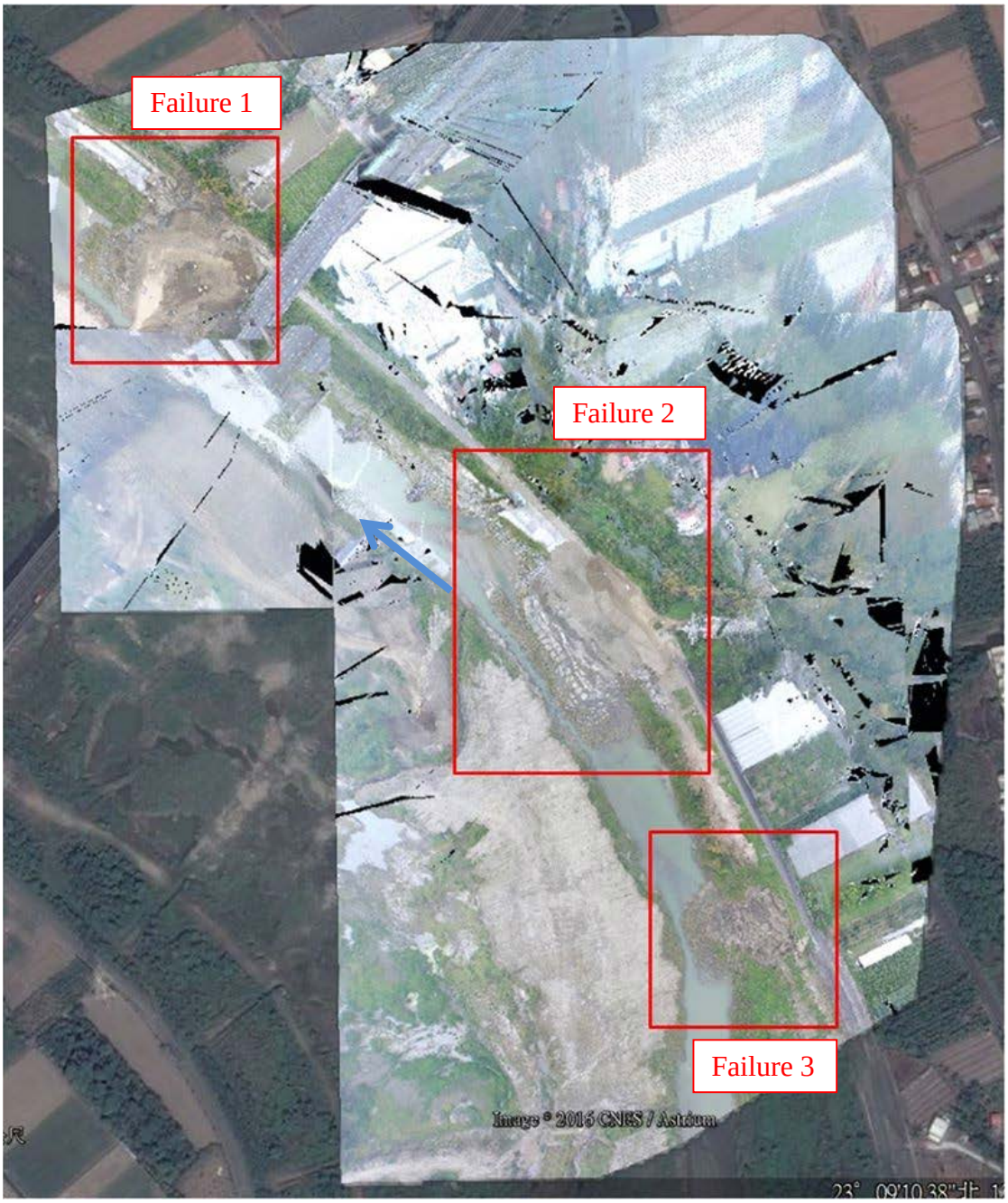

Figure 8-1: Location of Three RiXin Levee Failures.

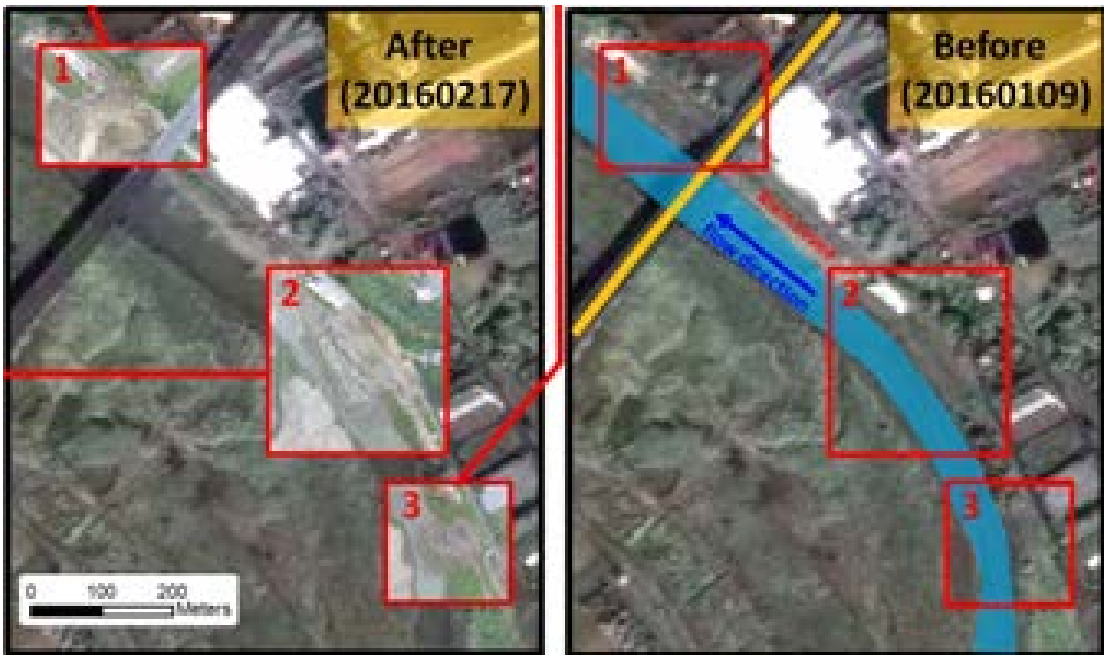

Figure 8-2: Pre- and Post-Failure Geometries of the Levee Slopes.

Figure 8-3: Aerial View of Failure No.1. (Photo provided by W.-K. Huang) (23° 9'12.40", 120°20'37.68"). Note the construction repair operation underway.

Figure 8-4: Bird's View of Failure No.1. (Photo provided by W.-K. Huang) (23.154135, 120.342255).

Figure 8-5: Layout of Failure No. 1 (23° 9'12.40", 120°20'37.68").

Figure 8-6: Failure 1 Looking Northwest (23.1537, 120.3434).

鑽　探　及　試　驗　報　告　表

BORING AND TESTING DATA

名　稱：
Project：

曾文溪橋

孔　號：P2
Hole No：

地面標高　：9.296 m
Elevation

地下水位　：4.30 m
Ground water Table

鑽探時間：101.07.29
Date of Boring

試驗時間：
Date of Testing

SPT N

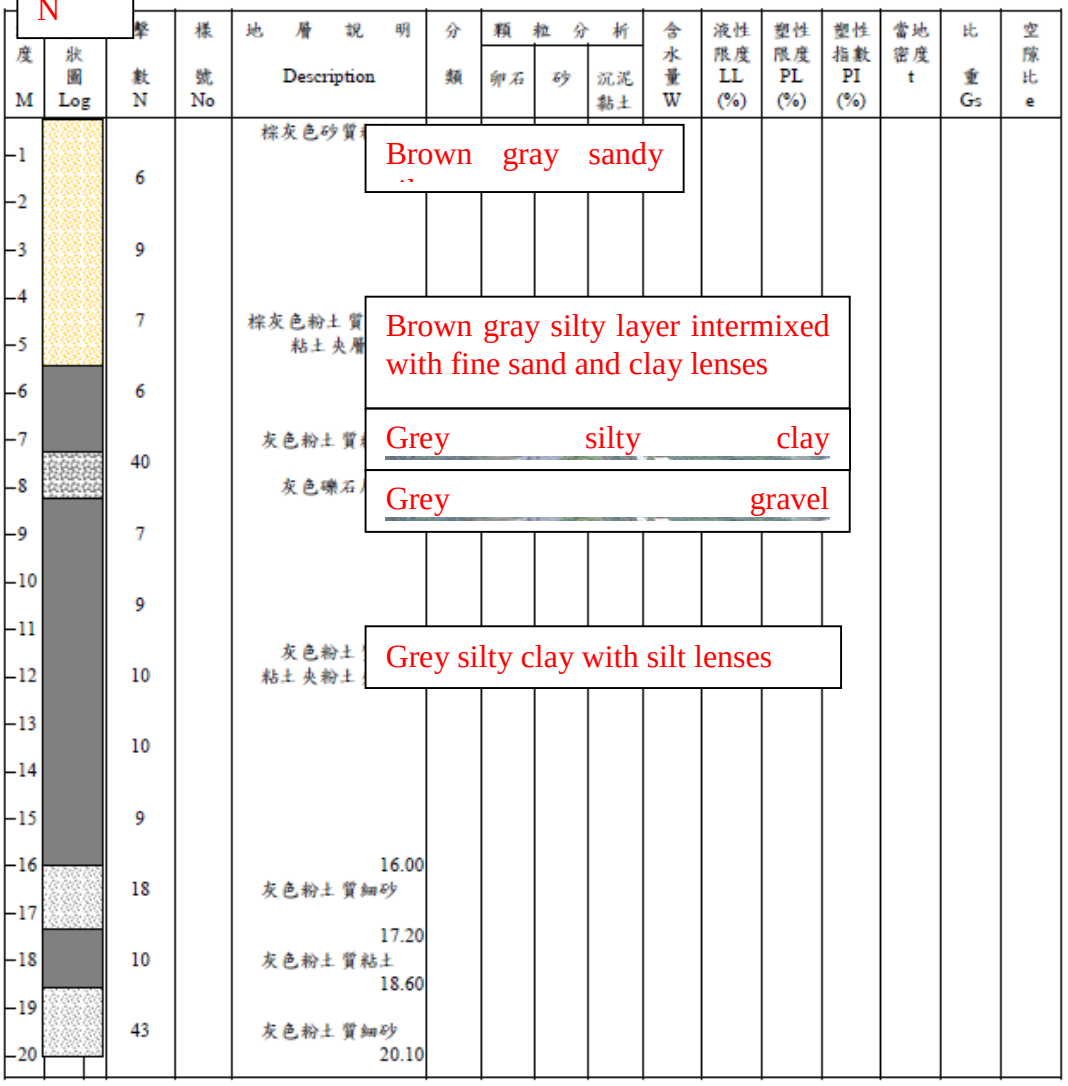

Figure 8-7: Boring Log (500m from Failure 1).

Figure 8-8: Seepage at Base of Scarp at Impervious Contact (23.1537, 120.3434).

Figure 8-9: Southwest Margin of Failure 1 (23.153889, 120.343178).

Figure 8-10: Arcuate Crack Extending to the Bridge Piers (23.153583, 120.343650).

Figure 8-11: Nested Arcuate Cracking Behind the Piers (looking northwest) (23.153514, 120.343736).

Figure 8-12: Settlement Around Bridge Prier is about 4 to 5 inches (23.153514, 120.343736).

Figure 8-13: Layout of Failure No. 2 and Layout (23° 9'3.26", 120°20'47.59").

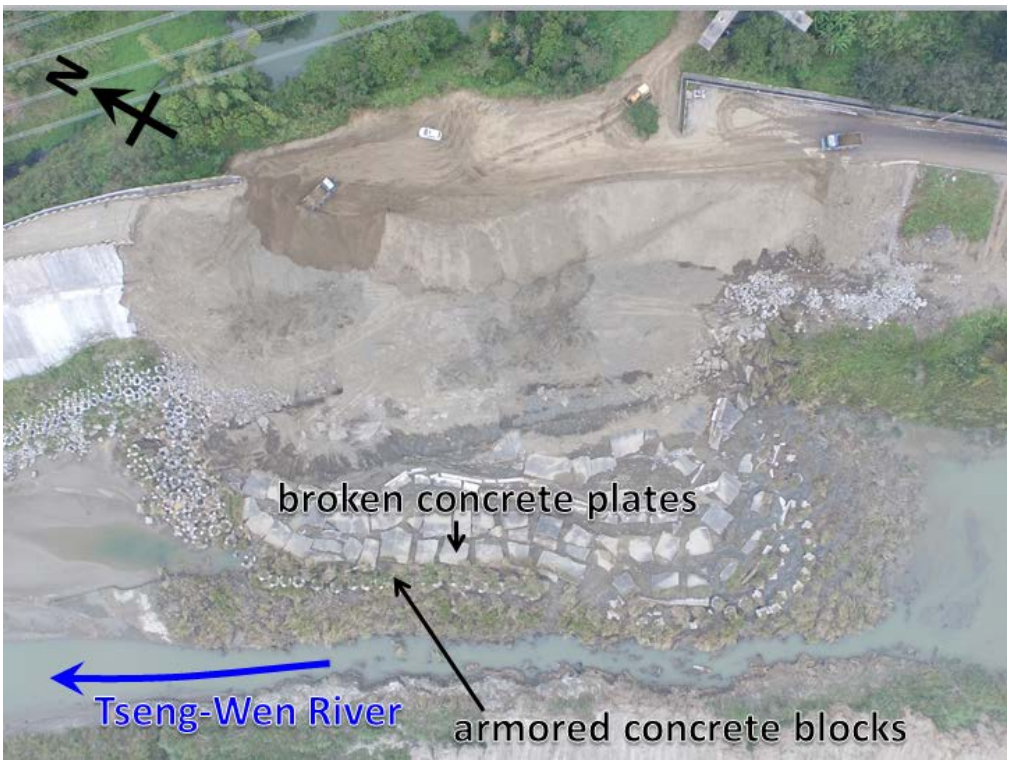

Figure 8-14: Aerial View of failure No.2. Notice the long runout distance of the materials. (Photo: W.-K. Huang) (23° 9'3.26", 120°20'47.59").

Figure 8-15: Bird's View of failure No.2. (Photo: W.-K. Huang) (23° 9'3.26", 120°20'47.59").

Figure 8-16 Concrete Slab and Piles Used to Protect Area near Levee Failure No.2. (23.151245, 120.346236).

Figure 8-17: Area of the Pushed Out Toe (23.150801, 120.345807).

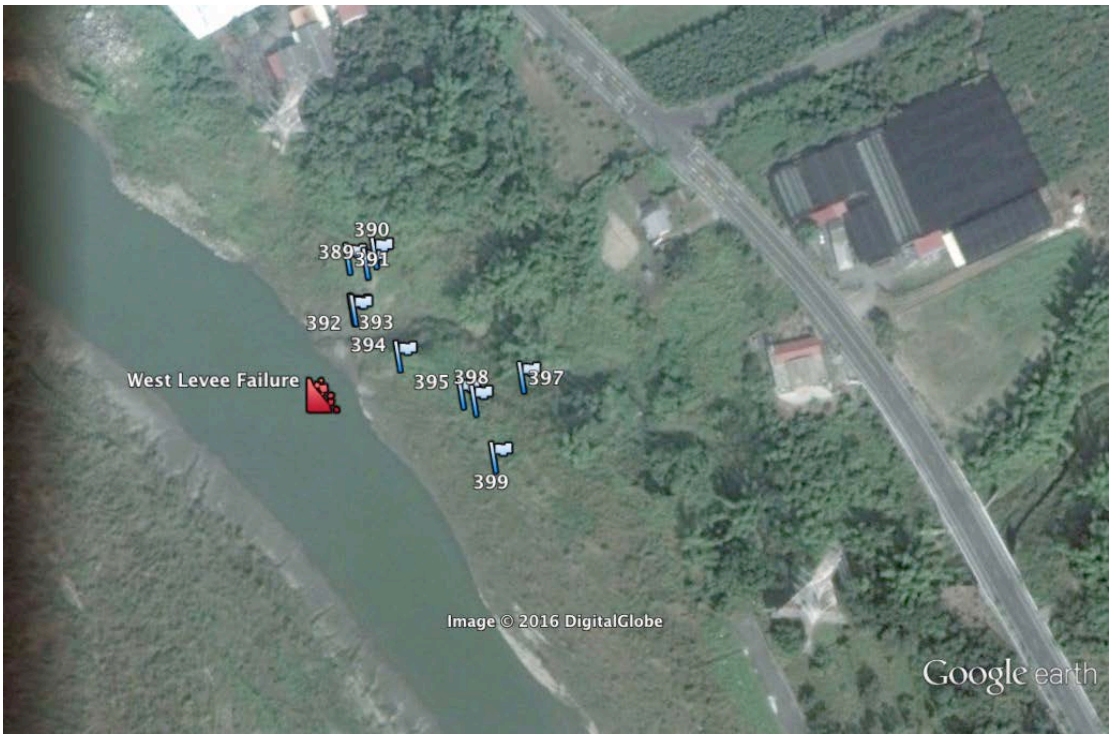

Figure 8-18: Google Image of region where Failure 2 occurred (image date in 1/2012).

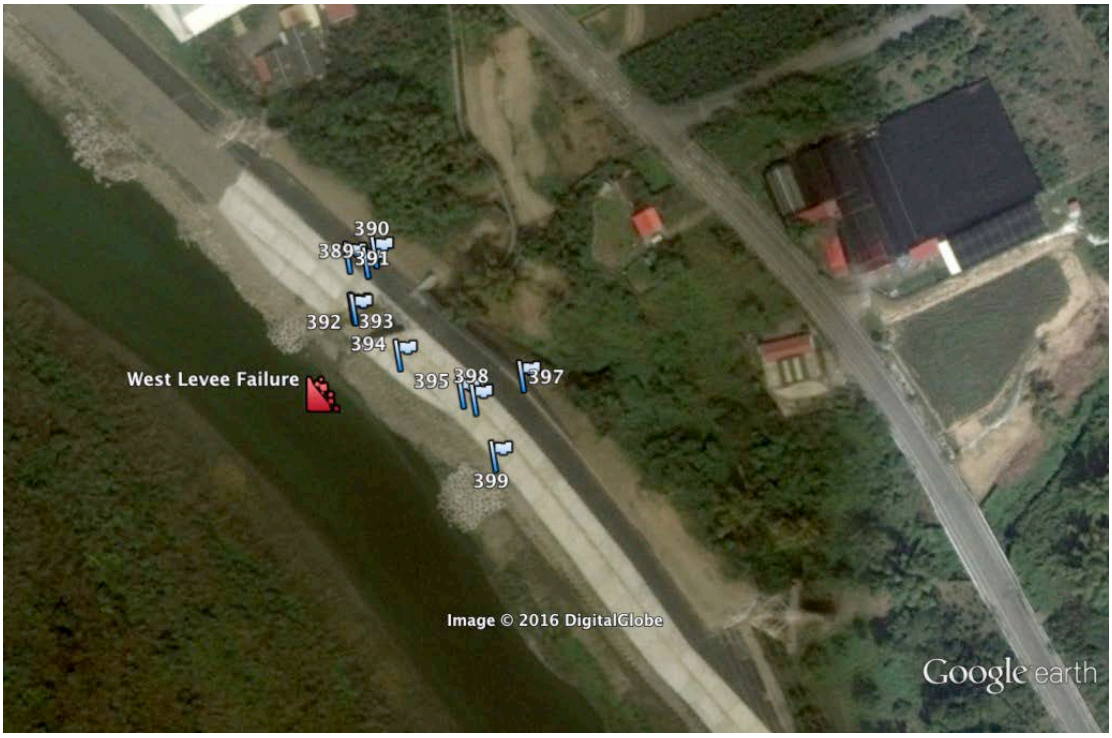

Figure 8-19: Google Image of region where Failure 2 occurred (image date: 4/2012).

Figure 8-20: Google Image of region where Failure 2 occurred (image date: 2/2014).

Figure 8-21: Google Image of region where Failure 2 occurred (image date: 5/2014) – note the visible constructed structural spillway.

Figure 8-22: Google Image of region where Failure 2 occurred (image date: 8/2014).

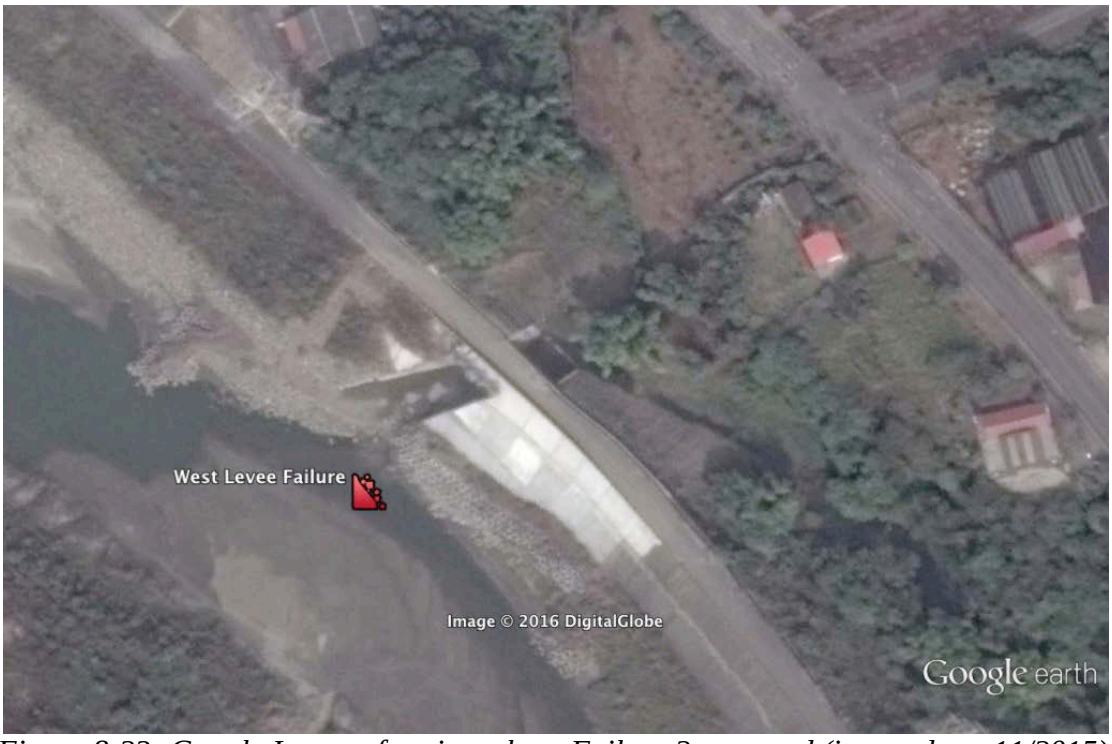

Figure 8-23: Google Image of region where Failure 2 occurred (image date: 11/2015).

Figure 8-24: Emergency Backfill of the Levee (at Failure 2) (23.150949, 120.346590).

Figure 8-25: Historical Failure Near Failure No.2. (Photo: W.-K. Huang). (23.150949, 120.346590).

Figure 8-26: Layout of Failure 3.(23.148325, 120.347631)

Figure 8-27: Aerial view of failure No.3. (Photo: W.-K. Huang). (23.148325, 120.347631)

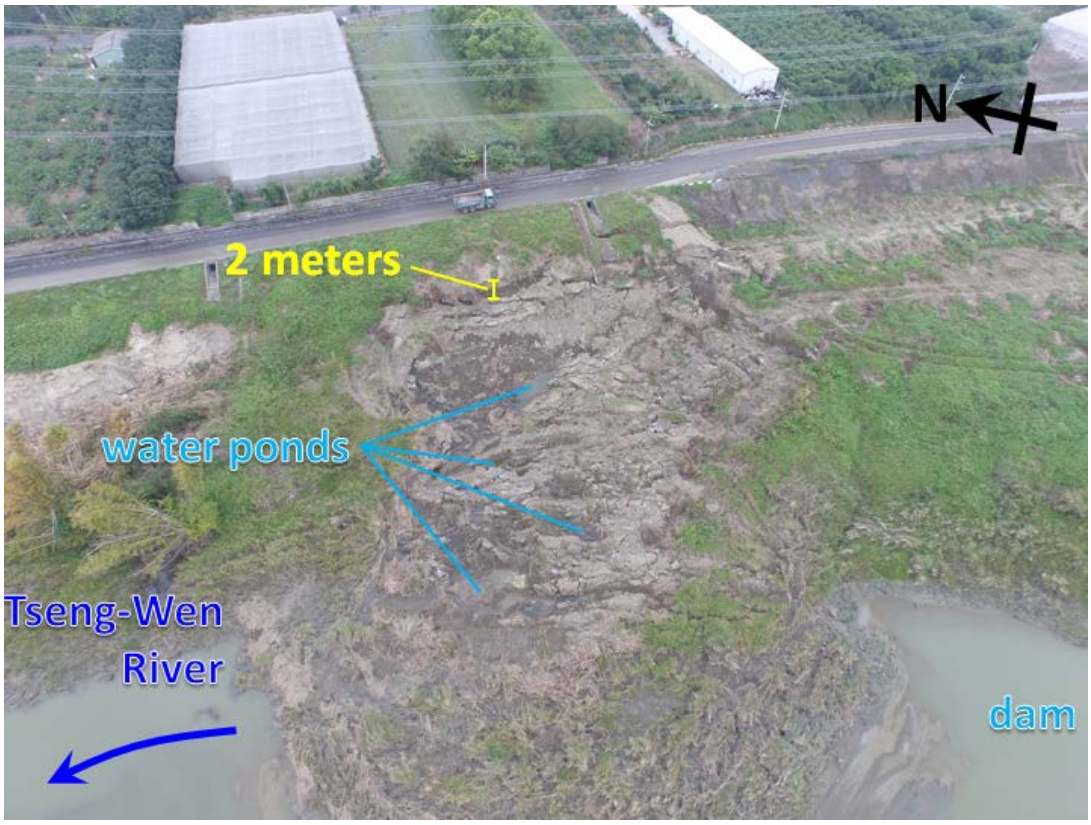

Figure 8-28 Bird's view of failure No.3. (Photo: W.-K. Huang). (23.148325, 120.347631)

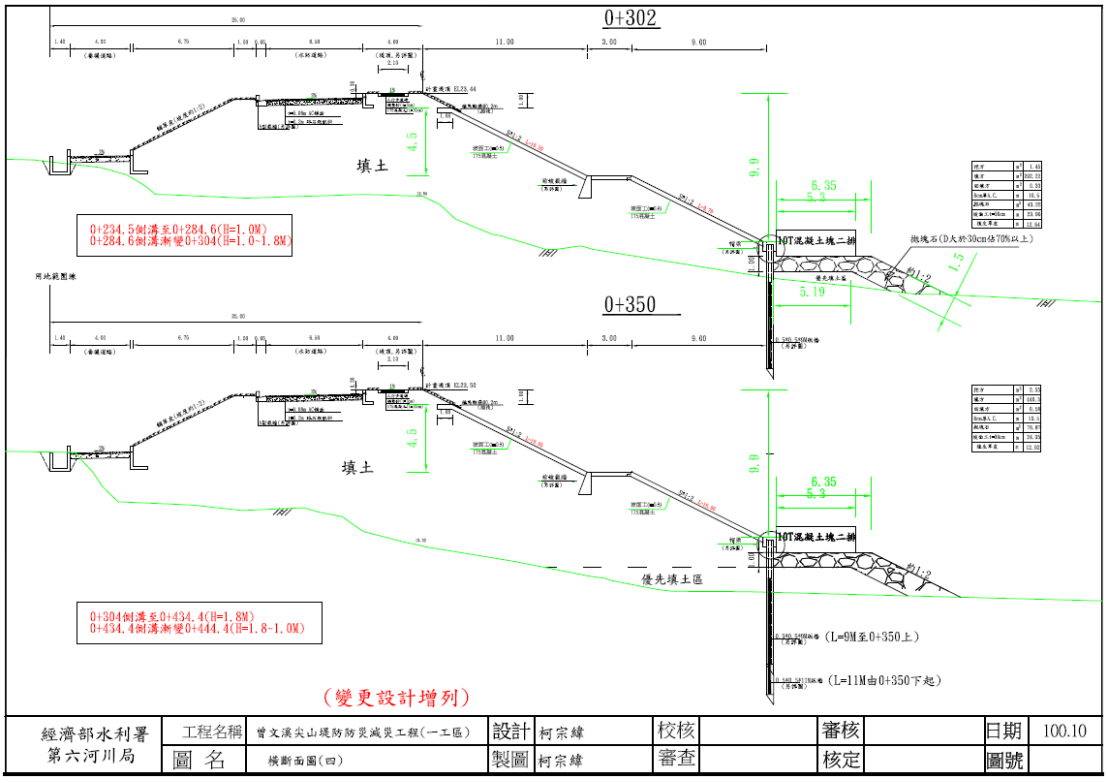

Figure 8-29: Portion of the Levee Protected Piles (between Failure 1 and 2) Serviced the Earthquake.

Figure 8-30: Aerial View of ErXi Bridge Levee Failure Site.

Figure 8-31: Distress of Concrete Slab Bank Protection (23.121176°,120.379569°).

Figure 8-32: Buckling of Repaired Slab (23.121176°,120.379569°).

Figure 8-33: Shear Cracking of the Repaired Concrete Slab (23.121176°,120.379569°).

Figure 8-34: Re-cracking of Recently Repaired Cracking (23.121176°,120.379569°).

Figure 8-35: Slab Damage at Levee Toe (23.121176°,120.379569°).

Figure 8-36: Patches of Sand Deposited on Bench (23.121329, 120.379284).

Figure 8-37: Evidence of Liquefaction on Land slide of Levee (23.120823, 120.378989).

Figure 8-38: Undulation of Levee Crest Road (23.120114, 120.379819).

Figure 8-39: Cracking Occurring along Landslide Toe (Photo from NCREE).

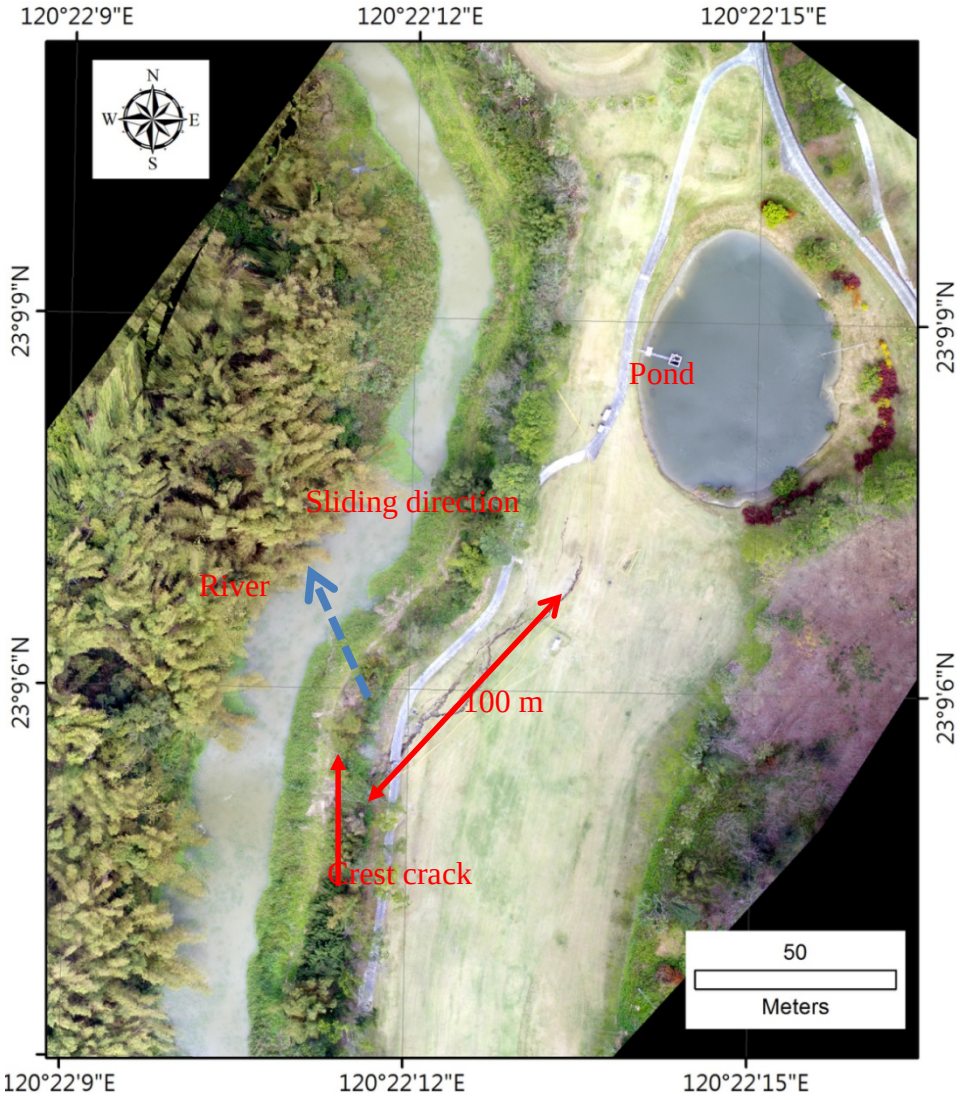

Figure 8-40: Overview of slope failure at Nan-Bao golf course (source: NCREE field survey on 2016/02/13).

Figure 8-41: Maximum vertical drop at the south end of the Nanboa golf course (23.151721, 120.370245)

Figure 8-42: Surface rupture at the crest of sliding mass at Nanboa golf course (23.151721, 120.370245).

Figure 8-43: Watering pipes along the surface rupture. (23.151721, 120.370245)

Figure 8-44: broken drainage pipe.(23.151721, 120.370245)

9. DAM PERFORMANCE

A total of 14 dams were shaken by the Meinong Earthquake as listed in Table 9-1. The estimated shaking intensities shown in this table were based on an intensity scale developed by the Taiwan Central Weather Bureau (Table 9-2). The GEER team did not visit the dam sites. Instead, information presented in this section was provided to GEER by Mr. Pin-Kun Lu (盧炳堃) of Taiwan Water Resources Agency 經濟部水利署 (WRA) and its consultants (Sinotech Engineering Consultants 中興工程公司 and LiMing Engineering黎明工程公司 Consultants) who performed the post-earthquake inspection.

These dams are regulated by Taiwan WRA and most of the affected dams are located in WRA's Southern Division (經濟部水利署南區水資源局). WRA staff and its consultants were immediately dispatched to complete emergency post-earthquake inspections. Other than Hu-Tou-Pi dam, which developed minor cracking on the dam crest, all other dams performed satisfactorily from an engineering standpoint, including a semi-hydraulic fill dam (Wu-Shan-Tou) that experienced shaking in excess of 0.2g at its base. Most of the larger dams were instrumented by seismometers at the crest and in the freefield and/or dam toe. Section 9.1 provides a more detailed description of the dams and the recordings.

Dam Name	Dam Name	Dam Type	Dam Height (m)	Intensity
Nan-Hwa	南化	Embankment	87.5 m	6* (250-400 gal)
Tseng-Wen	曾文	Embankment	134m	5 (80-250 gal)
Wu-Shan-Tou	烏山頭	Semi-Hydraulic Fill	56 m	5 (80-250 gal)
Ren-Yi Lake	仁義潭	Embankment	28m	5 (80-250 gal)
Lan-Tan Lake	蘭潭水庫	Embankment	34 m	5 (80-250 gal)
Jan-Shan Pi	尖山埤	Embankment	30m	5 (80-250 gal)
Bai-Ho	白河	Embankment	42.5m	5 (80-250 gal)
Hu-Tou Pi	虎頭埤	Embankment	15.3 m	5 (80-250 gal)
Ah-Gong-Dian	阿公店水庫	Embankment	31 m	4 (25 – 80 gal)
Gin-Mian	鏡面	Concrete	36m	5 (80-250 gal)
Kao-Ping Diversion Weir	高屏攔河堰	Concrete	Low height structure	4 (25 – 80 gal)
Jian-Sian Diversion Weir	甲仙攔河堰	Concrete	Low height structure	3 (8-25 gal)
Chi-Chi Diversion Weir	集集攔河堰	Concrete	Low height structure	3 (8-25 gal)
Sheki-Kong	石岡壩	Concrete	Low height structure	3 (8-25 gal)
Li-Yu-Tan	鯉魚潭	Embankment	96 m	3 (8-25 gal)

*Potential instrument error.

Table 9-1: Dams Shaken by Meinong Earthquake.

世界各種地震震度分級比較表

震度分級		我國現用 震度階 2000 年 cm/s²(gal)	日本氣象廳 震度階 1996 年	M.S.K. 震度階 1964 年 cm/s²(gal)	新 MERCALLI 震度階 1956 年 cm/s²(gal)	CANCANI 震度階 1903 年 cm/s²(gal)	DE ROSSIFOREL 震度階 1833 年
0	無感	0.8 以下	0	Ⅰ無感	O 0.5 以下	Ⅰ0.25 以下	Ⅰ
						Ⅱ0.25~0.5	
					Ⅰ0.5~1.0	Ⅲ0.5~1.0	
1	微震	0.8~2.5	1	Ⅱ極輕	Ⅱ1.0~2.1	Ⅳ1.0~2.5	Ⅱ
					Ⅲ2.1~5.0	Ⅴ2.5~5.0	
2	輕震	2.5~8.0	2	Ⅲ弱			Ⅲ
					Ⅳ5~10	Ⅵ5~10	
3	弱震	8~25	3	Ⅳ 大部分人有感	Ⅴ10~21	Ⅶ10~25	Ⅳ
				Ⅴ12~25			Ⅴ
					Ⅵ21~44		
4	中震	25~80	4	Ⅵ25~50		Ⅷ25~50	Ⅵ
				Ⅶ50~100	Ⅶ44~94	Ⅸ50~100	
5	強震	80~250	5 弱		Ⅷ94~202		Ⅶ
			5 強	Ⅷ100~200		Ⅹ100~250	
6	烈震	250~400	6 弱	Ⅸ200~400	Ⅸ202~432		Ⅷ Ⅸ
			6 強			Ⅰ250~500	
7	劇震	400 以上	7	Ⅹ400~800			Ⅹ
				XI,XII 800 以上	X,XI, XII 432 以上	XII 500~1000	

備註:日本震度階僅爲示意圖,實際日本震度階是由加速度值與地震動持續時間經計算而得,無法僅由加速度值得知。

Table 9-2: Taiwan Earthquake Intensity Scale by Central Weather Bureau (http://scman.cwb.gov.tw/eqv5/eq100/100/035.HTM).

9.1 Seismic Recordings at Dam Sites

Seismic instruments at six dam sites were triggered by the Meinong earthquake. Table 9-3 lists the peak ground accelerations (PGAs) recorded at the dam crests and in the freefield or at the dam toe. This list includes the highest embankment dam in Taiwan (Tseng-Wen) and the only semi-hydraulic fill dam (Wu-Shan-Tou).

Name	Name	Instrument Location	Peak Ground Acceleration (gal)		
			Vertical	Longitudinal	Transverse
Hu-Tou Pi	虎頭埤	Freefield	108.9	194.0	294.6
Tseng-Wen	曾文	Crest (MSM3)	69.3	125.7	261.4
		Toe(MSM2)	44.4	129.4	152.3
		Freefield (FSM1)	27.3	47.2	68.6
		Freefield (FSM2)	28.0	56.6	64.9
Wu-Shan-Tou	烏山頭	Crest	93.2	233.1	174.3
		Toe	50.6	148.2	158.6
		Freefield	97.0	272.1	164.6
Nan-Hwa	南化	Crest (DMT)	139.2	251.1	237.1
		Crest (DML) *	222.4	431.8	271.6
		Mid-Slope (DMC)	147.2	287.5	263.6
		Toe (DMB)	77.5	136.4	150.3
		Freefield (CTR)	70.3	99.6	124.4
		Freefield (CTL)	107.6	194.2	253.3
Ah-Gong-Dian	阿公店	Crest (ED01)	66.5	104.1	175.2
		Toe (ED03)	25.0	47.3	36.8
Gin-Mian	鏡面	Crest (DMT)	123.6	228.7	308.7
		Toe (DMB)	126.1	270.9	248.4

*Potential instrument error.

Table 9-3: Ground Motions Recorded on Dams during 2016 Meinong Earthquake.

9.2 Tseng-Wen Dam

Tseng-Wen Dam is the tallest compacted embankment dam in Taiwan. Built in 1973, the 133-m-high dam has a central core and a chimney/blanket filter and drain system downstream of the core (Figure 9-1). The embankment lifts were compacted to modern standards and construction was reviewed by the United States Bureau of Reclamation (USBR). Figure 9-2 shows the peak ground accelerations (PGA) recorded at various parts of the dam, and Figure 9-3 through Figure 9-5 show selected acceleration time histories recorded at the crest, toe, and freefield. Emergency inspection performed immediately after the earthquake did not identify any damage to the dam.

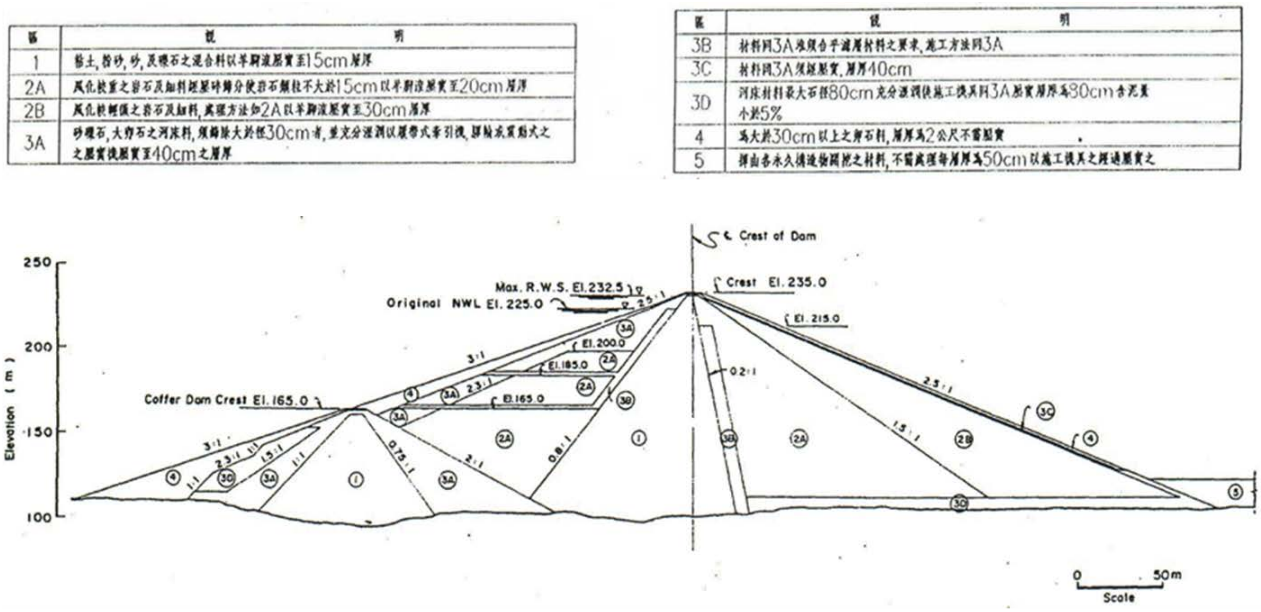

Figure 9-1: Cross Section of Tseng-Wen Dam.

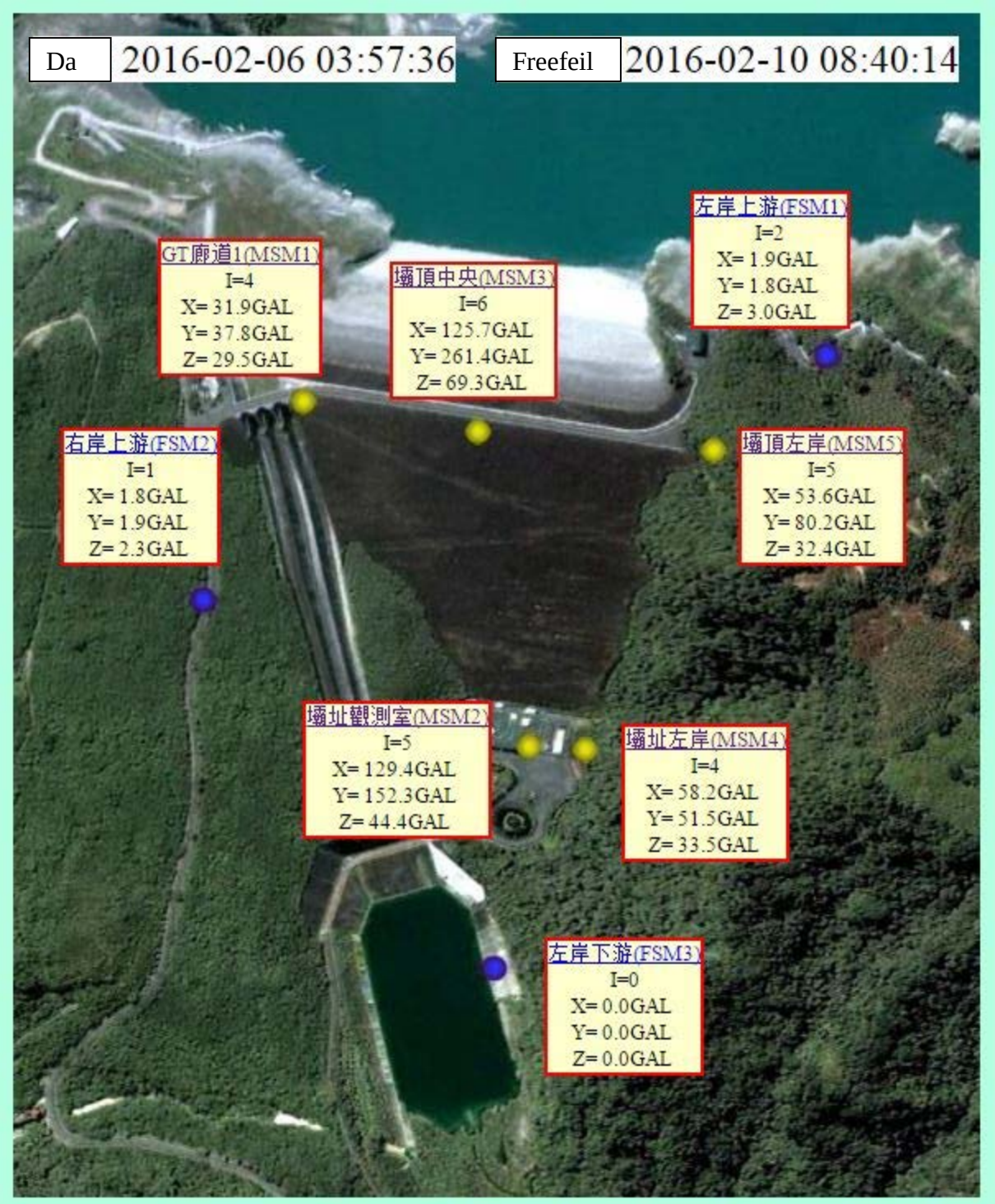

Figure 9-2: PGA Recorded on the Tseng Wen Dam Face (Freefield is from an aftershock).

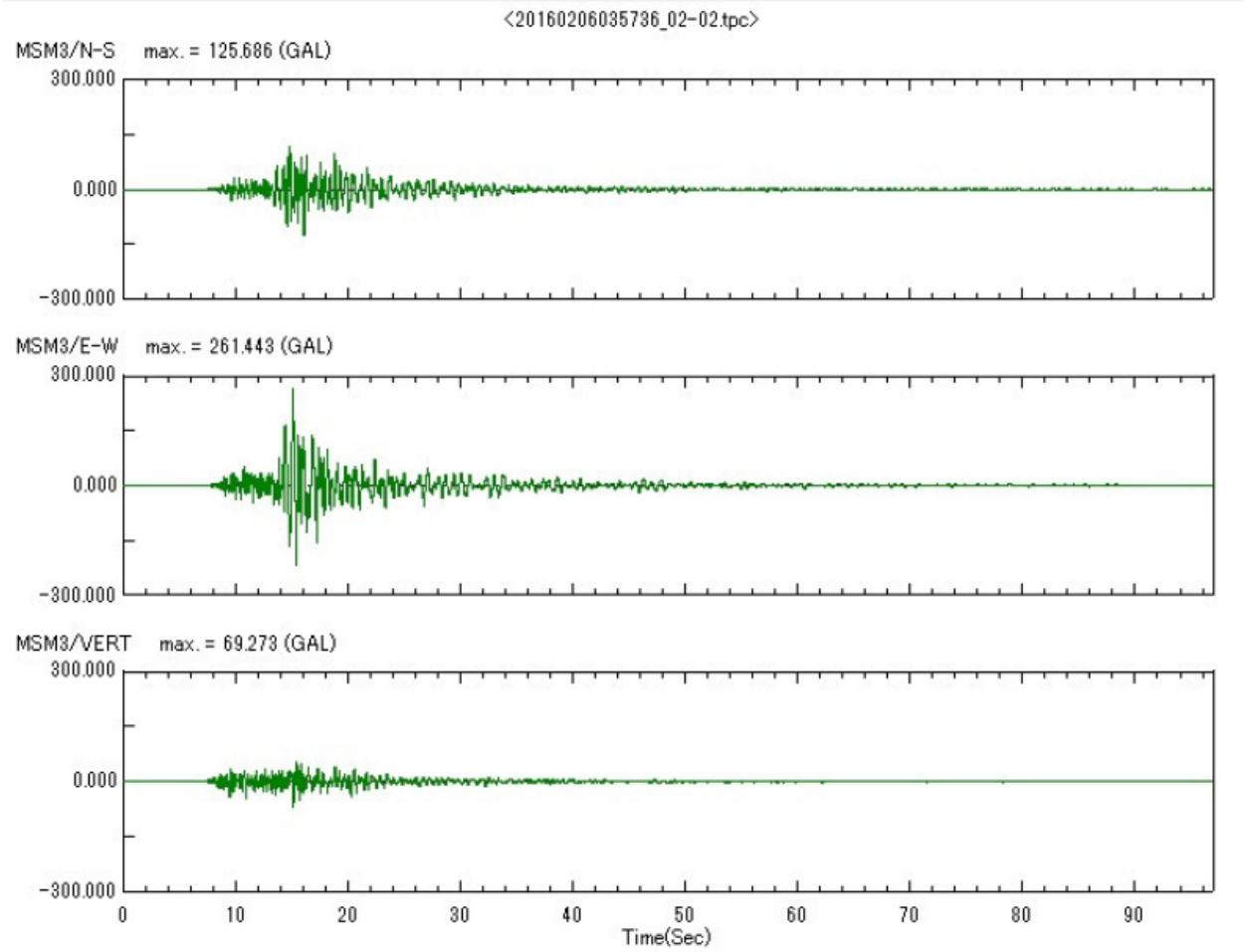

Figure 9-3: Acceleration Time Histories Recorded at Tseng Wen Dam Crest.

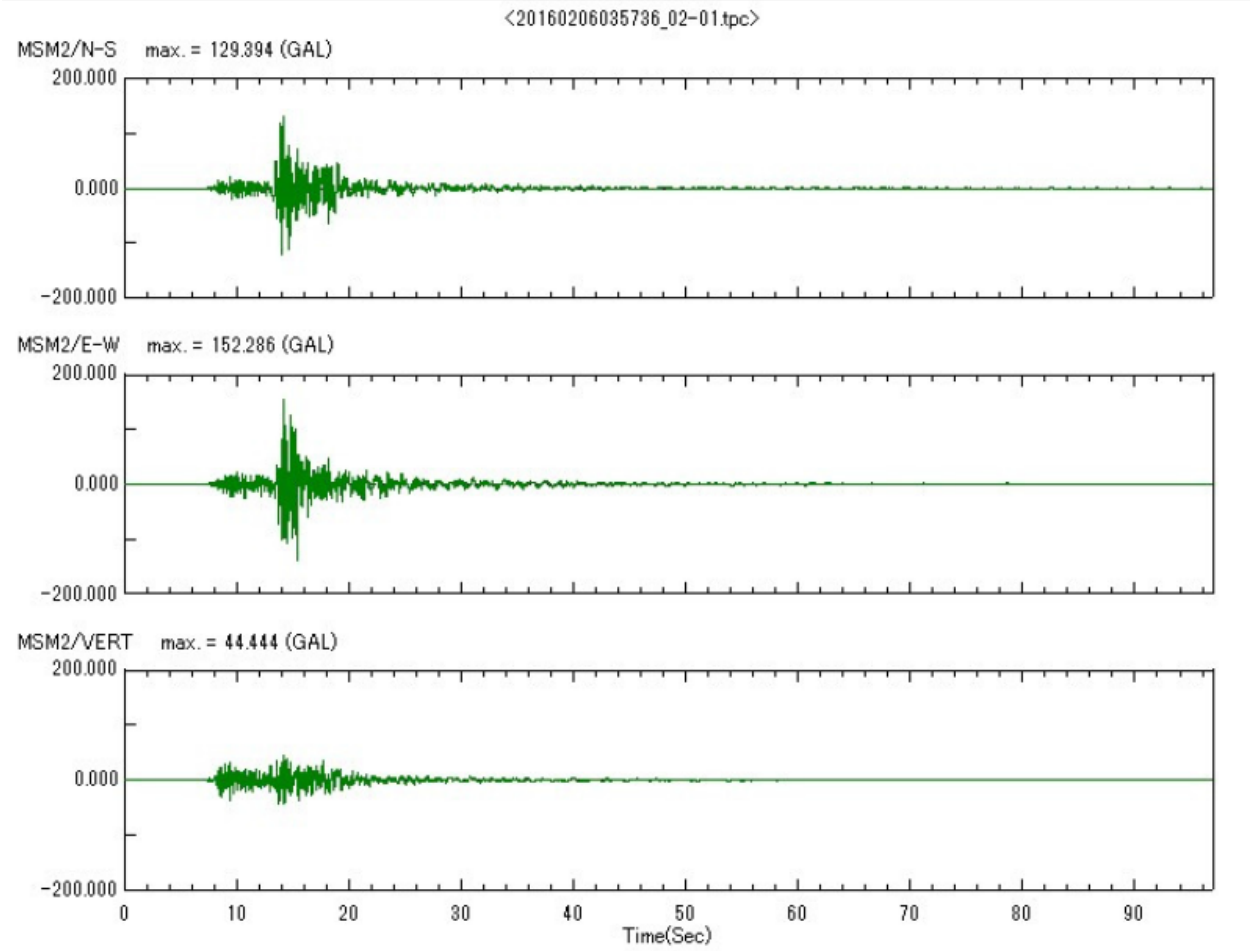

Figure 9-4: Acceleration Time Histories Recorded at Tseng Wen Dam Toe.

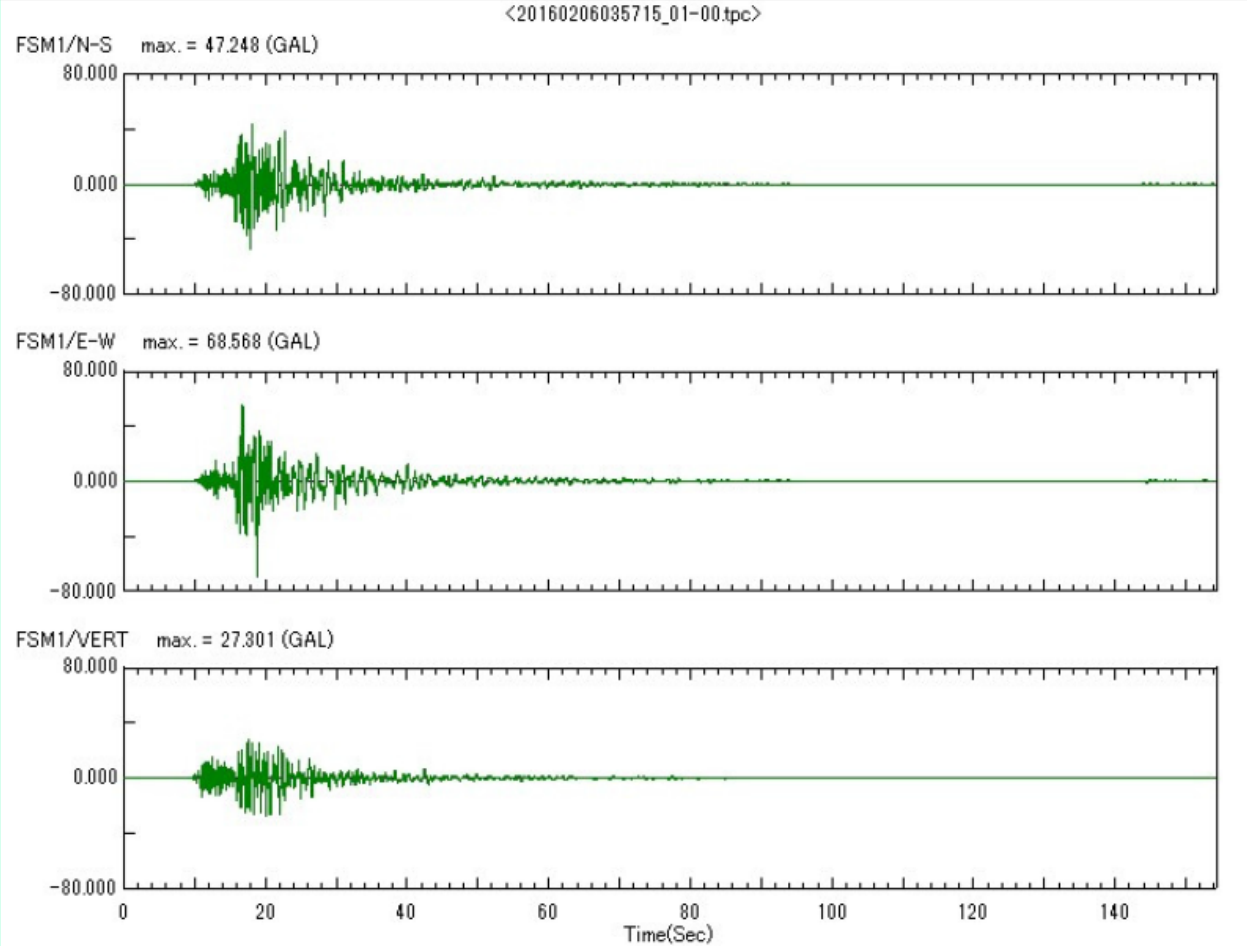

Figure 9-5: Acceleration Time Histories Recorded in the Tseng Wen Freefield.

9.3 Nan-Hwa Dam

Built in 1993, Nan-Hwa Dam is an embankment dam with a curved axis as can be seen in Figure 9-6. The cross section shows the 87.5-m-high dam has a central core and is protected by sandwiched chimney and blanket drains. The dam was compacted to modern standards and its design was reviewed by USBR. Figure 9-7 shows the cross section of the dam and the embankment material properties. Extensive instrumentation was used to monitor the dam performance as shown in Figure 9-6. Immediately after the earthquake, inspection of the dam was made and no damage was reported; however, some of the seismic instruments malfunctioned and reported erroneous readings. The PGAs report in this report should be considered preliminary until they can be verified.

Figure 9-6: Aerial View of Nan Hwa Dam with Instrumentation Locations.

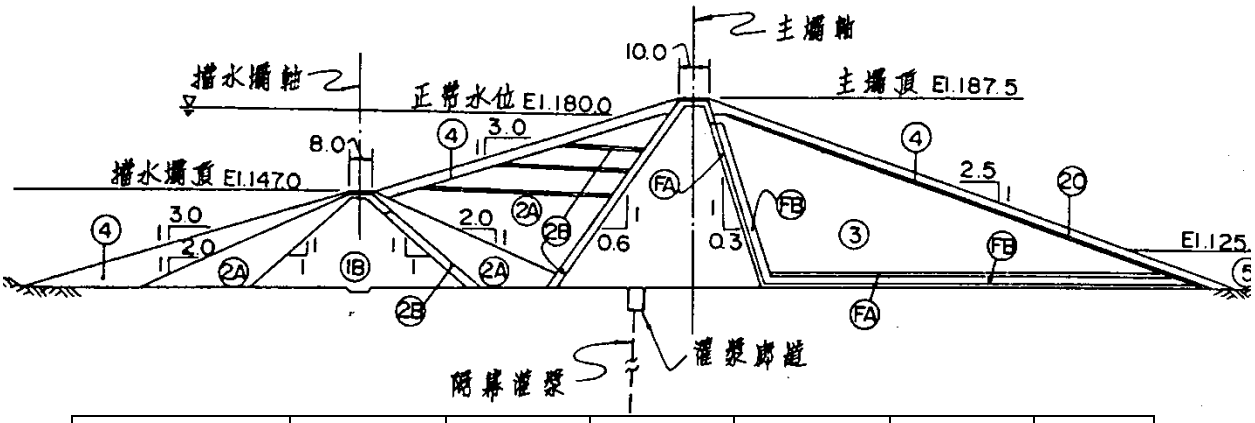

Zone	USCS	Gravel	Sand	Fines	LL	PI
1A	CL	0	8	92	30	14
1B	CL-ML	11	10	79	23	6
2A	GM	65	19	16	14	-
2B	GW	65	30	5	-	-
3	GC-GM	54	18	28	22	5

Figure 9-7: Cross Section showing Embankment Material Properties.

9.4 Wu-Shan-Tou Dam

Building of Wu-Shan-Tou Dam started in 1920 and was completed in 1930. This is one of the earliest large dams built in Taiwan. The dam is a semi-hydraulic fill dam, i.e., using wide starter dikes on both the upstream and downstream sides as shown in Figure 9-8 and hydraulic fill in between. The starter dikes, comprised mostly of gravelly fill (GP and GM) were lightly compacted by old hauling equipment. The interior part of the dam was hydraulically filled and formed a coarser outer shell zone (comprised of predominantly SM and ML) next to the starter dike, and a puddle core inner zone comprised mostly of CL and ML between the shell zones. The upstream and downstream slopes of the dam are both 3:1 (H:V). The dam did not amplify the ground motion much in the transverse direction where the motion at the toe was recorded at a PGA of about 0.15g and was amplified at the crest to 0.17g. However, in the longitudinal direction, the crest motion was amplified to just below 0.25g. Inspection immediately after the earthquake showed there was no damage to the dam.

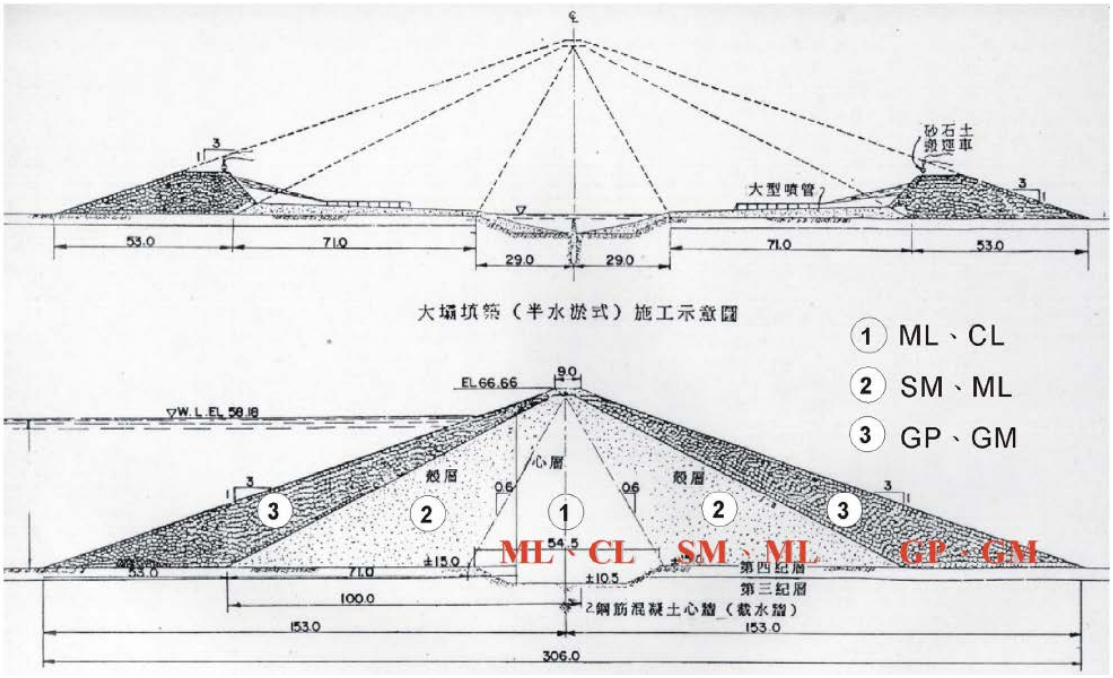

Figure 9-8: Cross Section of Wu-Shan-Tou Dam.

9.5 Hu-Shan-Pi Dam

This is the first dam built in Taiwan. Construction started in 1831 and completed in 1846. Since its original construction, the dam has experiencedfour damaging earthquakes. The 1906 and 1946 Chia-Yi earthquake and Hsinghwa earthquake both casused the dam to be breached after which it was later rebuilt, with the current layout likely reflecting the 1946 re-build (Figure 9-9). The current dam is 15.3 meters high and has a 3:1 (H:V) downstream slope and a similar slope but with a steep upstream drop on the upstream side as shown in Figure 9-11. No internal drain or toe drain was installed along the maximum section. Figure 9-10 shows a downstream view of the dam. Based on the vintage of the dam, it is expected that minimal compaction effort (animal walking) was made during construction. The 2010 M6.4 Jiashian earthwake caused the dam to crack again and develop a tranverse crack 6 meters long and 4 meters deep (Figure 9-12). The crack was excavated and repared. The 2016 Meinong earthquake caused the dam to experience longitudinal compression and bulging of the AC pavement, and ten tranverse cracks listed in Table 9-4 and shown in Figure 9-13. The deepest crack measured 100 cm deep and occurred at the same location as the 2010 post-Jiasian earthquake repaired crack. Most other cracks are surficial. The dam experienced about 0.3g ground motion in the freefield. Figures 9-14 through 9-16 show the cracking created by the Meinong earthquake.

			裂縫		
ID	Sta.	El (m)	Length (m)	Width (cm)	Depth (cm)
no. 1	0+200.6	310.103	3.2	0.5	3
no. 2	0+205.4	310.092	3.2	3.0	100
no. 3	0+211.5	310.015	3.2	0.3	5
no. 4	0+226.4	38.837	3.4	0.9	5
no. 5	0+241.8	38.713	1	1.0	1
no. 6	0+283.5	38.72	3.5	0.1	1
no. 7	0+292.1	38.803	3.5	0.1	1
no. 8	0+302	38.877	3.5	0.3	3
no. 9	0+311.3	38.883	3.5	0.3	3
no. 10	0+322	38.918	3.5	0.8	10

Table 9-4: Crack Measurement for Hu-Shan-Pi Dam.

Figure 9-9: Plan Veiw of Hu-Shan-Pi Dam.

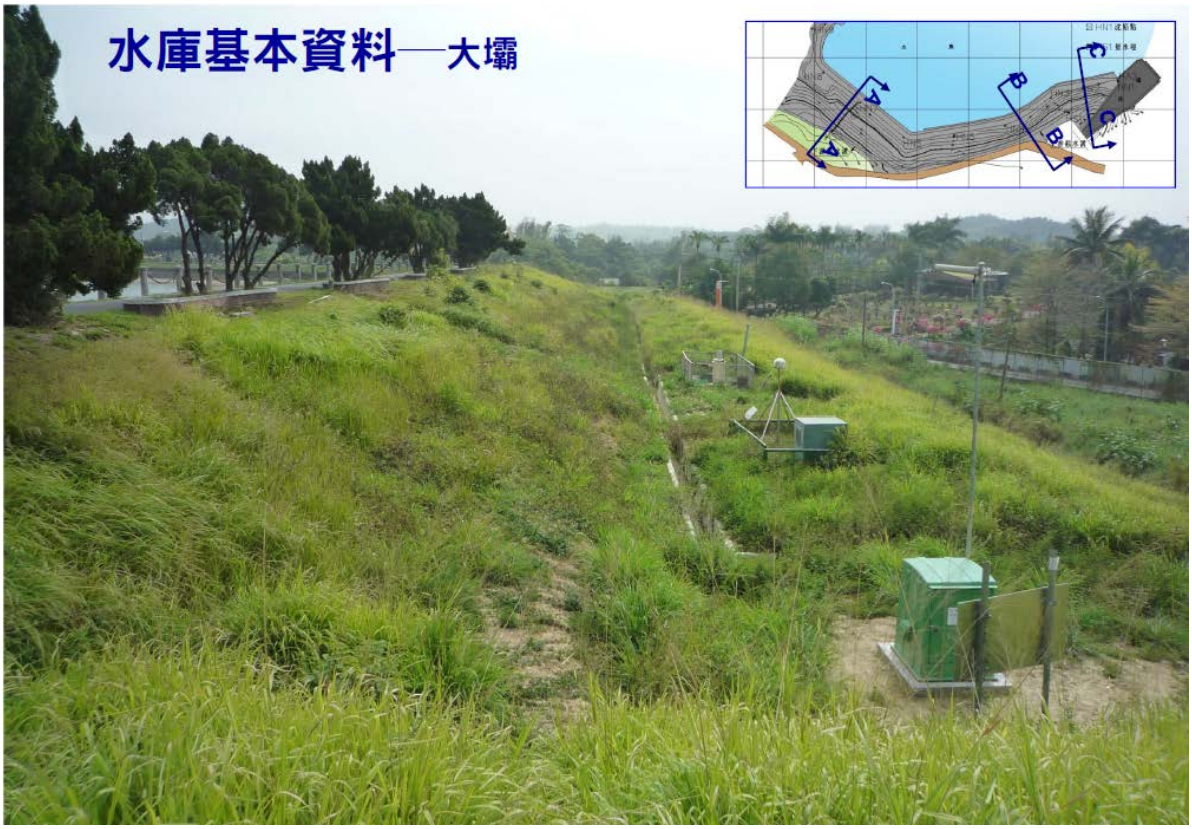

Figure 9-10: Downstread View of Hu-Shan-Pi Dam.

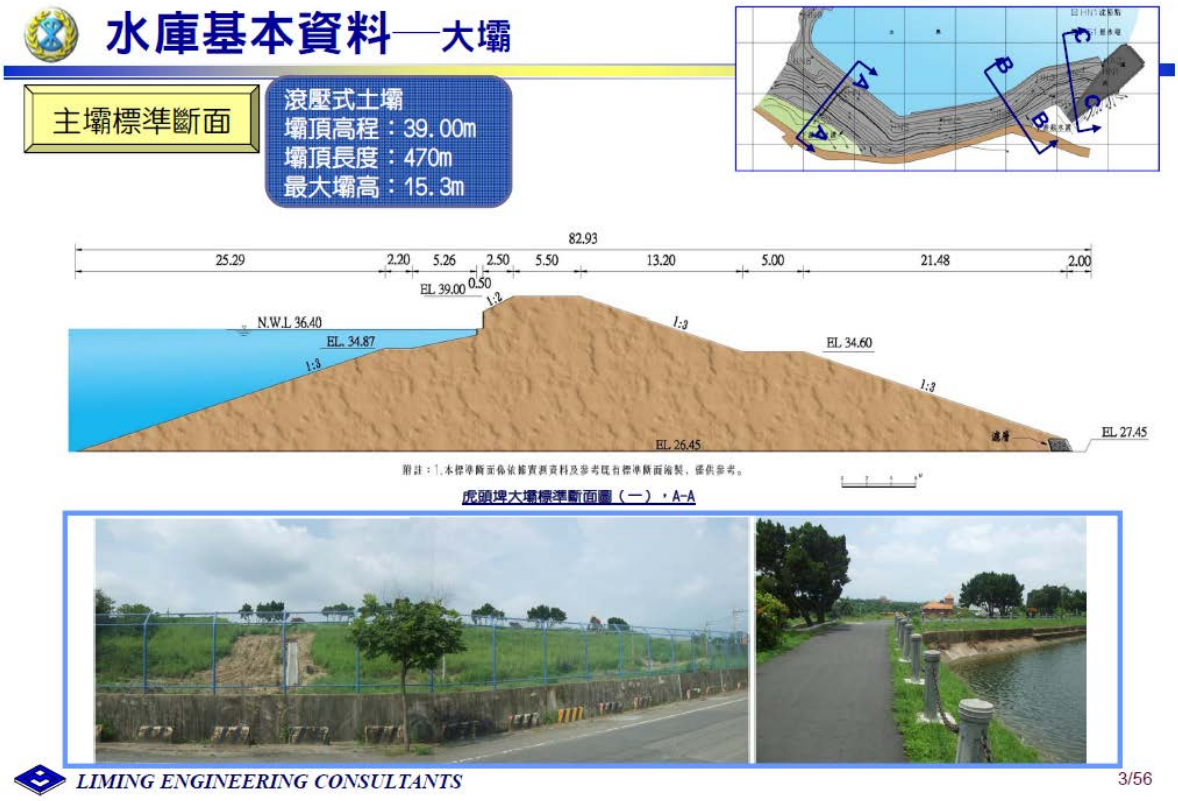

Figure 9-11: Cross Section of Hu-Shan-Pi Dam.

Figure 9-12: Earthquake Induced Transverse Crack from 2010 Jiasian Earthquake.

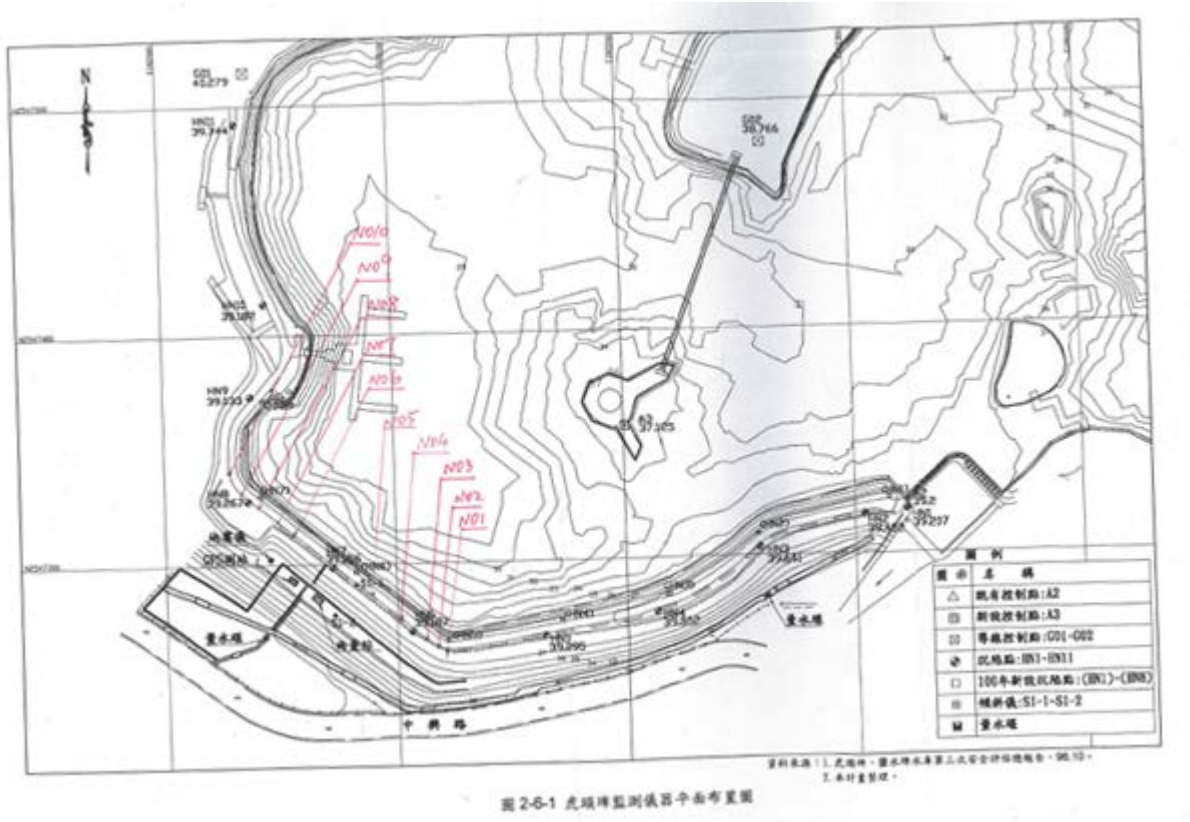

圖 2-6-1 虎頭埤監測儀器平面布置圖

Figure 9-13: Cracking caused by 2016 Meinong Earthquake.

Figure 9-14: Cracking of the AC Pavement (Lat: 23.025606, Long: 120.337445).

Figure 9-15: Cracking Developed in the Downstream Embankment (Lat: 23.025497, Long: 120.337569).

Figure 9-16: Cracking Developed in the Embankment (Lat: 23.026056, Long: 120.336966).

9.6 Gin-Mian Dam

The Gin-Mian Dam is a concrete gravity dam. The ground motion was amplfied from it toe of 0.25g to the crest of about 0.30g. No damage was reported at this dam.

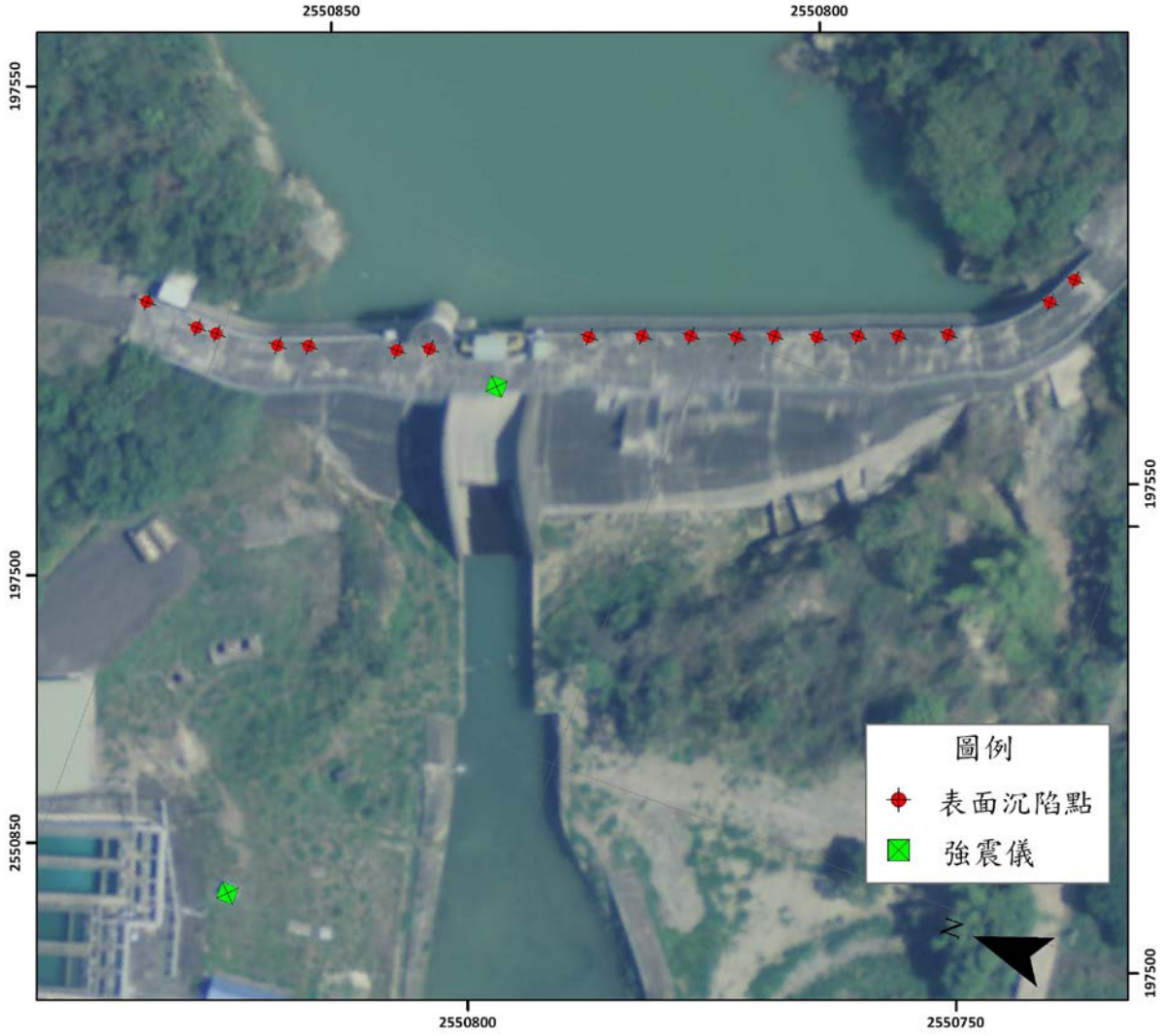

Figure 9-17: Aerial view of the Gin-Mian Dam.

10. SUMMARY AND CONCLUSIONS

The overall distribution of seismically triggered damage resulting from the Mw 6.3 February 6, 2016 Meinong Earthquake is asymmetrical with respect to the epicenter, with pronounced damage to the west, near Tainan City, and comparatively little damage elsewhere. The earthquake occurred at approximately 16 km depth on an unknown left lateral fault with minor reverse motion that did not rupture the ground surface. About a third of Taiwan experienced an intensity V shaking, which was scaled with a PGA of 80 to 250 gal. The earthquake ruptured from east to west and produced a noticeable velocity pulse observed in many stations near Tainan City. The asymmetric damage pattern is indicative of regional directivity effects as well as the complex nature of the earthquake mechanism. Concentrated distributions of aftershocks near the epicenter and over 25 km (15 mi.) to the west at typically greater depths, along with the observed long period velocity pulse suggest this earthquake may have resulted from a complex earthquake mechanism. Current studies suggest that this earthquake might have started with a relative smaller event followed by a larger main event with a rupture direction toward the northwest. The large PGA and PGV velocity pulse observed in Tainan region is mainly caused by this main event source mechanism with its directivity effect.

The earthquake complexity is further evident in a sharp, N-S trending, vertical displacement lineament measured by InSAR that appears to be the result of triggered slip on a previously unmapped fault trace now referred to as the Guanmiao fault. Movement along this west dipping Guanmiao fault may also be responsible for the higher degree of earthquake damage in the Tainan area. Earthquake effects include infrastructure and building losses, very limited landsliding, and numerous ground failures resulting from liquefaction and lateral spreading.

Liquefaction occurred primarily in Tainan City, approximately 40 km from the epicenter of the Meinong earthquake. While this liquefaction may appear unusual due to the relative small magnitude and large distance, it does agree with the lower bound from liquefaction case histories summarized by Ambraseys (1988) as shown in Figure 10-1. Based on ground response presented in Chapter 4, the thick alluvial deposit may have responded to the distance earthquake and amplified the attenuated ground motion and lengthen duration of the surface motion. This is similar to the 1989 Loma Prieta earthquake where liquefaction occurred in the Marina District of San Francisco located 90 km from the epicenter of the Mw 6.9 earthquake. In this case, the loose backfill liquefied because the soft Bay mud underlying the sandy fill amplified the weak attenuated motion.

Soil gradation curves obtained from ejecta material taken at liquefied sites show that the soils that liquefied did not fall outside the recognized material susceptible to liquefaction. However, similar to the New Zealand Christchurch earthquake, the grain size distributions for Meinong liquefied soils fall on the finer grain range as shown in Figure 10-2. Similar to The Christchurch earthquake, the Xinhua site that liquefied in this event liquefied in the 2010 Jiasian earthquake with the same magnitude and epicenters separated by less than 10 km,

Most of the liquefied sites appeared as isolated pockets that have been identified as primarily backfill material for either old fish ponds or levees. These areas contain material with the highest

potential for liquefaction. It is important to note however, that had the Meinong earthquake generated larger amplitude ground motions and/or longer durations of shaking, the extent of liquefaction would have been much more widespread. Nonetheless, as part of the GEER reconnaissance effort, NCKU used non-intrusive MASW geotechnical tests to measure the shear wave velocity of subsurface soils and subsequently used these profiles to successfully correlate liquefied sites and non-liquefied sites. This inexpensive method thus demonstrated itself as a promising screening tool to identify areas that require detailed geotechnical investigation are needed.

Although liquefaction occurred in a number of local regions within the city of Tainan, as noted, these were localized during this event to areas supported on prior pond features where poor quality backfill had been utilized. While this highlighted the historical significance of these features, the resulting building performance was generally good when well-connected foundations were used. On the other hand, features of buildings lacking well connected foundations (such as car ports and other additions) suffered extensive damage, in some case with propagation of large shear strains into the structure resulting in development of structural hinges (e.g. Figure 10-3). Modern Taiwanese design adopting continuous grade beam features will no doubt result in improved performance (e.g. Figure 10-4). The presence of basements below buildings was also noted to result in good performance of the superstructure of the building; despite adjacent liquefaction ground failure.

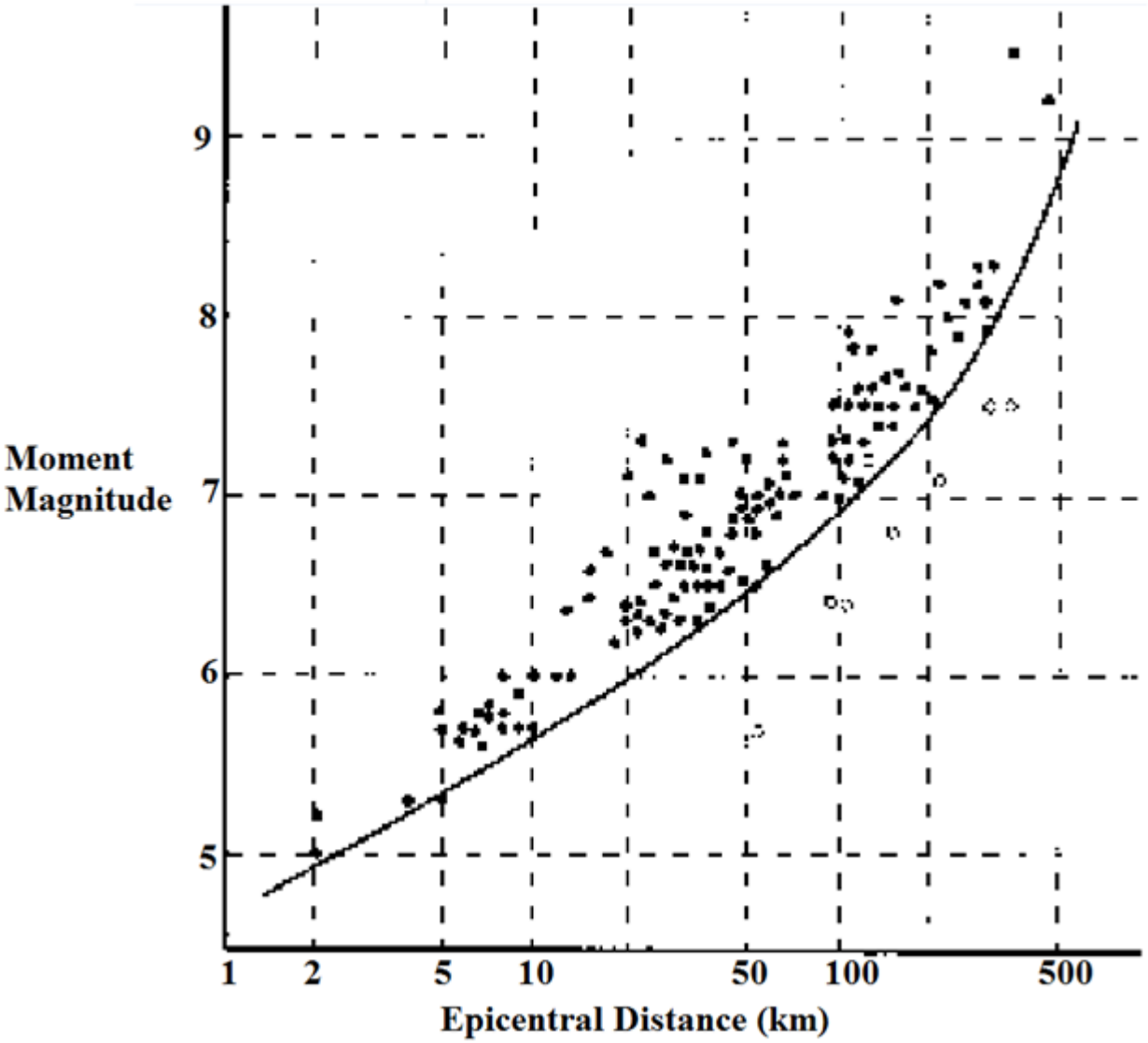

Figure 10-1: Historical Observation of liquefaction Case Histories (Ambraseys, 1988).

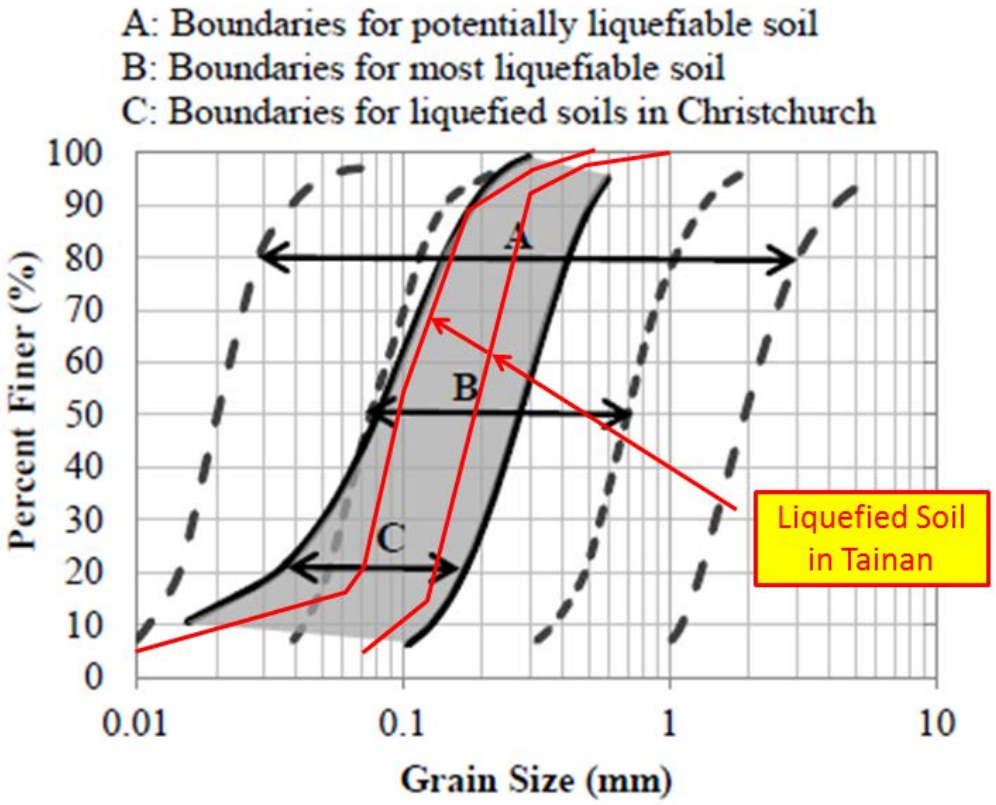

Figure 10-2: Comparison of Liquefiable Soil in New Zealand and Tainan (Modified after USGS).

Figure 10-3: Development of a structural hinge within a beam supporting a carport at the Xinshi site due to column heave (right side) and settlement (left side) of structure. This carport was demolished, while the interior of the building supported on grade beams connecting spread footings performed well (23.08096, 120.30258).

Figure 10-4: Modern grade beam design in Taiwan (building under construction in Tainan City).

REFERENCES

Andrus, R.D., Stokoe II, K.H., 2000. Liquefaction resistance of soils from shear-wave velocity. Journal of Geotechnical and Geoenvironmental Engineering, ASCE 126 11), 1015–1025.

Central Geological Survey, 2005, Geologic Map of Tainan

Chang, W. J., Ni, S. H., Huang, A. B., Huang, Y. H., and Yang, Y. Z. 2011. "Geotechnical Reconnaissance and Liquefaction Analyses of a Liquefaction Site with Silty Fine Sand in Southern Taiwan," Engineering Geology, Vol. 123, pp. 235-245.

Chen, H.Y., 2006, Crustal deformation analysis of southern Taiwan: GPS observations in southern Taiwan from 1995 to 2005, Master's Thesis, National Taiwan University, 156p.

Chen et al. 2016. 20160206 Tainan EQ Geotechnical Damage Field Survey v1.0 NCREE Geotechnical Division. (in Chinese)

Degenkolb blog (2016). Courtesy of Mr. Daniel Zepeda. http://degenkolb.com/blog

European Commission – Research General Directorate (2004) "Guidelines for the Implementation of the H/V Spectral Ratio Technique on Ambient Vibration Measurements, Processing and Interpretation." SESAME European Research Project. WP12 – Deliverable D23.12.

Foti, F., Lai, C., Strobbia, C, and Rix, G, (2014) "Surface Wave Methods for Near-Surface Site Characterization" *CRC Press*, ISBN 9780415678766

Hsieh, M.-C., L. Zhao and K.F. Ma, 2014. Efficient waveform inversion for average earthquake rupture in three-dimensional structures, *Geoph. J. Int.*, 198, 1279-1292.

Huang, C.-Y., P. B. Yuan, C.-W. Lin, T. K. Wang, and C.-P. Chang (2000), Geodynamic processes of Taiwan arc-continent collision and comparison with analogs in Timor, Papua New Guinea, Urals and Corsica, *Tectonophysics*, *325*, 1 – 21.

Huang, C.Y., Yuan, P.B., and Tsao S.J., 2006, Temporal and spatial records of arc-continent collision in Taiwan, a synthesis, GSA Bulletin, v. 118, no 3 / 4, p. 274-288.

Kao, H., G.-C. Huang, and C.-S. Liu (2000), Transition from oblique subduction to collision in the northern Luzon arc – Taiwan region: Constraints from bathymetry and seismic observations, *J. Geophys. Res.*, *105*, 3059 – 3079.

Lee, S. J., W. T. Liang, H. W. Cheng, F. S. Tu, K. F. Ma, H. Tsuruoka, H. Kawakatsu, B. S. Huang, and C. C. Liu, 2013. Towaes real-time regional earthquake simulation I: real-time moment tensor monitoring (RMT) for regional events in Taiwan, *Geoph. J. Int.*, doi:10.1093/gji/ggt371.

Lee, S. J., W. T. Liang, L. Mozziconacci, Y. J. Hsu, W. G. Huang and B. S. Huang, 2013. Source complexity of the 4 March 2010 Jiashian, Taiwan Earthquake determined by joint inversion of teleseismic and near field data. *Journal of Asian Earth Sciences*, 64, 14-26, http://dx.doi.org/10.1016/j.jseaes.2012.11.018.

Nakamura, Y., (1989). A Method for Dynamic Characteristics Estimation of Subsurface using Microtremor on the Ground Surface. Quarterly Report of RTRI. 30:1, 25-33.

NCREE (2016a). 0206 Meinong Earthquake, Seismology and impact in Tainan City. Digital presentation version 1.0. February 19, 2016.

NCREE (2016b). February 6, 2016 (local time) M_L-6.4 Meinong Earthquake Kaohsiung City, Taiwan. Digital presentation version 5.0.

SGH blog (2016). Courtesy of Mr. Kevin Moore. http://sghblogs.com/

Shyu, J. B. H., K. Sieh, Y. G. Chen, and C. S. Liu, 2005, Neotectonic architecture of Taiwan and its implications for future large earthquakes, J. Geophys. Res., 110, no. B0, 8402, doi 10.1029/2004JB003251.

Suppe, J., 1984, Kinematics of arc-continent collision, flipping of subduction, and back-arc spreading near Taiwan, Mem. Geol. Soc. China 6, 21–33.
Suppe, J. (1987), The active Taiwan mountain belt, in *Anatomy of Mountain Chains*, edited by J. P. Schaer and J. Rodgers, pp. 277 – 293, Princeton Univ. Press, Princeton, N. J.
Teng, L. S. (1990), Late Cenozoic arc-continent collision in Taiwan, *Tectonophysics*, *183*, 57 – 76.
U. S. Geological Survey, 2016, http://earthquake.usgs.gov/earthquakes/eventpage/us20004y6h#general_region: website accessed Feb. 27, 2016.
Wu, F.T, Rau, R.J., and Salzberg, D., 1997, Taiwan orogeny: thin-skinned or lithospheric collision, Tectonophysics, v. 274, p. 191-220.
Wu, Y. M., D.Y. Chen, T. L. Lin, C. Y. Hsieh, T. L. Chin, W. Y. Chang, W. S. Li, and S. H. Ker, 2013. A High-Density Seismic Network for Earthquake Early Warning in Taiwan Based on Low Cost Sensors by Yih-Min Wu, Seismo. Res. Lett., 84, SRL-2013085 1048..1054.
Yu, S. B., H. Y. Chen, and L. C. Kuo, 1997, Velocity field of GPS stations in the Taiwan area, Tectonophysics 274, 41–59.